2011-08-18

Nuclear Import of Smad: A Dissertation

Xiaochu Chen
University of Massachusetts Medical School

Graduate School of Biomedical Sciences

GSBS Dissertations

University of Massachusetts Medical School Year 2011

NUCLEAR IMPORT OF SMAD: A

DISSERTATION

XIAOCHU CHEN

University of Massachusetts Medical School,

NUCLEAR IMPORT OF SMAD

A Dissertation Presented

By

XIAOCHU CHEN

Submitted to the Faculty of the

University of Massachusetts Graduate School of Biomedical Sciences, Worcester

in partial fulfillment of the requirements for the degree of

DOCTOR OF PHILOSOPHY

August 18th, 2011

Interdisciplinary Graduate Program

NUCLEAR IMPORT OF SMAD
A Dissertation Presented

By

XIAOCHU CHEN

The signatures of the Dissertation Defense Committee signifies completion and approval as to style and content of the Dissertation

_____
Lan Xu, Ph.D., Thesis Advisor

_____
Peter Siegel, Ph.D., Member of Committee

_____
Thoru Pederson, Ph.D., Member of Committee

_____
Gregory Pazour, Ph.D., Member of Committee

_____
David Lambright, Ph.D., Member of Committee

The signature of the Chair of the Committee signifies that the written dissertation meets the requirements of the Dissertation Committee

_____
Roger Davis, Ph.D., Chair of Committee

The signature of the Dean of the Graduate School of Biomedical Sciences signifies that the student has met all graduation requirements of the School

_____
Anthony Carruthers, Ph.D.,
Dean of the Graduate School of Biomedical Sciences

Interdisciplinary Graduate Program

August 18, 2011

ACKNOWLEDGEMENTS

I am truly grateful to my thesis advisor Dr. Lan Xu. With his unique patience and intelligence, Dr. Lan Xu has made my graduate study such an exciting and rewarding one. I thank Dr. Lan Xu for providing outstanding research opportunities, challenging me with new ideas, teaching me how to properly conduct experiments and communicate science with people, all of which I have benefited and will continue to benefit from throughout my scientific career.

My sincere thank also goes to my advisory committee members, Dr. Roger Davis, Dr. Peter Siegel, Dr. Gregory Pazour, Dr. Thoru Pederson, Dr. Craig Peterson, and Dr. David Lambright., for the valuable discussions, reagents, critiques and guidance. I would like to thank our collaborators Ip lab, especially Alla, Maddy, Guoqiang and Tony, for sharing their reagents and ideas, and for all the help and technical support they provided during my research.

I also thank all of the past and present Xu lab members for your help and guidance, especially, Dr. Charisa Cottonham, Dr. Satoshi Kaneko, and Dr. Xiaohao Yao. And to my neighbors in Biotech Two, including the Davis lab, for sharing their equipments and joyful lunch time together. Especially Claire and Caroline, thank you for critiquing my

presentations. I would also want to thank Meng-Tse Lee for his help in revision of my thesis writing. I would like to thank Dr. Juerg Straubhaar for the help on statistic analysis of my screen data.

I am so fortunate to be able to accomplish this challenging work because the love and support from my friends here. I would like to thank Dr. Yuanfei Wu, Dr. Lue Dai, Lixia Li, Dr. Shuyun Dong, Dr. Hanhui Ma, Fan Zhang, Tingting Huang and many others for their emotional support and laughs we have shared. Additionally, I would like to send a special thank you to my family in China, especially my parents and my grandma. I would not have gone so far without their love and support. They have always been supportive for my career choice no matter what. I want to thank them for all the sacrifice they made for me by letting me go abroad for my Ph.D. study. I am the luckiest person in the world for having them as my family and I will try my best to make them feel proud of me. I love all of you, Mom, Dad, and grandma!

ABSTRACT

Signal transduction by transforming growth factor β (TGF-β) cytokines is mediated by an evolutionarily conserved mechanism that depends on the Smad proteins to transduce an extracellular stimulus into the nucleus. In the unstimulated state, Smads spontaneously shuttle across the nuclear envelope and distribute throughout the cell. Upon TGF-β or bone morphogenetic protein (BMP) stimulation, the receptor-activated Smads are phosphorylated, assemble into complexes with Smad4, and become mostly localized in the nucleus. Such signal-induced nuclear translocation of activated Smads is essential for TGF-β–dependent gene regulation that is critical for embryonic development and homeostasis. The molecular machinery responsible for this process, especially how the activated Smads are imported as complexes, is not entirely clear. Thus, I became interested in investigating the molecular requirements for nuclear targeting of Smads upon stimulation.

Recently, whole-genome RNAi screening offers a complementary cell-based approach to functionally identify molecules that mediate nuclear accumulation of Smads in response to TGF-β. In the first part of this dissertation, I performed a genome-wide RNAi screen that uncovered the importin moleskin (Msk) required in nuclear import of Dpp-activated MAD. Both genetic and biochemical studies further confirmed this finding. I also investigated Smad interactions with the Msk mammalian orthologues, Importin7 and 8 and validated that Smads are bona fide cargos of Imp7/8.

Besides the importin Msk, the screen also uncovered a subset of nucleoporins as required factors in signal-induced nuclear accumulation of MAD. Thus in the second part of this thesis, I focused on how the NPC mediates this Msk-dependent nuclear import of activated MAD. Most of these nucleoporins, including Sec13, Nup75, Nup93 and Nup205, were thought to be structural nucleoporins without known cargo-specific functions. We, however, demonstrated that this subset of nucleoporins was specifically used in the Msk-dependent nuclear import of activated MAD but not the constitutive import of cargos containing a classic nuclear localization signal (cNLS). I also uncovered novel pathway-specific functions of Sec13 and Nup93.

Regulation of TGF-β signaling can be achieved not only by modulating Smad nuclear translocation but also by modifying Smad phosphorylation status. Previously we identified a kinase, Misshapen (Msn), that caused the linker phosphorylation of MAD, resulting in negative regulation of Dpp signaling (*Drosophila* BMP). In the third part of this thesis, I investigated the biological relevance of Msn kinase to Dpp signaling in *Drosophila* wings. Both over-expression and RNAi studies suggest that Msn is a negative regulator of the Dpp/MAD pathway *in vivo*.

As a whole, my findings delineated two critical requirements for MAD nuclear import: the importin Msk and a unique subset of nucleoporins. For the first time, structural Nups are implicated in the direct involvement of cargo import, providing a unique trans-NPC mechanism.

TABLE OF CONTENTS

LIST OF TABLES

LIST OF FIGURES

LIST OF ABBREVATIONS

TGF-β (transforming growth factor β)

BMP (bone morphogenetic protein)

GDFs (growth and differentiation factors)

Dpp (decapentaplegic)

MAD (mothers against decapentaplegic)

DAD (daughters against decapentaplegic)

cNLS (classic nuclear localization signal)

NES (nuclear export signal)

NTF (nuclear transport factor)

Msk (Moleskin)

NPC (nuclear pore complex)

Nup (nucleoporin)

FG (phenylalanine-glycine repeats)

MAPK (mitogen-activated protein kinase)

GSK3 (glycogen synthase kinase 3)

CDK (cyclin-dependent kinase)

Msn (Misshapen)

GFP (green fluorescent protein)

DAPI (4',6-diamidino-2-phenylindole)

COPYRIGHT INFORMATION

The chapters of this dissertation have appeared in whole or part in publications below:

1 Xu L, Yao X, Chen X, Lu P, Zhang B, Ip YT. (2007) Msk is required for nuclear import of TGF-β/BMP-activated Smads. *Journal of Cell Biology* 178(6):981-94.

2 Yao X, Chen X, Cottonham CL, Xu L. (2008) Preferential utilization of Imp7/8 in nuclear import of Smads. *Journal of Biological Chemistry* 283(33):22867-74**.**

3 Chen X**,** Xu L. (2010) Specific Nucleoporin Requirement for Smad Nuclear Translocation. *Molecular Cell Biology* 30(16):4022-34

4 Kaneko S, Chen X, Lu P, Yao X, Wright TG, Rajurkar M, Kariya K, Mao J, Ip YT, Xu L. (2011) Smad inhibition by the Ste20 kinase Misshapen. *Proc Natl Acad Sci U S A.* 108(27):11127-32.

CHAPTER I: INTRODUCTION

1. 1 TGF-β Signal Transduction

First identified in the early 1980s, transforming growth factor β (TGF-β) has been shown to regulate a wide range of biological functions, including cellular proliferation, differentiation, adhesion, migration and death as well as developmental processes, in species ranging from *Drosophila*, *Caenorhabditis elegans* to mammals (Massagué 2000; Ten Dijke et al. 2002). The TGF-β superfamily is comprised of many secreted dimeric ligands, categorized as TGF-βs, bone morphogenetic proteins (BMPs), growth and differentiation factors (GDFs), activins and nodal. These ligands signal through a rather simple and evolutionarily conserved pathway, involving trans-membrane receptor serine/threonine kinases, intracellular Smad effectors as well as other signaling proteins.

A TGF-β ligand initiates signaling by binding to and bringing together type I and type II receptors in a heterotetrameric complex (Shi and Massague 2003) (**Fig. 1.1**). The constitutively active type II receptors then phosphorylate and activate their cognate type I receptors. Activation of the type I receptor results in phosphorylation of the Smad proteins, which then form complexes and translocate into the nucleus, functioning as transcription factors.

1.1.1 The Smad proteins

Smad proteins contain three domains: an N-terminal MAD-homology 1 (MH1) domain that harbors a nuclear localization signals (NLS) and a DNA-binding motif; a C-terminal MH2 domain that binds to type I receptors and mediate Smad homo- or hetero-oligomerization; and a linker region that connects the MH1 and MH2 domains. The linker region is enriched with prolines and phosphorylatable serines and threonines, providing interaction sites for ubiquitin ligases and other proteins (**Fig. 1.2**) (Moustakas and Heldin 2009).

In mammals, there are eight distinct Smads, classed into three functional groups: the receptor-activated Smad (R-Smad), the Co-mediator Smad (Co-Smad) and the inhibitory Smad (I-Smad) (Shi and Massague 2003; Xu 2006). R-Smads (Smad1,2,3,5,and 8) contain an C-terminal SXS motif which is phosphorylated by ligand-activated TGF-β receptor kinases. TGF-β/activin signals through Smad2 and Smad3 while BMP/GDF pathways signal via Smad1, Smad5 and Smad8. Co-Smad lacks the SXS motif at its C-terminus and is not phosphorylated by TGF-β receptor kinases. The C-terminal phosphorylation of the R-Smads allows them to associate with the Co-Smad, Smad4. The resulting Smad complexes consists of two R-Smad molecules and a single Smad4 and are translocated into the nucleus. Together with other cofactors, the R-Smad/Smad4 complexes regulate

the transcription of target genes. The expression of I-Smads is induced by TGF-β- or BMP-specific Smad complexes. I-Smad negatively regulates TGF-β signaling by competing with R-Smads for receptor or Co-Smad interaction and by targeting the receptors for ubiquitylation and degradation (**Fig. 1.2**).

1.1.2 TGF-β signaling in *Drosophila*

The TGF-β family is conserved throughout metazoan evolution (**Fig. 1.1**). Forward genetic screens in *Drosophila* have been identified core components of the TGF-β family members. *Drosophila melanogaster* has seven TGF-β family members and five receptors. The BMP-like ligands Decapentaplegic (Dpp), Screw (Scw) and Glass bottom boat (Gbb), bind the type II receptors Punt (Put) and Wishful thinking (Wit), which form complexes with the type I receptors Thickveins (Tkv) and Saxophone (Sax), and signal via a single R-Smad (MAD, Mothers against decapentaplegic) and a single Co-Smad (Medea) (Affolter and Basler 2007). The TGF-β/activin-like ligands dActivin and Daw bind the same type II receptors Put and Wit but pair with the type I receptor Baboon (Babo), and signal through dSmad2 (Smox) (an R-Smad) and Medea (Zhu et al. 2008). A single I-Smad, daughters against decapentaplegic (DAD), was described in wing imaginal disc development. DAD inhibits BMP-like signaling but not the activin-like signaling (Kamiya, et al. 2008).

1.1.3 Smad nuclear transport

At unstimulated states, R-Smads and Smad4 are present mostly in the cytoplasm or evenly throughout the cell (Xu et al. 2002; Inman et al. 2002). Upon TGF-β stimulation, R-Smads and Smad4 form oligomeric complexes that concentrate in the nucleus, which allows Smads to function as transcription factors in a signal-dependent manner. Moreover, the amount and duration of Smad association with their target promoters in the nucleus determines the strength and time span of transcriptional outcomes (Xu 2006). Therefore, effective regulation of TGF-β signal transduction is essentially achieved by spatial and temporal control of intracellular trafficking of Smads.

The subcellular localization of Smads revealed by immunofluorescent staining only showed a static moment of constantly moving Smads. In fact, R-Smad and Smad4 all undergo spontaneous bi-directional shuttling across the nuclear envelope as revealed in two previous studies using *in vitro* nuclear transport assays (Xu et al. 2002; Inman et al. 2002). Additional live cell analyses further validated this conclusion (Nicolás et al. 2004; Schmierer and Hill 2005). Using photoactivation technology, the dynamics of a particular pool of photo-activatable GFP-fused Smad2 (PAGFP-Smad2) can be visualized in live cells. After photoactivation, either the cytoplasmic or nuclear pool of PAGFP-Smad2 was shown to continuously shuttle between the cytoplasm and the nucleus in

unstimulated cells. Likewise, in Fluorescence Loss in Photobleaching (FLIP) analysis, after photobleaching of either the cytoplasmic or nuclear pools of GFP-fused Smad2 or Smad4, the remaining GFP-Smads in the other subcellular compartment quickly redistributed and refilled the bleached region. These live-cell analyses suggest the constant import and export of R-Smads as well as Smad4 in establishing R-Smads and Smad4 subcellular localization.

From cell membrane to the nucleus, the cytoplasmic trafficking of Smads is often mediated by motor proteins that are associated with microtubules. Kinesin1 interacts with Smads and recruits Smad2 to the receptor complexes for its phosphorylation and activation in Xenopus and mammalian cells (Batut and Hill 2007). Other motor proteins, such as Dynein light chain km23-1 (DYNLRB1), facilitate Smad traffic towards the nucleus of mammalian cells (Jin and Mulder 2007; Jin et al. 2009).

Smad Nuclear Import

For translocation across the nuclear envelope, Smad nuclear import requires both Nuclear Pore Complexes (NPCs) and importins. Smad2 and Smad3 can interact with nucleoporins Nup214 and Nup153 directly through a hydrophobic region in the C-terminus of Smad2 and Smad3 (Xu et al. 2002). Point mutations in this nucleoporin-binding region resulted in impaired nuclear import of

unphosphorylated Smad2, confirming the requirement of nucleoporins in Smad2 nuclear shuttling in the basal state. All Smads have a conserved nuclear localization signal (NLS) in their MH1 domain, which interacts with specific importins, such as importin β, importin α and Msk. Importin β has been shown to interact directly with the NLS motif in the MH1 domain of activated Smad3, but not Smad2 (Kurisaki et al. 2001), as Smad2 contains two unique inserts flanking the NLS motif, which impairs Smad2 interaction with Importin β (**Fig. 1.2**). Recently, we identified Msk (Imp7 and Imp8 in mammals) as the importin for C-terminal phosphorylated Smads in *Drosophila* MAD and in mammalian cells Smad1, Smad2 and Smad3 (Xu et al. 2007). These findings suggest R-Smads employ different import routes for nuclear import with or without TGF-β stimulation. Smad4 may also enter the nucleus through multiple pathways. In mammalian cells, Imp 7/8 are required for the nuclear import of Smad4 in response to TGF-β (Yao et al. 2008). Overexpression of Imp8 is sufficient to drive the nuclear import of Smad4 without TGF-β stimulation. Smad4 can also directly interact with Nup214 and enter the nucleus without importins in the nuclear import assay reconstituted *in vitro* (Xu 2003). In *Drosophila* cells, it remains unclear which importin is responsible for the signal-independent nuclear import of Medea (Smad4 homolog in *Drosophila*), as it does not require Msk or importin β (Yao et al. 2008).

Smad Nuclear Export

Smad nuclear export requires exportin and NPCs. Smad proteins contain characterized nuclear export signals (NESs) in their MH2 (Smad1, Smad3) or linker domains (Smad4) (**Fig. 1.2**). The NESs interact with specific exportins for Smads export. Smad3 nuclear export is mediated by exportin 4 (Kurisaki et al. 2006) while Smad1 and Smad4 nuclear export depends on exportin 1, also known as CRM1. Recently, a new exportin, RanBP3 was described for Smad2 and Smad3 nuclear export (Dai et al. 2009).

Signal-induced phosphorylation of Smads triggers the assembly of R-Smads and Smad4 oligomeric complexes, which creates a completely different cargo for nuclear import, compared to Smad monomers in the unstimulated state. How does TGF-β target Smads into the nucleus? Given that the dynamic shuttling of Smads in and out of the nucleus, it can be proposed that upon TGF-β stimulation, either an increase in nuclear import or a decrease in nuclear export causes the concentration of Smads in the nucleus. An increased nuclear import rate can be due to enhanced Smads affinity to nucleoporins or the recruitment of new import factors whereas the export rate can be affected by Smads affinity to exportins and nucleoporins, C-terminal dephosphorylation of Smads as well as sumoylation and ubiquitylation in the nucleus. In fact, phosphorylation of R-Smads did not affect its affinity to nucleoporins (Xu et al. 2002). Whether the nuclear import rates for

activated Smads increases is under debate. Faster import of pseudophosphorylated R-Smads was observed when compared with wild-type unphosphorylated R-Smads *in vitro* (Kurisaki et al. 2001). In a live cell analysis, the initial import rate of Smad2 (first 3 minutes) did not change significantly in response to TGF-β. However, at later time points, the import of phosphorylated Smad2 sustained while the import of unphosphorylated Smad2 plateaued (Schmierer and Hill 2005). A following study by the same group found that a mathematical model allowing faster import of Smad complexes better fitted the experimental data from live cell analyses than the model assuming identical import rates between Smad complexes and monomeric Smads (Schmierer et al. 2008). This finding strongly suggests that TGF-β-induced nuclear accumulation of activated Smads requires their enhanced nuclear import. Furthermore, the same *in vivo* study reported that TGF-β signaling significantly decreased the export rate of Smad2, indicating that an inhibition of nuclear export of Smad2 is also required for its signal-dependent nuclear accumulation (Schmierer and Hill 2005). Indeed, phosphorylation of R-Smads was shown to cause some decrease in binding to exportin 4 (Kurisaki et al. 2006). But it is not sufficient to target R-Smads to the nucleus by only blocking the export by depletion of exportin 4 using siRNA, which did not cause much change in R-Smads localization at basal state. Other elements, such as dephosphorylation, sumoylation and ubiquitylation of Smads in the nucleus, also contribute to the TGF-β induced nuclear accumulation of Smads (**Fig. 1.3**). For example, Smad3 is

sumoylated by the Sumo ligase protein inhibitor of activated Stat y (PIASy) and sumoylation promotes Smad3 nuclear export in mammalian cells (Imoto 2003). Sumoylation of Medea in early *Drosophila* embryonic cells also promotes its nuclear export, leading to the negative regulation of dpp signaling (Miles et al. 2008). It has been described that monoubiquitylation of Smad4 by the nuclear ubiquitin ligase TIF1γ also promoted its nuclear export and inhibited its association with Smad2 and Smad3 (Dupont et al. 2009). It is possible that *in vivo* dephosphorylation, sumoylation and ubiquitylation of Smads ensure the continuous Smad shuttling and that TGF-β might inhibit these post-translational modifications of Smads to shift the shuttling equilibrium favoring the nuclear accumulation of Smads.

In addition, nuclear retention factors can also control Smad compartmentalization by regulating how long Smad complexes reside in the nucleus. An exclusively nuclear protein, FoxH1, when it is over-expressed, is capable of retaining Smad2 mostly in the nucleus in the absence of a TGF-β signal (Xu et al. 2002). Several other Smad interacting proteins, such as ATF2 (Kang et al. 2003) and TAZ (Varelas et al. 2008), also target Smads to the nucleus. FoxH1 and ATF2 both bind to the MH2 region of Smad2, shielding the NES in the MH2 region from exposure to export factors and therefore sequester Smads in the nucleus.

1.2. Nuclear Pore Complexes and Nuclear Transport

1.2.1 Structure of Nuclear Pore Complexes

In eukaryotic cells, the exchange of macromolecules between the nucleus and cytoplasm is mediated by nuclear pore complexes (NPCs) embedded in the nuclear envelope, providing a size-selective gate for bidirectional transport (Strambio-De-Castillia and Rout 2010; Wente and Rout 2010). Analysis of electron microscope images revealed the NPC as a cylindrical pore structure with strong octagonal symmetry. Embedded in the plane of the nuclear envelope is a core structure, a central hole surrounded by eight spokes in a radially symmetrical manner. Attached to the central core are peripheral filaments emanating into the cytoplasm and nucleoplasm. On the cytoplasmic side, filaments extend from NPC and associate with the protein synthesis machinery and the cytoskeleton. On the nuclear side, emanating fibrils converge at their distal ends to form a cage-like structure referred to as the nuclear basket. Proteomic analyses of the composition of the NPC have revealed that each NPC is composed of multiple copies of ~30 unique proteins, called nucleoporins (Nups) (Cronshaw et al. 2002). It is estimated that each NPC in eukaryote contains around 400 individual proteins.

A recent work using a computational approach that combined proteomic, biophysical and imaging data suggested a detailed molecular architecture of the

NPC, assigning each Nup to particular subcomplexes in the NPC (Alber et al. 2007). Nups can thus be grouped into three classes (**Fig. 1.4**): transmembrane Nups, FG-Nups and non-FG Nups. Three transmembrane Nups in both yeast and vertebrates constitute a lumenal ring that anchored the central core to the nuclear envelope. FG-Nups containing phenylalanine-glycine repeats (FG-repeats) are largely unfolded proteins that constitute the peripheral filaments lining the surface of central channel from the nuclear to the cytoplasmic face. Non-FG Nups assembled into four spoke rings, two outer rings sandwiching two inner rings, with eight-fold symmetry to form the central core. The inner rings include the Nup170 subcomplex (yeast) or Nup155 (vertebrates) subcomplex, while the outer rings contain the Nup84 subcomplex (yeast) or Nup107-160 subcomplex (vertebrates, **Fig. 1.4**).

Non-FG Nups are evolutionarily conserved across all eukaryotes. Structurally, non-FG Nups are composed entirely of either a β-propeller fold, an α-solenoid (helix-turn-helix) fold, or a distinctive combination of both—a combination that is characteristic of a particular family of membrane coating complexes such as clathrin, COPI and COPII (Devos et al. 2004; Devos et al. 2006). The similarity between non-FG Nups and the COP complex proteins supports the "proto-coatomer hypothesis", indicating the common evolutionary origin of these two groups. Analogous to the curved membrane of a vesicle being stabilized by a

clathrin or COP coat, the non-FG Nups hug and stabilize the curved surface of the pore membrane. Particularly, Sec13 is a shared component between the NPC and COPII complex. Sec13 contains six WD40 repeats that fold into an open six-bladed β-propeller, which is complemented by a seventh blade from β-stranded region of Nup145C or Sec31, forming Sec13-Nup145C pair in the NPC or Sec13-Sec31 pair in the COPII complex respectively (Hsia et al. 2007; Brohawn et al. 2008).

The Nup84 subcomplex that forms the outer rings in yeast is a well-characterized heptameric complex consisting of Nup84, Nup85, Nup120, Nup133, Nup145C, Sec13, and Seh1 (Siniossoglou et al. 2000; Allen 2001; Lutzmann 2004). A negative-stain electron microscopy study on the heptamer assembled from recombinant proteins revealed a 400Å long Y-shaped complex and established the relative position of its members. The arrangement of the seven Nups is linear with Nup133 and Nup84 at the base, the Sec13-Nup145C pair in the center, and the Seh1-Nup85 pair and Nup120 as two arms of the Y respectively. Four crystal forms of Seh1-Nup85 pair and two crystal forms of Sec13-Nup145C pair were unveiled in crystallographic analyses (Hsia et al. 2007; Brohawn et al. 2008). High structural similarity exists between Seh1-Nup85 pair and Sec13-Nup145C pair as revealed by superimposition, despite low sequence identity between protein pairs.

The inner rings consist of the Nup170 subcomplex which is less well characterized (Lusk et al. 2002). It appears to contain Nup157/Nup170, Nup188, Nup192/Nup205, Nup53, Nup59 and Nic96/Nup93. Among these Nups, only Nic96 structure was solved by x-ray crystallography (Jeudy and Schwartz 2007).

Several putative models have been generated for the central core assembly. As mentioned previously, Alber et al., integrated proteomic, cryo-EM, and biochemical data in computational reconstitution of the NPC core structure and proposed the central core as two outer rings sandwiching two inner rings (**Fig. 1.4**). This model has a 16-fold symmetry due to the 8-fold rotational symmetry of the spoke and the 2-fold rotational symmetry between the nucleoplasmic and cytosolic halves of the NPC. A relative different “lattice like” model with the same symmetry was postulated by Schwartz group (**Fig. 1.5 A**). Nup84 and Nic96 complexes still assembled into outer rings and inner rings respectively, but the extended arm of the Y-shape Nup84 complex was positioned facing outward and the two arms of the Y facing inward formed a triskelion that conceptually resembled the lattice cages in vesicle coats. Hsia et al. observed both Sec13-Nup145C and Seh1-Nup85 hetero-octameric crystals and proposed that these two hetero-octamers formed alternating vertical poles that connected four horizontally arranged rings, each composed of eight heptamers (**Fig. 1.5 B**). Given

the determined length of heptamer (400Å), the resulting diameter of the ring would be about 1000Å, consistent with the outer dimension requirement established in cryoelectron microscopy (Yang et al. 1998). The resulting cylinder coat had 32 heptamers. The NPC core was therefore depicted as a series of concentric cylinders consisting of pore membrane proteins, coat nups (Nup84 complexes), adaptor nups (Nic96 complexes) and channel nups.

1.2.2. Nuclear Transport

The NPC is permeable to small metabolites, ions and molecules less than 40 kDa in mass or 5nm in diameter. To translocate through the NPC, macromolecules need to interact with the NPC directly or indirectly through soluble nuclear transport factors (NTFs) (Feldherr and Akin 1997). Most NTFs belong to the family of proteins known as the karyopherins (Kap). There are 14 Kaps in yeast and at least 20 in metazoans. In general, a Kap has a cargo-binding domain, an NPC-binding domain(s) and an N-terminal binding domain for Ran, a small Ras-like GTPase required for active transport (Vetter et al. 1999). High-resolution structural information obtained from importin studies suggested a common folding feature for Kaps. These proteins are comprised of tandem HEAT-repeats (helix-turn-helix), folding into a super-spiral structure. Interestingly, this structural feature resembles that found in non-FG Nups, indicating their common root in evolution. Most Kaps specialize to facilitate transport in only one direction, but

there are a few exceptional Kaps that can mediate both import and export. Not only can Kaps transport proteins, they can also mediate RNA transport.

In addition to the NTFs, another requirement for any facilitated transport is a transport ‘signal’, which can be recognized by either NTFs or adapter molecules. Different transport signals target different cargos to their specific transport routes. Many of these signals do not fit a well-defined consensus. In protein transport, specific amino acid residues serving for transport signal purpose are termed as nuclear localization sequences (NLSs) for import or nuclear export sequences (NESs) for export. A classical NLS is the simple five amino acid peptide KKKRK, necessary and sufficient for targeting its attached protein to the nucleus (Goldfarb et al. 1986). Additional nuclear import signals may exist for proteins lacking a classical NLS. Recently, a 3 amino acid domain SPS in ERK2 was identified as a general nuclear import signal. Phosphorylated SPS interacts with Imp7 and directs nuclear translocation of ERK2 (Chuderland et al. 2008). Smad3 contains an SPS domain in its MH2 region. Phosphorylation of SPS also results in Smad3 nuclear localization while nonphosphorylatable Smad3 with the SPS replaced by AAA remains cytoplasmic (Chuderland et al. 2008). However, the role of Imp7 and Imp8 in the SPS-directed nuclear import of Smad3 has not been characterized in this study.

Nuclear transport can be formulated as three conservative steps (Akey and Goldfarb 1989). First, NTFs recognize their cognate substrates through transport signals and assemble into a NTF-cargo complex. Second, the NTF-cargo complex binds to the NPC and translocates through the NPC. Third, once the NTF-cargo complex reaches its target compartment (either the nucleoplasm or cytoplasm), the complex dissembles. In Kap-mediated transport, Kap-cargo interactions and transport directionality are regulated by the small GTPase Ran. Ran has either GTP- or GDP-bound state. Conversion between these two states is regulated by two Ran-specific proteins: A cytosolic GTPase-activating protein (GAP) that converts Ran-GTP to Ran-GDP, and a nuclear guanine exchange factor (GEF) that converts Ran-GDP to Ran-GTP. Because Ran-GAP is located exclusively in the cytosol and Ran-GEF is located only in the nucleus, cytoplasmic Ran is primarily in the GDP-bound state whereas the nucleus primarily contains Ran-GTP. Such a Ran-GTP gradient, across the two faces of the NPC, is essential for the directionality of Kap-mediated transport (Kuersten et al. 2001). Overall, Ran-GTP decreases the affinity of importins for their import cargos while in export cases, Ran-GTP binding increases the affinity of exportins for their export cargos. For nuclear import, a specific cargo is loaded onto its cognate importin in the cytoplasm where Ran-GTP levels are low and released from the importin in the nucleus where Ran-GTP levels are high. The released importin is now bound to Ran-GTP and then recycled back to the cytoplasm. GTP hydrolysis of Ran on the

cytoplasmic side frees the importin for further cycles of nuclear import. For nuclear export, exportin-cargo complexes are formed via Ran-GTP association in the nucleus and dissembled in the cytosol through GTP hydrolysis of Ran by GAP.

Exactly how the NPC facilitates transport is controversial. A favorable transport model should fit the following observations. First, selectivity of the transport should be explained. Second, the model should explain the fast transport rate which is in a range of milliseconds. Third, the model should provide the physical path taken by transport complexes. Lining along both the nucleoplasmic and cytoplasmic faces of the central tunnel of the NPC, FG-Nups were thought to function as an entity, providing docking sites for cargo-free or cargo-loaded NTFs. Many NTFs, such as NTF2, Tap/NXF1 and Impβ, were found to bind to FG-Nups.

From a thermodynamic point of view, entry from the large volume of the cell compartment into the small volume of the NPC channel is a non-spontaneous process that requires energy, in other words an entropy-loss process. Analogous to an enzyme that catalyzes a reaction, the milieu formed by the FG Nups interacts with the transport complex, whose binding energy compensates for the loss in entropy, and allows the entry of specific molecules into the narrow pore. Conversely, molecules that cannot bind FG milieu are repelled as there is no gain of energy to overcome the diffusion barrier. Thereby, the NPC ensures the

selectivity as a virtual or entropic gate without the need for individual structural elements to move with respect to each other (Rout 2003). Molecular organization of the FG milieu is still a matter of vigorous debate. At physiological concentrations, recombinant FG-Nups were shown to form a hydrogel *in vitro* under certain conditions (Frey and Görlich 2007). Such a hydrogel is the result of intra- and intermolecular interactions of cohesive hydrophobic clusters within FG-Nups. Therefore, the selective phase/hydrogel model was postulated as the FG-Nups form "a hydrogel-based" three-dimensional sieve that allows translocation of small molecules but restricts that of large ones (**Fig. 1.6 A**). Indeed, the constructive hydrogel *in vitro* recapitulated some of the transport characteristics of the NPC, allowing rapid diffusion of only NTF-containing transport complexes at a comparable rate as *in vivo* transport (Frey and Görlich 2009).

When FG-regions of Nup153 were attached to gold nanodots, extended brush-like polymer filaments were observed by atomic force microscopy (Lim et al. 2006). Molecular dynamics simulations also suggested that FG-Nups would form brush-like structures when tethered to a surface at a physiological density (Miao and Schulten 2009). These observations suggest that FG-Nups may exhibit a polymer brush-like behavior, pushing away non-specific macromolecules. A transient passage through the meshwork is created when FG-Nups are bound by

NTFs and collapsed (Lim et al. 2007) (**Fig. 1.6 B**).

All the above models cannot explain the observation that cargo-free or cargo-bound importin β mostly travels at the periphery of the nuclear pore rather than the axial NPC channel (Ma and Yang 2010). Other features should be implemented in order to better explain such observations. A recent reduction of dimension (ROD) model contends that FG-Nups are essentially saturated with NTFs and therefore a coherent FG Nup-NTF bilyer is coating the inner wall of the central channel (Peters 2009) (**Fig. 1.6 C**). The diameter of the middle free space of the central channel thus determines the size of molecules that can diffuse through. While in the case of facilitated transport, NTFs or NTF-containing transport complexes might interact with FG-Nups that already collapsed to the inner wall of the central tube, competing away cargo-free NTFs from their binding sites and finally walk through the channel. This periphery path has been described to be the preferred transport area in a recent single molecule study (Ma and Yang 2010). In contrast to phase selective and polymer brush model, increasing NTF concentration will collapse more FG-Nups and thus widen the inner tube of the central channel.

In the hydrodynamic study, Rexach and colleagues described two distinct conformations that can be adopted by FG-domains: a globular collapsed-coil

conformation and an extended-coil conformation (Yamada et al. 2010). As a result, FG-Nups can be divided into two groups: ‘shrubs’, those FG-Nups that are completely collapsed and anchored to the inner wall of the central channel; or ‘trees’, those FG-Nups that contain an attached extended-coil domain which supports a collapsed-coil domain (**Fig. 1.6 D**). Several collapsed-coil domains of trees converge at the center of the NPC, forming a tunnel transporter structure serving as a primary transport route (zone1). The space between ‘shrubs’ and ‘trees’ provides an alternative peripheral transport route (zone2). Transport through these two routes can then occur according to principles described above. Large cargos were postulated to be preferred substrate of zone1 while cargo-free NTFs or NTFs loaded with small cargos might preferentially translocate through zone2. The forest model combines features of previous described models, as the FG-domains in zone1 allow for sieving effects whereas the FG-domains in zone2 functioning as entropic brushes for virtual gating. However, to distinguish between the presented models, biophysical properties of FG-Nups *in situ* have to be further determined.

There still remains an unresolved issue: how do NPCs distinguish different cargos resulting in different transport capacities? As FG-Nups can be categorized into several classes, one explanation to the specificity of the NPC is that each class of FG-Nup recognizes only certain kinds of NTF-cargo complexes. Differential

expression among FG-Nups subclasses causes differences in transport capacities. Supporting evidence for this has been found from *in vivo* studies using target combination of different FG region deletions. Certain deletion combinations affect passage of one transport factor through the NPC without affecting another (Strawn et al. 2004). However, in the same study, the FG-regions of asymmetric Nups could be deleted without major effects on transport and viability. This redundancy among FG-Nups suggests that other players might be more crucial in determining specificity of the NPC. The discovery of the peripheral transport route in the NPC raises the possibility that non-FG Nups in the vicinity may regulate the transport specificity (Ma and Yang 2010). In fact, emerging evidence has supported this idea. Mice with the deletion of the non-FG nucleoporin, Nup133 or Nup155 developed distinct phenotypes, arguing for specific functions of these non-FG Nups (Lupu et al. 2008; Zhang et al. 2008).

1.2.3 Specific Functions of Nucleoporins

In addition to transport function, FG-Nups and non-FG Nups participate in several regulatory events that occur on either side of the nuclear envelope, such as releasing cargo from the NTF-cargo complex, directing cargo to the NPC, and modification of cargo for further processing. On the cytoplasmic side, yeast Nup159 (homologous to mammalian Nup214/CAN) and Nup42 (homologous to mammalian NupL2) on cytoplasmic filaments are engage in the dissociation of

mRNP-Mex62-Nab2 export complexes as they leave the NPC transport channel and enter the cytoplasm (Stewart 2007b). One critical factor in this process is the RNA helicase DEAD box protein Dbp5, whose function involves alteration of RNA structure and aiding the dissociation of RNA-binding proteins. To release Mex62 and Nab2 from mRNP, Dbp5 ATPase needs to be activated by Gle1 and its cofactor inositol hexkisphosphate (IP6). Structurally juxtaposed Nup159 and Nup42 interact with Dbp5 and Gle1, respectively, allowing for the activation of Dbp5. Activated Dbp5 then triggers the release of Mex62 and Nab2, which in turn terminates mRNP export and prepares the mRNA for translational initiation in the cytoplasm.

Nup358 also plays a role in the release of nuclear export cargo from exportins. The high affinity docking sites provided by Nup358 also promote the recruitment of import cargo to the NPC (Hutten et al. 2009). For example, the regulator of virion expression (Rev) protein of HIV-1 uses Nup358 for NPC docking. Additionally, Nup358 has a domain with small ubiquitin-related modifier (SUMO) ligase activity, capable of binding to the sumolylation cofactor enzyme Ubc9 to facilitate the addition of SUMO to nuclear transport cargoes, thus modifying their protein-protein interaction properties (Pichler et al. 2002;Reverter and Lima 2005). Nup358 also harbors a cyclophilin A homologous domain that might regulate 26S proteasome function (Yi, Friedman, and Ferreira 2007). Moreover, the N-terminal

domain of Nup358 binds to microtubules during interphase as well as kinetochores in mitosis, indicating its role in regulating microtubule assembly, stability and dynamics (Joseph et al. 2004;Joseph and Dasso 2008).

On the nuclear side of the NPC, fibrils emanating from the nuclear basket interconnect to form a meshwork, extending both in parallel and perpendicularly to the nuclear envelope plane. This basket-associated meshwork is involved in the post-transcriptional control of gene expression, the epigenetic control of gene expression as well as chromatin maintenance and repair. Before a mature mRNA reaches the cytoplasm through the NPC, its quality is controlled by several surveillance factors in the vicinity of the NPC, whose function can lead to the retention and subsequent degradation of aberrant mRNA. These factors, including Esc1, Pml1, Pml39, Swt1 and Nab2, have been either genetically or functionally linked to the basket, indicating a platform function of the basket meshwork in recruiting factors for post-transcriptional mRNA surveillance (Dziembowski et al. 2004; Galy et al. 2004; Lewis et al. 2007; Peters 2009).

The basket-associated protein network can also recruit active genes to the vicinity of the NPC and retain them for subsequent transcriptional reactivation. This phenomenon was described in studies of chromatin boundaries and the rapid reactivation of inducible yeast genes, such as INO1 and GAL1 (Brickner and

Walter 2004; Casolari 2005; Kundu et al. 2007; Schmid et al. 2006). The interaction of the NPC with the 3' untranslated region and promoter of specific genes allows the organization of an optimal microenvironment for the modulation of gene expression, which is dependent on the SWI-SNF complex and non-canonical histone variant H2A.Z. A subset of Nups, sec13 and Nup50, is capable of interacting with active gene loci in the nuclear interior, apart from the nuclear periphery and NPCs, and facilitate transcriptional activation during development and cell cycle progression (Capelson et al. 2010;Kalverda et al. 2010).

Nups also have a role in DNA repair and telomere integrity (Towbin, Meister, and Gasser 2009). Mutations of Mlp, the main molecular component of the basket, increase the occurrence of DNA damage and aberrations of telomere length. The NPC has been shown to physically associate with stalled DNA replication fork and several factors in SUMO-dependent DNA repair pathway (Therizols et al. 2006).

1.3 Crosstalk pathways that modulate Smad Signaling

Smad signaling is subject to additional regulation from other extracellular signals. The linker regions of R-Smads are phosphorylated by mitogen-activated protein kinases (MAPK), GSK3 kinase or cyclin-dependent kinases (CDK2/4/8/9).

Kretzschmar et al. (1997) first showed that Smad1 undergoes phosphorylation by MAPK in the central linker region in human tissue cultured cell lines (Kretzschmar, Doody, and Massague 1997). Such phosphorylations activated by Epidermal Growth Factor Receptor (EGFR) occur at four specific MAPK/Erk recognition consensus sites (PXS[PO3]P) within the linker region of Smad1. Smad1 linker phosphorylation, as opposed to the C-terminal phosphorylation of R-Smads, causes cytoplasmic localization of Smad1 and inhibition of Smad1 transcriptional activity. In addition, linker phosphorylation of Smad1 leads to Smad1 association with the E3 ubiquitin ligases Smurf1 or Nedd4L and subsequent proteasomal degradation of Smad1 in perinuclear centrosomes (Sapkota et al. 2007;Gao et al. 2009). In *Xenopus*, fibroblast growth factor 8 (FGF8) and insulin-like growth factor 2 (IGF2) induce phosphorylation of the linker region of Smad1 via mitogen-activated protein kinase (MAPK), ensuring the normal neural induction by inhibition of BMP signaling. Thus, FGF/IGF signaling provides negative feedback to BMP signaling in the developing nervous system. The regulatory cross-talk between the BMP and MAPK pathways was also demonstrated in knock-in mouse model. Knock-in mice were generated which contain Smad1 forms that lack all four MAPK phosphorylation sites. Embryonic fibroblasts from these knock-in mice were used for a BMP reporter assay. While FGF inhibited BMP signaling in Smad1 wildtype knock-in cells, FGF failed to inhibit BMP signaling in Smad1 linker phosphorylation-resistant

knock-in mutant mouse embryonic fibroblasts (Sapkota et al. 2007). MAPKs can also antagonize the growth inhibitory function of TGF-β in epithelial cells via linker phosphorylation of Smad2 and 3 (Kretzschmar et al. 1999).

Phosphorylation by MAPK has been shown not to be solely restricted to the linker domain. *Drosophila* MAD is phosphorylated by a MAPK-related kinase called Nlk (Nemo-like kinase) (Zeng et al. 2007). Nlk, an enzyme known to be involved in the Wingless/Wnt pathway, phosphorylates MAD at a conserved serine residue in its MH1 DNA binding domain. This phosphorylation inhibits Dpp/BMP signaling by preventing nuclear accumulation of C-terminal phosphorylated MAD, thus inhibiting the activation of Dpp/BMP-responsive genes.

The Wnt pathway component GSK3 also phosphorylates R-Smads in the linker region. GSK3 phosphorylation requires a phosphorylated Ser/Thr residue located four amino acids downstream (S/TXXXS/T[PO3]). In Smad1, GSK3 phosphorylation can be primed by phosphorylation of the MAPK sites. Linker phosphorylation by GSK3 negatively regualtes BMP signal transduction because mutation of the GSK3 sites into Alanines resulted in strongly ventralized phenotypes (high BMP signaling) in injected Xenopus embryos (Fuentealba et al. 2007). Wnt signaling induces GSK3 degradation, leading to decreased Smad1 linker phosphorylation by GSK3. Therefore, at high Wnt levels the BMP signal is

of longer duration. GSK3 also directly phosphorylates basal state Smad3 in its MH1 domain in mammalian cells and target basal state Smad3 to ubiquitylation and proteasomal degradation, providing inhibitory controls of TGF-β signaling (Guo et al. 2008).

As demonstrated in pulse-chase experiment, C-terminal phosphorylation of Smad1 driven by BMP precedes linker phosphorylations by MAPK and GSK3 (Fuentealba et al. 2007). Thus, the MAPK/GSK3-mediated phosphorylations provide a negative feedback for TGF-β and BMP signaling by regulating the protein level of Smads. However, recent research suggested that linker phosphorylation could enhance Smad signaling before terminating the signal by Smad turnover (Alarcón et al. 2009). In this study, CDK8/9 phosphorylate activated Smads in their linker regions and promote Smad interaction with the transcription factor YAP, resulting an enhanced Smad target gene expression while ultimately this linker phosphorylation event leads to eventual degradation of activated Smad proteins. These findings seem paradoxical in terms of integrating both activation and inhibition functions in the same phosphorylation event. The following study from the same group revealed a mechanism that switches Smad proteins from binding transcriptional cofactors to binding ubiquitin ligases (Aragon et al. 2011). In the BMP pahway, Smad1 linker phosphorylation by CDK8/9 induces the binding to YAP but also primes subsequent phosphorylation

by GSK3, which in turn switches Smad1 binding from YAP to the ubiquitin ligase Smurf1. Similarly in the TGF-β pathway, Smad3 phosphorylation by CDK8/9 enables enhanced transcriptional activity through Pin1 binding while this phosphorylation also primes subsequent phosphorylation by GSK3 and thus binding to ubiquitin ligase Nedd4L. This swich mechanism allows efficient regulation of TGF-β signaling by coupling TGF-β signal delivery to turnover of the signal transducer, Smad proteins.

Thesis Objective

Signal-induced nuclear translocation of activated Smad is essential for the TGF-β signaling. The mechanisms by which activated Smads are imported across nuclear membrane into the nucleus are not fully understood. So far, most studies employed *in vitro* reconstituted nuclear import assay to investigate nuclear import of Smads. However, conclusions from such assay are limited when apply to phosphorylated Smads in intact cells. These observations led to the **major aim of my thesis: to obtain a systemic overview of the molecules that are involved in transporting activated Smad from cell surface to the nucleus.**

To achieve this aim, I performed a gemone-wide RNAi screen in *Drosophila* to comprehensively identify molecules that mediate nuclear import of activated Smad in intact cells. Specifically, I pursued the following:

Aim 1: To identify and characterize the importin for nuclear import of activated Smad

Aim2: To identify and characterize the nucleoporins for nuclear import of activated Smad

These two aims covered two critical elements in nuclear import, the transport receptors (importins) and the nuclear pore complex. Overall, this thesis was to increase our comprehension of the molecular mechanism of nuclear translocation of activated Smad in TGF-β signaling.

Fig 1.1

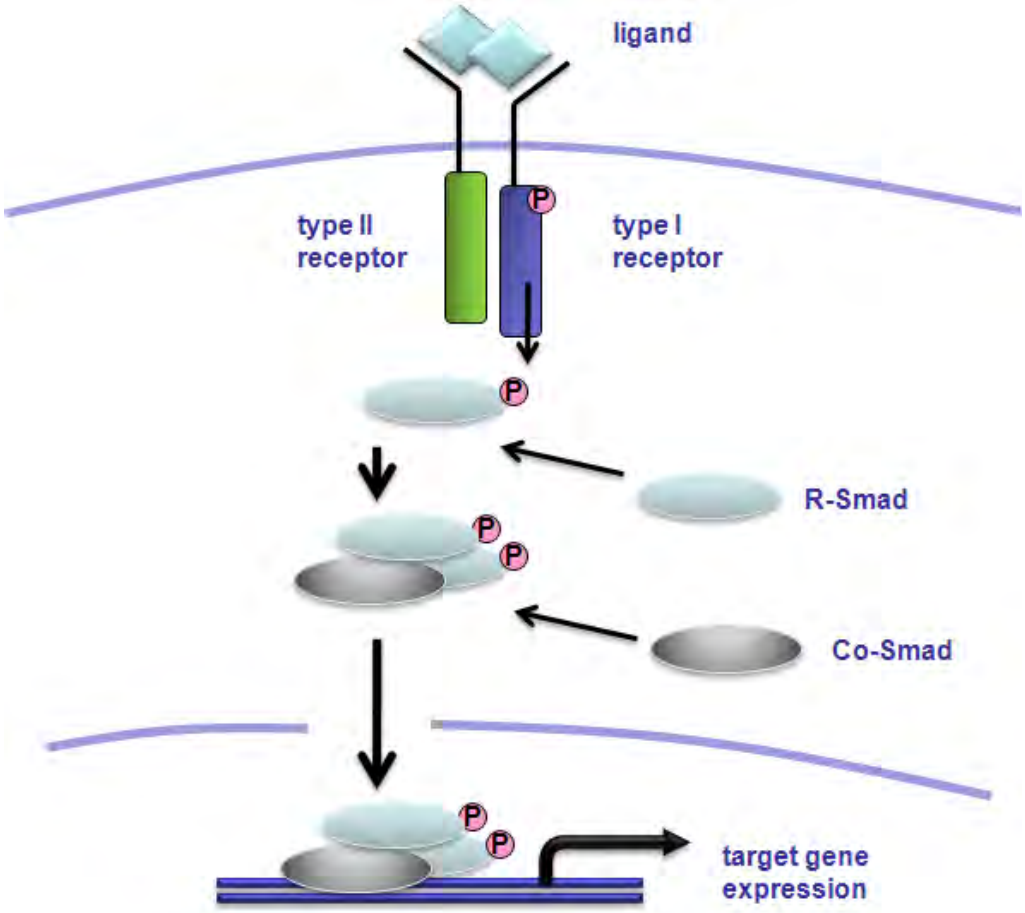

TGFβ pathways in mammals and Drosophila						
		H.sapiens			*D. melanogaster*	
Pathway		BMP	TGFβ		BMP	Activin
Ligand		BMP2,4	TGFβ1		Dpp	dActivin
		BMP5,6,7	TGFβ2		Gbb	Daw
		BMP8A,8B	TGFβ3		Scw	
		BMP9				
RII		BMPRII	TβRII		Put	Put
		ActRIIA ActRIIB			Wit	Wit
RI		ALK2	TβRI (ALK5)		Tkv	Babo
		ALK1	ALK1		Sax	
		BMPRIA(ALK3)	ALK2			
		BMPRIB(ALK6)	BMPRIA (ALK3)			
R-Smad		SMAD1,5,8	SMAD2,3		MAD	dSmad2
Co-Smad		SMAD4	SMAD4		Medea	Medea
I-Smad		SMAD6,7	SMAD7		Dad	?

Fig. 1.1 TGF-β and BMP signaling in mammals and *Drosophila* (A) Components of the TGF-β pathway. (B) Comparison of TGF-β pathway components in mammals and *Drosophila*.

Fig 1.2 The family of Smad proteins

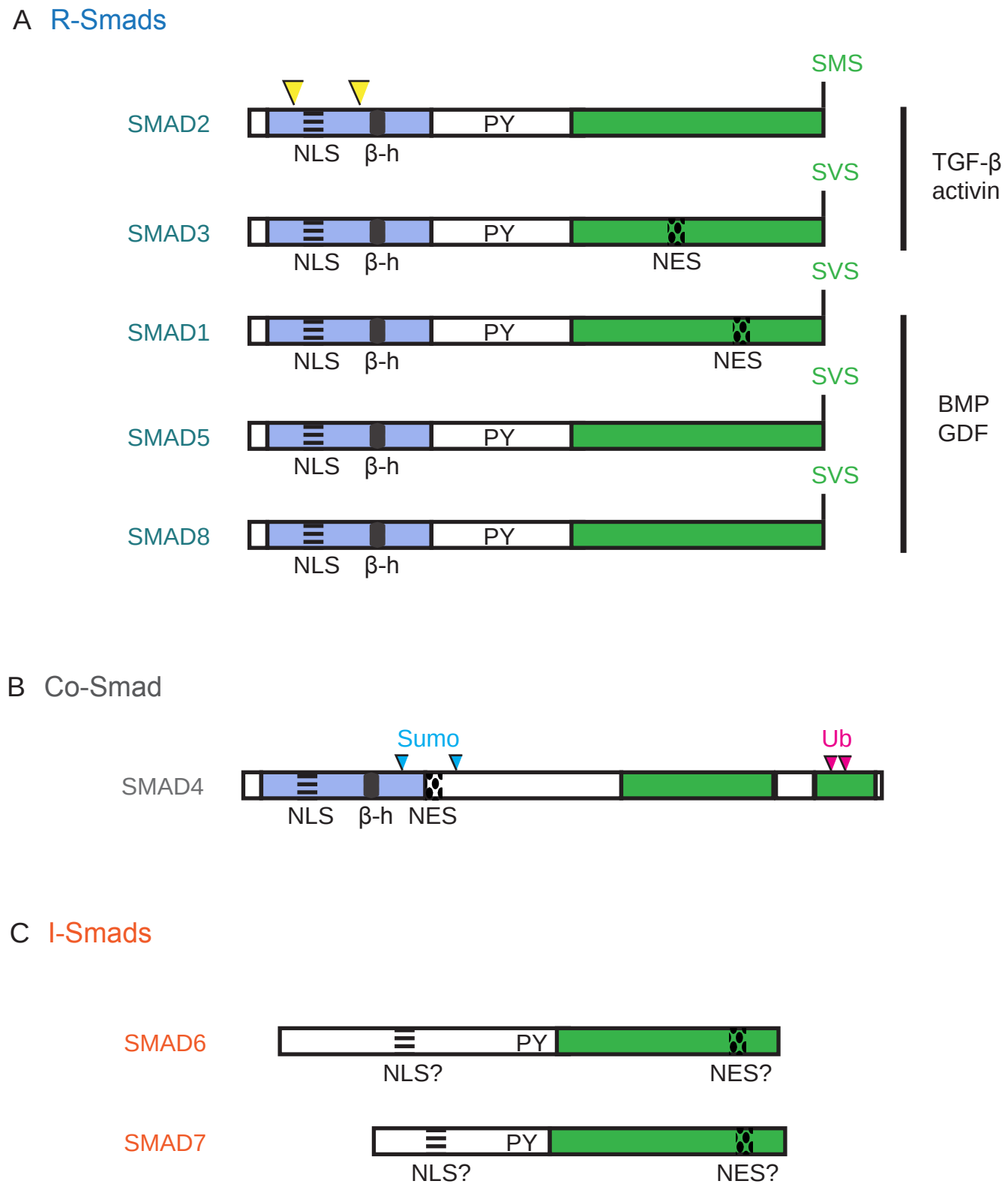

Fig. 1.2 The family of Smad proteins. Schemetic drawing of the eight human Smad proteins classified into (A) Receptor-activated Smads (R-Smads); (B) common-mediator Smad (Co-Smad); and (C) inhibitory Smads (I-Smads). The conserved N-terminal MAD-homology 1 (MH1) (blue) and C-terminal MH2 (green) domains are shown. SMS or SVS: the C-terminal serines that are phosphorylated by the type I receptor kinases; NLS: nuclear localization signal (striped box); the two unique inserts in SMAD2 (yellow triangles); β-h: the β-hairpin domain that binds to DNA (black box); PY: the proline-tyrosine motif in the linker domain that is recognized by the WW domain of Smurf family proteins; NES: the nuclear export signal (dotted box); Sumo: Sumoylation (blue arrows); Ub: ubiquitylation (pink arrows).

Fig 1.3 Regulation of TGF-β-induced nuclear accumulation of Smads

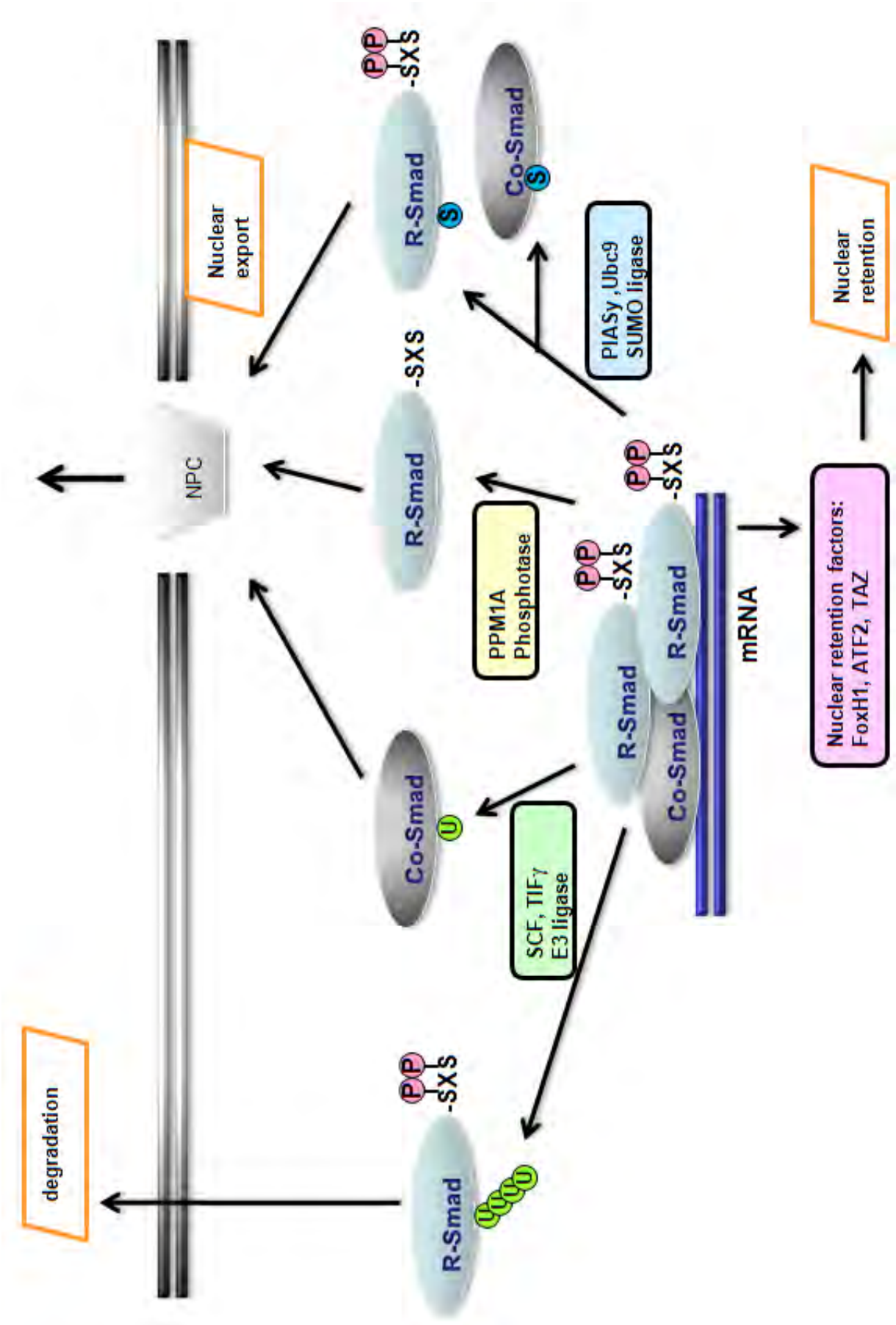

Fig. 1.3 Regulation of TGF-β-induced nuclear accumulation of Smads. Smad protein complex dissociates and R-Smads are de-phosphorylated by nuclear phosphatases (like PPM1A) and exported into the cytosol. SUMO ligases (PIAS and Ubc9) sumoylate (**S**) Smad3 and Smad4, promoting their nuclear export. Nuclear Smad4 can also be mono-ubiquitinated (**U**) by an E3 ligase TIF1γ leading to its enhanced nuclear export and reduced affinity to R-Smads. SCF/Roc1 target receptor-phosphorylated R-Smads for ubiquitylation (U), resulting in nuclear export followed by degradation. Above are all negative regulations of TGF-β signaling. Nuclear retention factors, such as FoxH1, ATF2 and TAZ, sequester Smads in the nucleus and thus positively regulate TGF-β signaling.

Fig 1.4 NPC structure

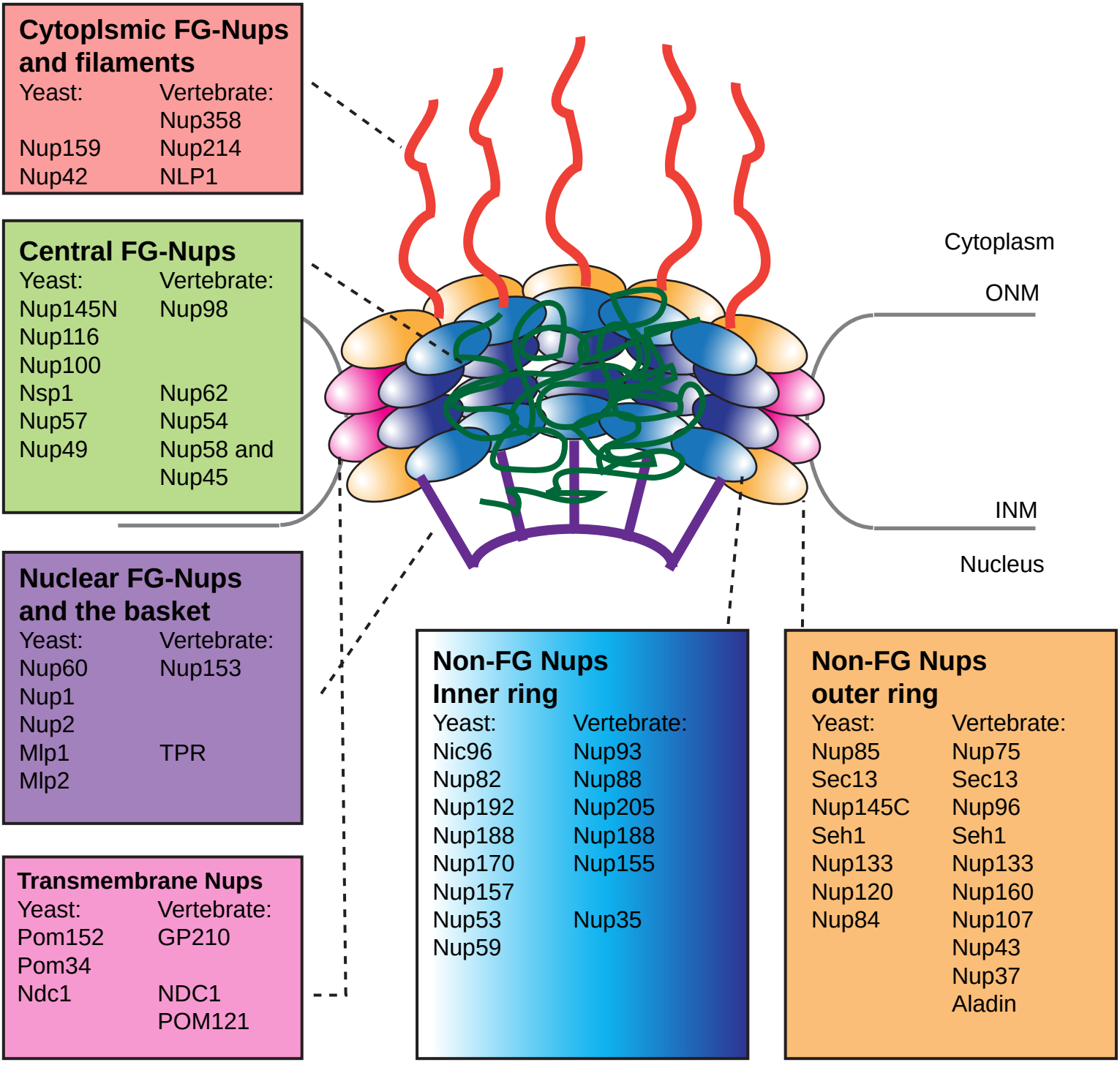

Fig. 1.4 Structure of Nuclear Pore Complexes. Each nuclear pore complex (NPC) is a cylindrical structure comprised of eight spokes surrounding a central tube that connects the nucleoplasm and cytoplasm. NPC-associated peripheral structures consist of cytoplasmic filaments, the basket and a distal ring. The NPC components called nucleoporins can be grouped into transmembrane Nups, Phe-Gly (FG) Nups and non-FG Nups.FG Nups line and fill the central tube. The NPC is anchored to the nuclear envelope by transmembrane nucleoporins (Nup) that connect to inner rings and outer rings formed by Non-FG Nups. The Nups that are known to constitute each NPC substructure are listed, with yeast and vertebrate homologues indicated. Both inner and outer ring Nups form biochemically stable NPC subcomplexes. The inner rings consist of the Nup170 subcomplexes. The outer rings consist of the Nup84 subcomplexes (yeast) or the Nup107-160 subcomplexes (vertebrate). GP210, glycoprotein 210; Mlp, myosin-like protein; Ndc1, nuclear division cycle protein 1; Nic96, Nup-interacting component of 76 kDa; NLP1, Nup-like protein 1; Pom, pore membrane protein; Seh1, SEC13 homologue 1; TPR, translocated promoter region.

Fig 1.5 Different models of NPC

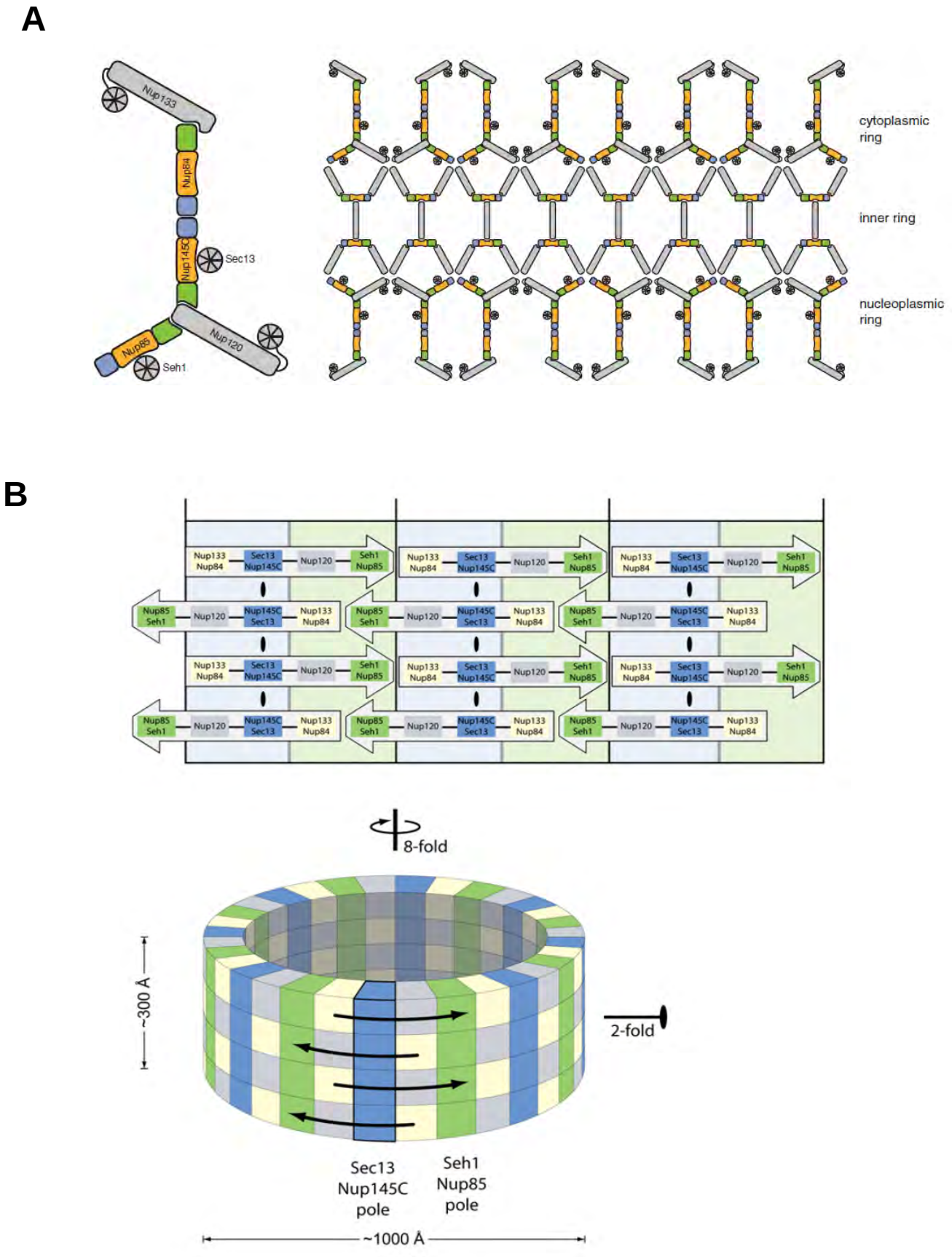

Fig. 1.5 Different models of NPC (A) The **l**attice model for the Nup84 complex and the structural scaffold of the NPC. The entire scaffold (eight spokes) is illustrated unwrapped and laid flat in two dimensions. The Nup84 complex comprises the nuclear and cytoplasmic rings, whereas the Nic96-containing complex makes up the inner ring. The relative position and interactions between the seven proteins in the Nup84 complex are shown with Sec13, Seh1, Nup133, and Nup120 colored in gray. The remainder of the Nic96 complex (Nup157/170, Nup188, and Nup192) is illustrated in gray. (Figures from Brohawn et al. 2008) (B) Eight heptamers are circumferentially arranged in a head-to-tail fashion in four stacked rings. The Sec13-Nup145C and Seh1-Nup85 hetero-octamers serve as vertical poles connecting the four rings, thereby forming a scaffold. The poles are connected through their interaction with the remaining nups of the heptameric complex. Based on the two-fold axes of symmetry in the Sec13-Nup145C hetero-octamer, the heptameric complex rings are stacked with opposite directionality.(Figures from Hsia et al. 2007)

Fig 1.6 Nuclear Transport models

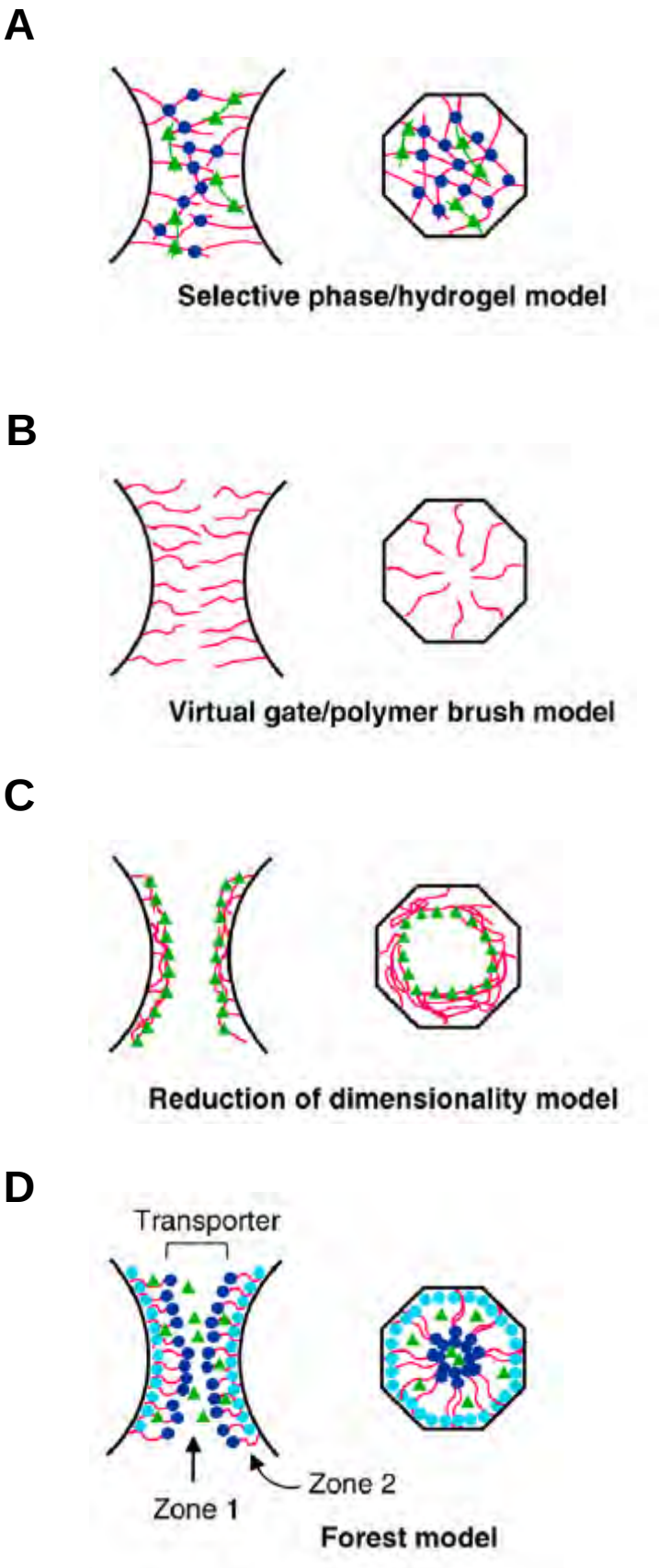

Fig. 1.6 N uclear transport models. (A) The selective phase/hydrogel model (Frey and Görlich 2009). FG-nucleoporins (pink) form a sieve-like structure that functions as a physical permeability barrier. FG–FG contacts (blue dots) form the meshes of the sieve. Transport receptors (green triangles) can bind to FG domains and partition into the barrier. Having multiple FG-binding sites, transport receptors might also add extra meshes to the sieve, increasing the permeability barrier. (B) The virtual gate/polymer brush models (Rout 2003; Lim et al. 2006). Largely non-cohesive FG-Nups arrange as 'repulsive bristles' or 'polymer brushes' (pink) forming an entropic barrier to repel large molecules. A transient passage through the meshwork is created when FG-Nups are bound by NTFs. (C) The reduction of dimensionality model (Peters 2009). Transport receptors (green) coat interact with FG-Nups to form a coherent FG Nup-NTF bilayer coating the wall of the transport channel. Passive diffusion of small molecules can occur through the inner tube of the channel. Transport complexes move by a random, two-dimensional walk on the inner wall of the channel. (D) The forest model (Yamada et al. 2010). FG-Nups that adapt a completely collapsed conformation are designated as shrubs (light blue dots). FG-Nups that contain FG-regions in both collapsed (dark blue dots) and extended-coil conformation (pink lines) are designated as trees. Together, these two groups of FG-Nups form a forest-like landscape. The globular domains of trees (dark blue dots) form the transporter in the middle of the channel, harboring transport zone 1. The peripheral zone 2

locates at the extended-coil regions of trees (pink lines). Transport receptors (green) can pass through zone 1 or 2, depending, for example, on the size of the transport complex. From (A-D) both side views (left) and top views (right) of the NPC are shown. (Figures from Wälde & Kehlenbach 2010).

CHAPTER II: MSK IS THE IMPORTIN FOR NUCLEAR IMPORT OF TGF-β/BMP-ACTIVATED SMADS

Disclaimer: The following chapter is a collaborative effort. Experiments for Figure 1 (A and C panel), 3 (C, D and E panel), 4 (in collaboration with Yao, X.), and table 2.1 were done by the author. Experiments for the remaining figures were done by Yao, X. (Figure 1B, 2, 3A and B).

Summary:

Cytoplasm-to-nucleus translocation of Smad is a fundamental step in transforming growth factor β (TGF-β) signal transduction. Using nuclear accumulation of the *Drosophila* Smad Mother against Decapentaplegic (MAD) as the readout, I carried out a whole-genome RNAi screen in *Drosophila* cells. The screen identified Moleskin (Msk) as a required factor for the nuclear import of dpp-activated MAD. Msk genetically and biochemically interacted with dpp signaling components. Biochemical interaction studies further confirmed that Smads are bona fide cargos of Imp7 and Imp8, the mammalian orthologues of Msk. Both MH1 and linker regions of Smad3 are required for the Smad interaction with Imp7/8. Moreover, such interaction was regulated by GTP-bound Ran, a hallmark that a substrate was the direct cargo of the importins.

Introduction:

Nuclear translocation of Smad proteins is a critical step in signal transduction of TGF-β cytokines. However, little is known regarding the molecular mechanism responsible for nuclear transloction of Smads, especially the activated Smads. Previous studies on this subject used mostly *in vitro* methods, including reconsitituted nuclear import assay which suggested either an importin-independent or importin β-mediated mechanism for nuclear import of Smads. Such conclusions are limited in answering whether phosphorylated Smads depend on the same mechanisms to enter the nucleus in an intact cell.

The development of RNAi techonology allows us to study gene functions in intact cells. Recently, a dsRNA library targeting the entire annotated *Drosophila* genome became available. Moreover, critical components of Decapentaplegic (Dpp; *Drosophila* BMP) signaling have been well characterized in *Drosophila* tissue culture cells. Therefore, it is feasible to perform a whole-genome RNAi screen in *Drosophila* tissue culture cells to genetically dissect the Dpp pathway and investigating molecular requirements for nuclear targeting of Smads upon stimulation.

Here, in a genome-wide RNAi screen, I identified Moleskin (Msk) as a required component in nuclear import of Dpp-activated Mad. Msk is a member of

importin-β superfamily of nuclear importers that can directly interact with NPC and the small GTPase Ran (Görlich et al. 1997). Genetic experiments with *Drosophila* embryos demonstrate that Msk is largely responsible for the nuclear import of activated ERK (Lorenzen et al. 2001). Msk has two orthologues in mammals, Imp7 and Imp8. Based on *in vitro* assays Imp7 has been suggested to import ribosomal proteins, histone H1, HIV reverse transcription complexes and glucocorticoid receptor into the nucleus (Jäkel et al. 1999a; Fassati et al. 2003; Freedman & Yamamoto 2004). Imp8 was recently shown to support nuclear import of the signal recognition particle 19 (SRP19) protein *in vitro* (Dean et al. 2001). However, it is unclear whether in intact cells Imp7 or 8 are required for nuclear import of these cargos.

Results:

Whole-genome RNAi screening identified molecular requirements for nuclear accumulation of activated MAD

I used nuclear translocation of MAD as the readout in our RNAi screen because this is an early event in Dpp signaling. Using a *Drosophila* S2R+ cell line inducibly coexpressing GFP-MAD and the receptor kinases Punt and Tkv, I established a robust assay to recapitulate phosphorylation/activation-dependent nuclear accumulation of MAD (**Fig 2.1.A**). When GFP-MAD was conditionally expressed in S2R+ cells, it was detected diffusively throughout the cell (**Fig**

2.1.A). In contrast, when the Dpp receptor kinases Punt and Thickvein (Tkv) were coexpressed, which caused MAD phosphorylation, the bulk of GFP-MAD became predominantly localized to the nucleus 1 hour after CuSO4 induction (**Fig. 2.1.A**). With this cell line (MAD+R), I performed an RNAi screening in which the cells were treated with a library of ~21,300 dsRNAs individually, which was pre-dispensed into 62 of 384-well screen plates, targeting over 95% of the annotated *Drosophila* genome (Perrimon and Mathey-Prevot 2006). dsRNAs against the GFP and the Punt/Tkv receptors combination were used as negative and positive controls. The subcellular location of GFP-MAD was recorded by high-throughput automated confocal microscopy. From each screen plate, top 20 candidates were selected based on the nuclear/cytoplasmic signal ratio measured using computer algorithms, followed by visual inspections to produce a list of primary hits. Among the primary hits (see **Appendix**), Msk was uncovered as a top one that was required in MAD nuclear translocation (**Fig. 2.1.C**). The block of MAD nuclear translocation was not due to off-target effects of the dsRNA as the same result were observed when we designed and tested a second non-overlapping dsRNA against *msk*. In contrast to RNAi against Punt and Tkv, RNAi of *msk* did not affect C-terminal phosphorylation of MAD (**Fig. 2.1.B**), suggesting that Msk functions downstream of MAD phosphorylation, perhaps in transporting MAD into the nucleus.

Since the screen was performed using a S2R+ cell line over-expressing exogenous GFP-MAD, it would be necessary to determine whether endogenous MAD nuclear import is regulated by Msk in the same manner. Dpp treatment of *Drosophila* S2 cells resulted in exclusive nuclear distribution of phosphorylated MAD, as revealed by immunofluorescent staining using a phospho-MAD-specific antibody PS1 (**Fig. 2.2.A**). Depletion of Msk by RNAi clearly inhibited nuclear concentration of phospho-MAD, while not affecting the level of phosphorylation of MAD at the carboxy-terminus.

Msk has been previously suggested to cooperate with the *Drosophila* importin β homologue Ketel in nuclear import of dERK, as mutations in either Msk or Ketel inhibited nuclear accumulation of dERK (Lorenzen et al. 2001). Moreover, the mammalian orthologs of Msk have been shown to associate with and function in conjunction with importin β (Görlich et al. 1997). Therefore we wanted to test whether Ketel might also be involved in nuclear translocation of MAD. After the depletion of Ketel by RNAi, endogenous phosphor-MAD was still detected predominantly in the nucleus, even the RNAi of Ketel resulted in reduced phosphorylation of endogenous MAD through an unknown mechanism. The nuclear to cytoplasmic ratio of phosphor-MAD signal intensity confirmed that RNAi against Ketel did not affect nuclear accumulation of phosphor-MAD (**Fig. 2.2.A**). Consistent with such finding, Western blot analysis of cytoplasmic and

nuclear fractions of S2 cells shown that depletion of Msk, but not Ketel, resulted in reduced amount of phosphor-MAD in the nuclear fraction and enhanced amount of phosphor-MAD in the cytoplasmic fraction (**Fig. 2.2.B**). The RNAi against Ketel effectively impaired nuclear import of classic NLS-fused GFP, the well known substrate of Ketel, while depletion of Msk had no effect (**Fig. 2.2.E**). From these results, we can conclude that the nuclear import of Dpp-activated MAD is independent of the importin β homologue Ketel.

In both S2R+ and S2 cells, treatment with Dpp results in transcriptional activation of *dad* (daughters against decapentaplegic), a known Smad target gene in mammalian cells as well (Nakao et al. 1996; Tsuneizumi et al. 1997). When Msk was depleted by RNAi, the Dpp-induced increase in dad expression was completely abolished (**Fig. 2.2.C**). The blocking effect of *msk* RNAi on *dad* expression was as strong as that caused by punt/tkv RNAi (**Fig. 2.2.C**). Thus, as expected for a factor mediating nuclear import of MAD, Msk is critical for MAD-mediated transcriptional output of Dpp.

Physical Interaction between Msk and MAD

To address the question if Msk is directly involved in transporting phospho-MAD into the nucleus, we tested interaction between endogenous Msk and Flag-tagged MAD. Indeed, endogenous Msk was co-immunoprecipitated with Flag-MAD in

S2 cell extract (**Fig. 2.2.D**). Under our experimental conditions, both basal state and phosphorylated MAD displayed comparable affinity with Msk (**Fig. 2.2.D**). This suggests that binding of Msk is not unique to phospho-MAD and Msk alone may not account for why only phospho-MAD accumulate in the nucleus. Therefore while Msk is crucial for phospho-MAD to enter the nucleus, additional factors are involved to retain only phospho-MAD in the nucleus.

A *msk* mutant allele genetically interacted with the dpp^{hr4} mutant allele

In a forward deficiency screen, the *Drosophila* chromosomal deficiency of region 66B-66C was found to genetically interact with *dpp* mutant alleles (Nicholls and Gelbart 1998). At the early embryonic stage, Dpp signaling activity specifies the dorsal-ventral patterning. While *dpp* expression is strictly zygotic at this stage, other factors in the Dpp dorsal-ventral patterning pathway are expressed maternally. The screen used the mutant dpp^{hr4} allele, a recessive embryonic lethal allele which provided barely sufficient *dpp* function for the flies to survive (Raftery et al. 1995) and was therefore very sensitive to levels of the maternal factors that affected *dpp* activity. The screen was designed to identify the deficiencies that reduced *dpp* function by depleting a maternally provided factor required for the *dpp* dorsal-ventral patterning pathway. When such a deficiency mutation was placed in combination with the dpp^{hr4} mutation, lethality occurred. The screen identified two novel deficiency regions, 54F-55A and 66B-66C, that

are required for *dpp* function but the genes were never identified (Nicholls and Gelbart 1998). Interestingly, *msk* maps to the 66B-66C region. Therefore I decided to test the genetic interaction between *msk* and dpp^{hr4} allele. I performed a similar experiment in which I crossed +/+; msk^{5}/$TM3^{sb}$ females to dpp^{hr4}/CyO; +/+ males. The maternal msk^{5} mutation allele substantially reduced the number of dpp^{hr4} progeny relative to their dpp^{wt} siblings in such a cross (33 progeny vs 463 progeny, **Table 2.1**). Note that there was a reduction in both classes of dpp^{hr4} mutant progeny (dpp^{hr4}/+; $TM3^{sb}$/+ and dpp^{hr4}/+; msk^{5}/+), indicating that it was not the msk^{5} in the progeny (progeny allele) but rather the msk^{5} in parental female flies (maternal allele) that caused the reduction. This result suggested that msk^{5} acted maternally to reduce *dpp* function in these heterozygous progeny.

Smads are direct nuclear transport substrates of Imp7 and Imp8

Msk closely relates to verterbrate orthologues Importin 7 and 8, each sharing over 50% identity in amino acid sequences with Msk. Imp7 and Imp8 (~60% identical between the two) belong to the family of Ran-binding proteins which share little sequence similarity but a common ability to bind the small GTPase Ran.

We investigated Smads interactions with Imp7 and 8 by coimmunoprecipitation experiments. Flag-tagged Smad1 or Smad2 were overexpressed in 293T cells and immunoprecipitated with anti-Flag antibody. In both cases, HA-tagged Imp7 or

Imp8 coimmunoprecipitated with either Smad1 or Smad2 (**Fig. 2.3.A and B**). Constitutively active BMP receptor (ALK3-QD) or TGF-β receptor kinase (ALK5-TD) was cotransfected to induce C-terminal phosphorylation of Smad1 and Smad2, respectively. Such phosphorylation of Smads did not affect their interaction with Imp7 or 8 (**Fig. 2.3.A and B**). Because phosphorylated Smad1, 2, and 3 readily assemble into complexes, our results suggest that monomeric and multimeric forms of Smads have similar interactions with Imp7 or 8 (Wu et al. 2001;Chacko et al. 2004).

For detailed analysis of Smad-Imp7/8 interaction, we focused on Smad3. We produced GST-fusions of the MH1, MH2, and linker plus MH2 domains of Smad3 in *Escherichia coli* and tested their ability to pull down endogenous Imp7 and 8 in HeLa cells. When comparable amount of GST fusion proteins were used, both the MH1 (aa 1–155) and the linker plus MH2 (aa 146–425) domains were able to bind endogenous Imp7/8, with the MH1 domain exhibiting stronger interaction (**Fig. 2.3.C**). The same assay barely detected any interaction between the Smad3 MH2 (aa 231–425) domain and Imp7/8 (**Fig. 2.3.C**). Therefore, interaction with Imp7/8 appears to involve multiple interfaces in the MH1 and linker regions of Smad3. The MH1 domains of Smad2 (aa 1–185) and Smad3 are highly similar except for two insertions in Smad2 that prevent Smad2 from binding to DNA (Zawel et al. 1998). But apparently such differences did not affect Smad2 binding to Imp7/8

through the MH1 domain (**Fig. 2.3.C**). Bacterially produced GST-Imp8 was able to pull down purified recombinant Smad1 or Smad3, suggesting that Imp8 could directly interact with Smad1 or Smad3 (**Fig. 2.3.D**)

One characteristic among importins is that the interaction with their cargos is regulated by Ran in its GTP-bound form (Gorlich et al. 1996; Mattaj and Englmeier 1998). To test if this is true between Smad3 and Imp8, we first pulled down HA-Imp8 using GST fusion of full-length Smad3. After washing off the unbound proteins, the constitutive active mutant RanQ69L-GTP or BSA was added to the GST beads for further incubation (**Fig. 2.3.E**). Indeed we found that compared to the BSA control, RanQ69L-GTP caused more release of Imp8 into the supernatant and correspondingly resulted in a decrease of Imp8 remaining bound to GST-Smad3 on the beads (**Fig. 2.3.E**). This suggested that association of Smad3 with Imp8 was disrupted upon binding of Ran-GTP, supporting the notion that Smad3 is a nuclear import cargo of Imp8.

A Lys-rich motif required for Imp8-mediated nuclear import of Smad3

In unstimulated cells, Smad4 mostly resided in the cytoplasm, presumably because the CRM-1 mediated nuclear export of Smad4 dominated over the Imp8 mediated nuclear import of Smad4. When export is inhibited by blocking the exportin CRM-1 by Leptomycin B (LMB) or import is enhanced by

overexpressing the importin Imp8, Smad4 became predominately nuclear without TGF-β signaling (Pierreux, Nicolas, and Hill 2000; Yao et al. 2008). A Lys-rich motif KKLK in MH1 domain of Smad4 has been identified as a required element for Smad4 nuclear accumulation in LMB treatment as well as Imp8 overexpression assays. Because R-Smads and Smad4 have highly homologous MH1 domains, including the KKLK motif at relatively the same positions (**Fig 2.4.A**), it is interesting to determine whether the KKLK motif also plays a role in R-Smads nuclear import. Similar to Smad4, changing the KKLK sequence to AALA in Smad3 also prevented Imp8 from importing this mutant Smad3 into the nucleus (**Fig 2.4.B**). Although the KKLK motif also presents in Smad2, overexpression of Imp8 has little effect in mediating nuclear import of Smad2 at the basal state, indicating that there are additional structural requirements in Smads that enable nuclear import via Imp8 and such structural elements are probably not present in Smad2. These results suggest that the KKLK motif is required but not sufficient for nuclear import of Smads.

Materials and methods

Plasmids

GFP-MAD, FLAG-MAD were cloned into pSH vector under the control of a metallothionein promoter that responses to $CuSO_4$ induction. Punt and Tkv were cloned into pMK33 vector also with a metallothionein promoter for expression in

Drosophila S2 and S2R+ cells. FLAG-tagged Smad1, Smad2 and Smad3, HA-Imp7, HA-Imp8, ALK3-QD, ALK5-TD were cloned into pCDNA3.1 vector for expression in HEK293T and HeLa cells while full-length Smad1, Smad2, Smad3, Smad3 deletions MH1, Imp8 were cloned into pGEX4T1 vector for cellular expression in *E. coli*. The constitutive active GTPase RanQ69L was cloned into pET32a for cellular expression in *E. coli*. FLAG-tagged mutant Smad3 3KA (^{40}KKLK to ^{40}AALA) was generated by PCR-based site directed mutagenesis.

Whole-genome RNAi screening

The dsRNA library targeting the whole *Drosophila* genome and the format for screening have been described previously (Armknecht et al. 2005). dsRNAs were deposited in 384-well plates, and in each plate one well is reserved for gfp dsRNA (negative control) and one for combined punt and tkv dsRNA (positive control). 10^4 S2R+ cells in 10 μl serum-free media were seeded in each well and incubated for 1 h, after which 30 μl of serum-containing media was added. After incubation for 3 d, the cells were induced with 0.5 mM $CuSO_4$ for 3 h followed by fixation with 4% paraformaldehyde in PBS (10 min) Automated microscopy was performed using the Opera system, the confocal microplate imaging reader system (Evo Techonology). The wells containing selected hits were reported to the *Drosophila* RNAi Screening Center (DRSC) at Harvard Medical School, which in

turn revealed the identities of the dsRNAs contained in those wells. The complete dataset including strong and weak hits in the screen is listing in the **Appendix**.

Cell culture, transfection, and immunofluorescent staining

Drosophila S2 and S2R+ cells were cultured in Schneider medium with 10% fetal bovine serum (Invitrogen) and transfected with Effectene (QIAGEN). HeLa and 293T cells were cultured in DME with 10% fetal bovine serum and transfected with Lipofectamine 2000 (Invitrogen). Cells with or without treatment (1 nM Dpp, 100 pM TGF-β, or 100 ng/ml BMP2 as indicated; all from R&D Systems) were processed for immunofluorescence staining as described previously (Xu et al., 2002). PS1 was a gift from P. ten Dijke (Leids University, Netherlands). Alexa 488– or Alexa 633–conjugated anti–rabbit secondary antibodies (Invitrogen) were used as indicated, and cells were mounted in Vectorshield (Vector Laboratories). Immunofluorescence microscopy and image acquisition were done with an inverted microscope (20×/0.45, 40×/0.6, 60×/1.40; Eclipse TE2000-S; Nikon) and digital camera (SPOT RT-KE; Diagnostic Instruments, Inc.) using vendor-provided software. For confocal microscopy, a DMIRE2 inverted microscope and the TCS scanning system from Leica were used. The images were captured with lasers at: UV (DAPI), 488 nm (Alexa 488 or GFP), and 633 nm (Alexa 633) wavelengths at room temperature using vendor-provided software. 20×/0.70, 40×/(1.25–0.75), and 63×/1.40 oil immersion objectives were used for

low and high magnification images. Final figures were assembled using Adobe Photoshop. For quantitation purposes, confocal sections with the strongest signal were selected, and the staining intensity in the nucleus and cytoplasm was measured using NIH ImageJ. Only cells with unsaturated signals were chosen for such analysis.

RNAi in Drosophila cells

General procedures for generating dsRNA and RNAi in *Drosophila* S2 and S2R+ cells were as described previously (Clemens et al. 2000). Two amplicons corresponding to different coding regions of *msk*, DRSC11340 and DRSC23929, were used to generate nonoverlapping dsRNA targeting *msk*. Amplicons DRSC17039, DRSC00861 and DRSC03328 were used to generate the long dsRNAs against *punt*, *tkv* and *ketel* respectively. Sequence information for the long dsRNA amplicons can be found at the DRSC website (http://www.flyrnai.org).

S2 cell fractionation

S2 cells were suspended in 20 mM Hepes, pH 7.6, 5 mM MgCl2, 10 mM KCl, 1 mM EGTA, 1 mM EDTA, 250 mM sucrose, and 0.025% digitonin (EMD Biosciences). Cells were passed through 18 ½ G syringes three times and incubated on ice for 5 min. The homogenate was centrifuged at 800 g for 10 min.

The supernatant was collected as the cytoplasmic fraction. The pellet was further extracted with 20 mM TrisCl, pH 7.5, 250 mM NaCl, and 0.5% NP-40 to yield the nuclear fraction.

Fly strains and crosses

The *Drosophila* lines dpp^{hr4}/CyO and msk^{5}/$TM3^{Sb}$ were from Dr. Stuart Newfeld. Male flies with genotype dpp^{hr4}/CyO; +/+ were cross with female flies with genotype +/+; msk^{5}/$TM3^{Sb}$. All progenies were collected and sorted into four groups according to the phenotypes: with or without curly wings (the CyO phenotype) in combination of with or without stubbly hairs (the TM3 phenotype). The number of flies in each group was compared to the total number of flies to calculate the percentage.

Protein–protein interaction assay

For coimmunoprecipitation experiments, *Drosophila* or 293T cells were lysed in 20 mM Tris Cl, pH 7.4, 200 mM NaCl, 5 mM Mg2Cl, 20 mM NaF, 20 mM $Na_4P_2O_7$, 2 0 mM β-glycerolphosphate, 0.5% NP-40, and 2 mM DTT supplemented with protease inhibitors. Cell extracts were incubated with anti-Flag conjugated to agarose beads (Sigma-Aldrich) at 4°C for 4–16 h, followed by 3× wash in the lysis buffer before immunoblotting. Anti-Msk was a gift from L.

Perkins (Harvard Medical School, Boston, MA). For GST pull-down experiments, HeLa or 293T cells were lysed as above and incubated with 10 μg purified GST fusion protein on glutathione beads at 4°C for 4–16 h. The beads were then washed 3× in the lysis buffer. For RanQ69L-GTP elution, GTP-loaded His-RanQ69L or BSA as the control (both at 0.4 μg/μl) were added to the washed beads and further incubated at room temperature for 45 min. At indicated time points, an aliquot of the supernatant was taken for immunoblotting. At the end point, the beads were washed once in the lysis buffer and the bound proteins were analyzed by anti-HA or anti-Imp7 (Imgenex). Full-length human Imp8, Smad1, and Smad3 were produced in E. coli and purified as GST fusions. GST-Smad1 (a gift from F. Liu, Rutgers University, NJ) and GST-Smad3 were digested with thrombin to remove the GST moiety (Novagen). 10 μg of GST-Imp8 on beads was incubated with Smad1 or Smad3 (0.5–1 μg/μl) at 4℃ with rotation for 4 h. The buffer contained 20 mM TrisCl, pH 7.5, 200 mM NaCl, 0.05% NP-40, 5% glycerol, and PMSF. The beads were washed 3× in the same buffer and the bound proteins were analyzed by immunoblotting.

Quantitative real-time RT PCR

Total RNA was isolated by RNasy spin columns (Qiagen) and was reverse transcribed using the iScript cDNA synthesis kit (Bio-Rad). Real-time PCR was conducted using the iQ SYBR green kit (Bio-Rad). The mRNA level of *dad* was

measured as well as the ribosomal protein *rp49*, which was used as the internal standard for quantification.

Forward primer for *dad*: GAAGCGACTGCCCACTTG;

Reverse primer for *dad*: CGGTGTTGGGGATTCTGT;

Forward primer for *rp49*: CGGATCGATATGCTAAGCTGT;

Reverse primer for *rp49*: GCGCTTGTTCGATCCGTA;

Fig 2.1

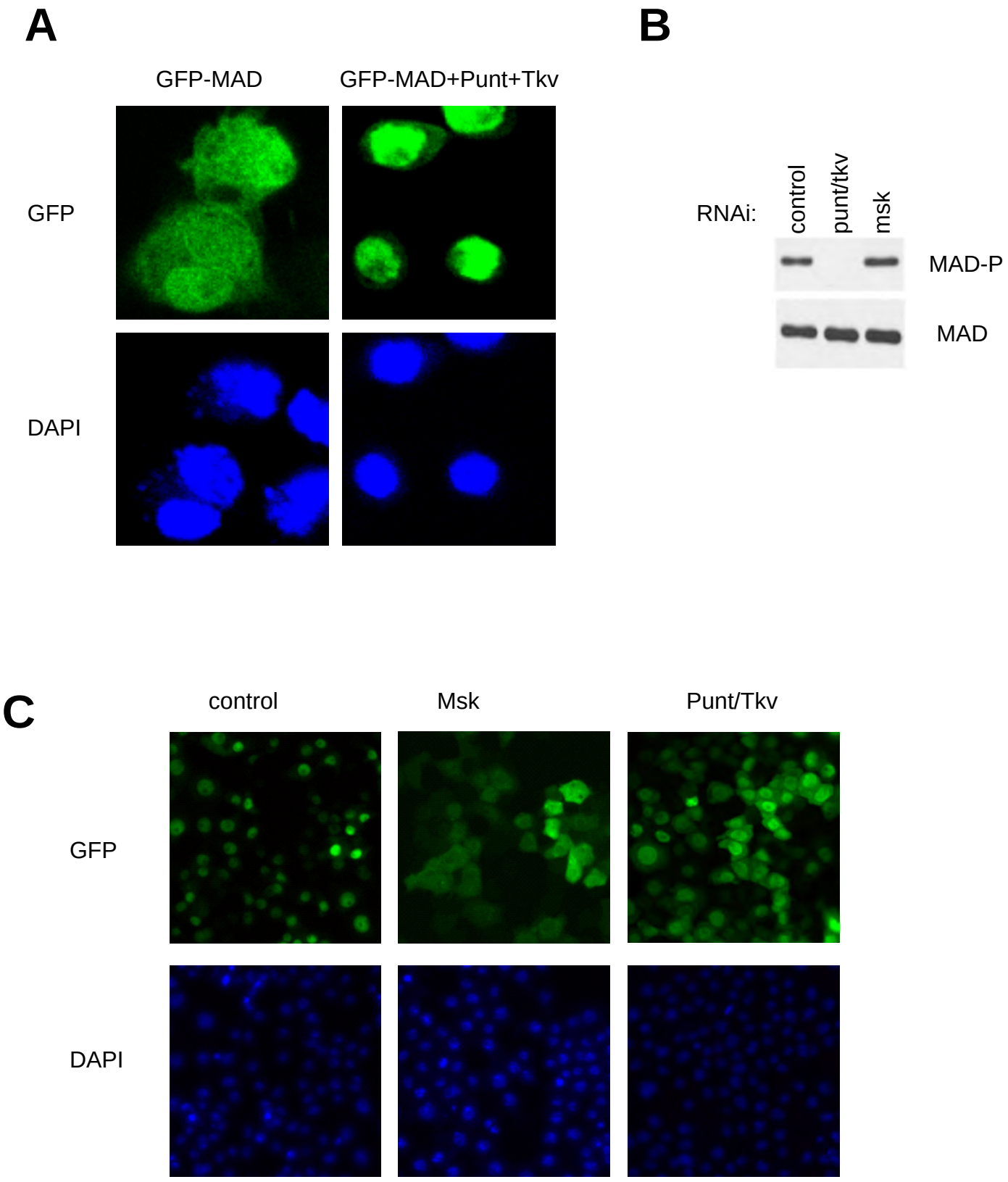
A
GFP-MAD
GFP-MAD+Punt+Tkv
GFP
DAPI
B
RNAi:
control
punt/tkv
msk
MAD-P
MAD
C
control
Msk
Punt/Tkv
GFP
DAPI

Fig 2.1 Whole-genome RNAi screening in S2R+ cells uncovered new components in the Dpp–MAD pathway. (A) Phosphorylation-dependent nuclear accumulation of GFP-MAD. S2R+ cells stably transfected with plasmids for GFP-MAD only, or GFP-MAD with receptors punt and tkv were induced to express these proteins with $CuSO_4$ for 1h. The nuclei were marked with DAPI. (B) In S2R+ cells induced to express GFP-MAD and Punt/Tkv, RNAi targeting either punt plus tkv or msk (with dsRNA different from that in A) blocked nuclear concentration of GFP-MAD. The cells and experimental procedure were as in A. (C) Same RNAi experiment as in B, and proteins were extracted from the cells and analyzed by immunoblotting with antibodies against phospho-MAD (MAD-P) or GFP.

Fig 2.2

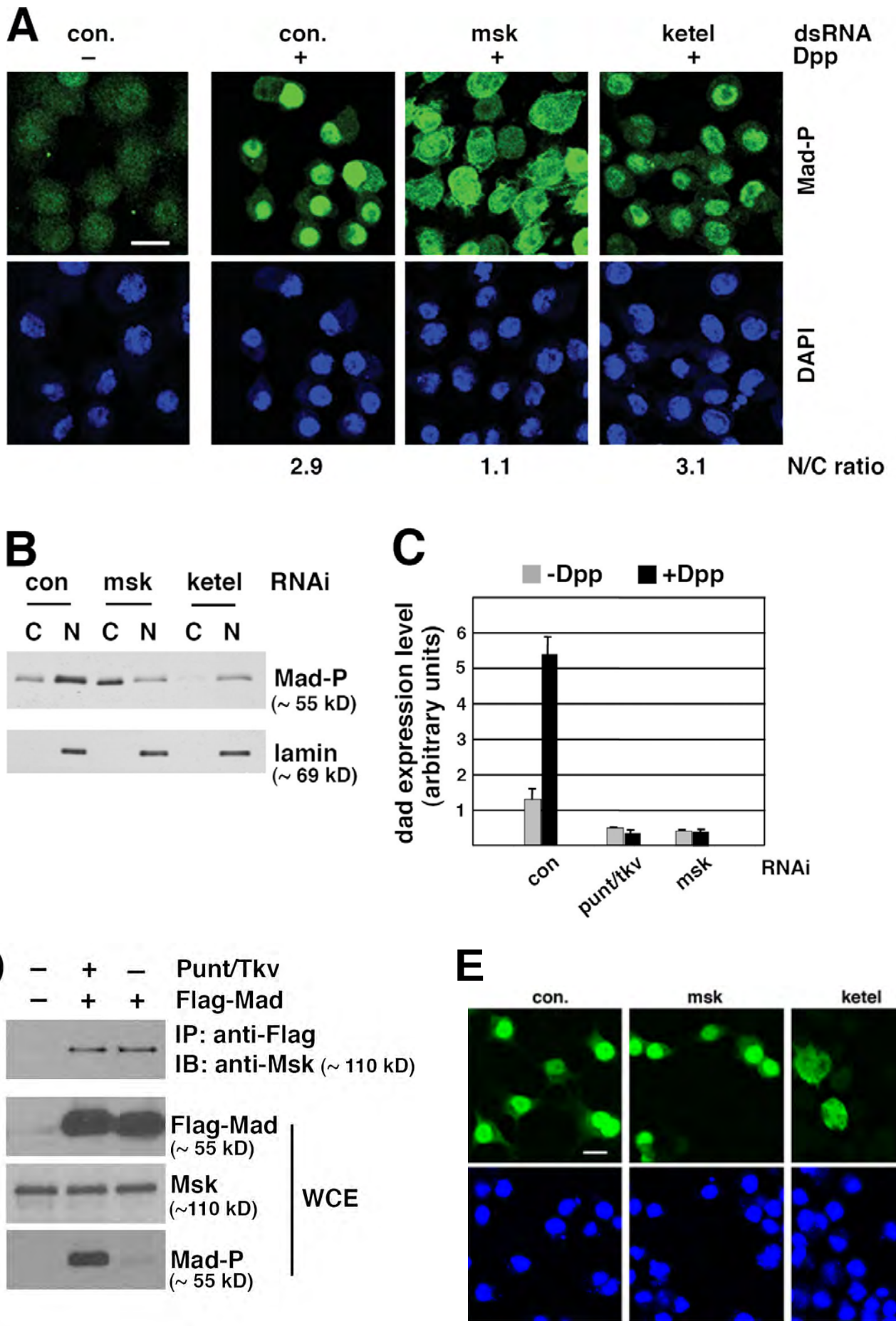
A
con.
–
con.
+
msk
+
ketel
+
dsRNA
Dpp
Mad-P
DAPI
2.9
1.1
3.1
N/C ratio
B
con
msk
ketel
RNAi
C N C N C N
Mad-P
(~ 55 kD)
lamin
(~ 69 kD)
C
-Dpp
+Dpp
dad expression level
(arbitrary units)
1
2
3
4
5
6
con
punt/tkv
msk
RNAi
D
– + –
Punt/Tkv
– + +
Flag-Mad
IP: anti-Flag
IB: anti-Msk (~ 110 kD)
Flag-Mad
(~ 55 kD)
Msk
(~110 kD)
Mad-P
(~ 55 kD)
WCE
E
con.
msk
ketel
RNAi
cNLS-GFP
DAPI

Fig 2.2 Msk is required for nuclear accumulation of endogenous MAD in Dpp-treated *Drosophila* S2 cells and co-immunoprecipitated with MAD. (A) S2 cells were treated with indicated dsRNA and then subject to Dpp stimulation (1 nM for 1 h). Distribution of phospho-MAD (MAD-P) was detected by immunofluorescence staining using the PS1 antibody. The phospho-MAD signal per unit area in the nucleus and cytoplasm was measured using NIH ImageJ, and the nucleus/cytoplasm (N/C) ratios are shown (>50 cells were counted per sample). Bar, 10 μm. (B) S2 cells treated with indicated dsRNA were stimulated with Dpp as in A. Subcellular fractions were prepared and examined for phospho-MAD (MAD-P) and lamin levels (C: cytoplasm; N: nucleus). (C) S2R+cells were subject to indicated RNAi. The cells were then stimulated with Dpp (1 nM) for 2 h and the mRNA level of dad was measured by real-time RT-PCR. The expression level of Rp49 was used as the internal standard for quantitation. The plotted data are derived from multiple experiments. Error bars indicate SD. (D) Co-immunoprecipitation of endogenous Msk with Flag-MAD. Whole-cell extract (WCE) was prepared from S2 cells transfected with Flag-MAD and Punt/Tkv as indicated and subject to immunoprecipitation using anti-Flag antibody conjugated to agarose beads. The bound proteins as well as input extract were analyzed by immunoblotting with indicated antibodies. (E) Expression vector encoding two copies of GFP fused to a cNLS (cNLS-GFP) was transfected into Drosophila S2R+ cells. After indicated RNAi, cNLS-GFP was expressed by $CuSO_4$ induction.

Table 2.1

- dpp^{hr4}/Cyo (male) × msk^{5}/ $TM3^{sb}$ (female)

Progeny Genotype	Number	Percentage
Cyo; msk^{5}	253	51.0%
Cyo; $TM3^{sb}$	210	42.3%
dpp^{hr4}; msk^{5}	25	5.0%
dpp^{hr4}; $TM3^{sb}$	8	1.6%
	496	

Table 2.1 *msk* genetically interacts with *dpp*. Male flies with genotype dpp_{hr4}/CyO; +/+ were cross with female flies with genotype +/+; msk_{5}/$TM3_{sb}$. All progenies were collected and sorted into four groups according to the phenotypes: with or without curly wings (the CyO phenotype) in combination of with or without stubbly hairs (the TM3 phenotype). The number of flies in each group was compared to the total number of flies to calculate the percentage.

Fig 2.3

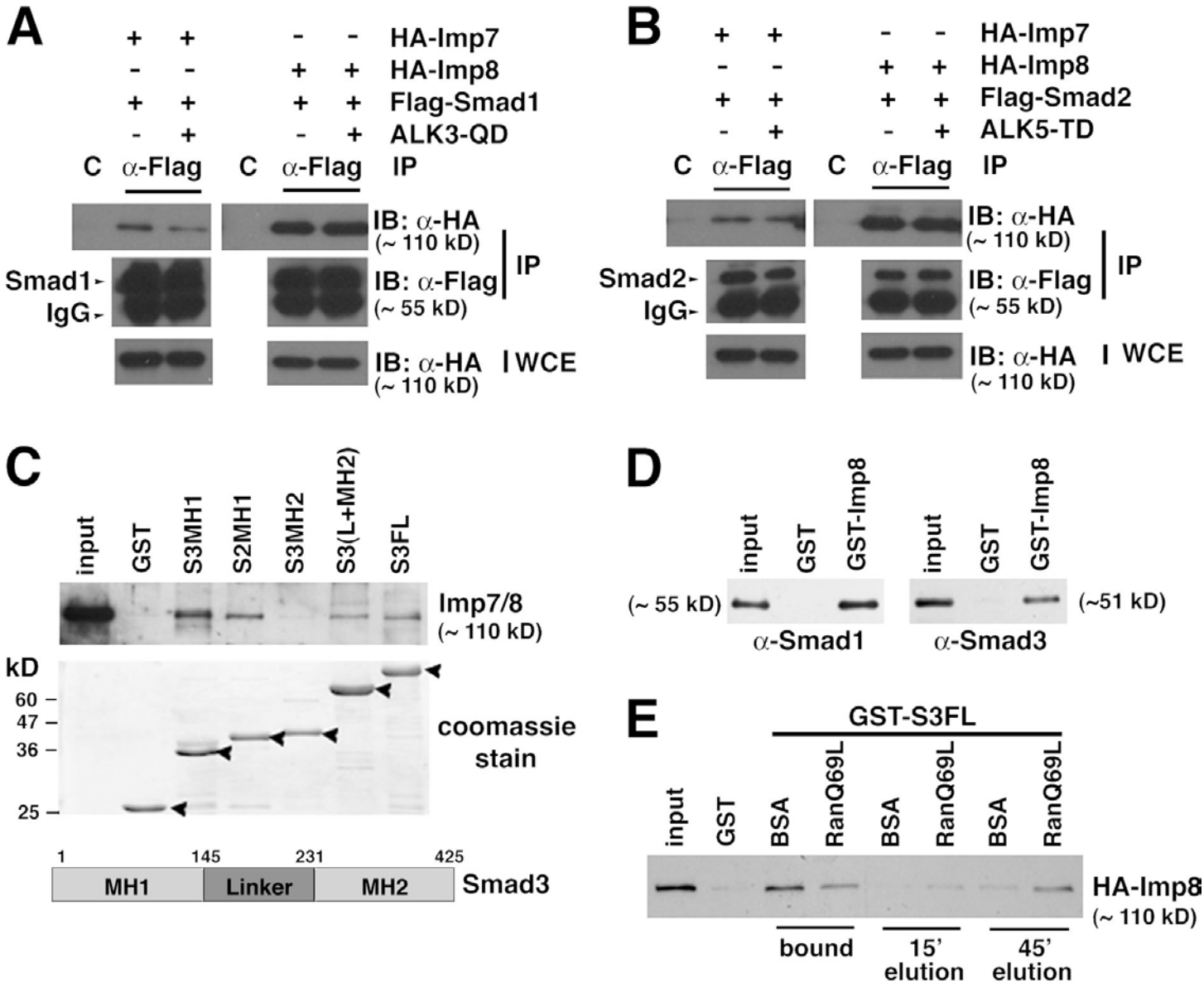
A
HA-Imp7
HA-Imp8
Flag-Smad1
ALK3-QD
C
α-Flag
IP
IB: α-HA
(~ 110 kD)
Smad1
IgG
IB: α-Flag
(~ 55 kD)
IP
IB: α-HA
WCE
B
HA-Imp7
HA-Imp8
Flag-Smad2
ALK5-TD
Smad2
C
D
input
GST
GST-Imp8
(~ 55 kD)
α-Smad1
α-Smad3
(~51 kD)
E
GST-S3FL
BSA
RanQ69L
bound
15' elution
45' elution
HA-Imp8
(~ 110 kD)
input
GST
S3MH1
S2MH1
S3MH2
S3(L+MH2)
S3FL
Imp7/8
(~ 110 kD)
kD
60
47
36
25
coomassie stain
1
145
231
425
MH1
Linker
MH2
Smad3

Fig 2.3 Interaction of Smads with Imp7 and Imp8, and the regulation by Ran-GTP. (A) Co-immunoprecipitation of Smad1 with Imp7 and Imp8. 293T cells were transfected with indicated expression plasmids and the whole-cell extract (WCE) was immunoprecipitated with anti-Flag antibody. Protein A/G bead was used as the control (c). The bound proteins and the input extract (WCE) were analyzed by immunoblotting as indicated. (B) Co-immunoprecipitation of Smad2 with Imp7 and Imp8. Same experimental design as in A, but with different expression plasmids transfected as indicated. (C) Mapping of Smad3 domains involved in interaction with Imp7/8. Recombinant GST fusions of indicated Smad3 or Smad2 fragments were used to pull down endogenous Imp7/8 in HeLa cells. The bound proteins were analyzed by an antibody that recognized both Imp7 and 8. Comparable amount of GST proteins was used in the pull down as judged by the Coomassie stain intensity. The arrowheads mark GST fusion proteins on the SDS-PAGE gel. S3MH1: aa 1–155;S2MH1: aa 1–185; S3MH2: aa 231–425; S3(L+MH2): aa 145–425; S3FL: full-length. Schematic drawing of Smad3 is also shown. (D) Purified GSTImp8 on glutathione beads was used to pull down purified recombinant Smad1 and Smad3. The bound proteins were examined by immunoblotting using indicated antibodies. GST was used as the control. (E) Ran-GTP interrupts association between Smad3 and Imp8. GST-fusion of full-length Smad3 (GSTS3FL) was used in a pull-down experiment as in C. The bound proteins were further incubated with RanQ69L-GTP or BSA, and proteins

released into the supernatant were collected and analyzed at indicated time points (15 min and 45 min elution). At the 45-min time point, the beads were washed again and proteins remaining bound to GST-S3FL (bound) were also examined by anti-HA immunoblotting.

Fig 2.4

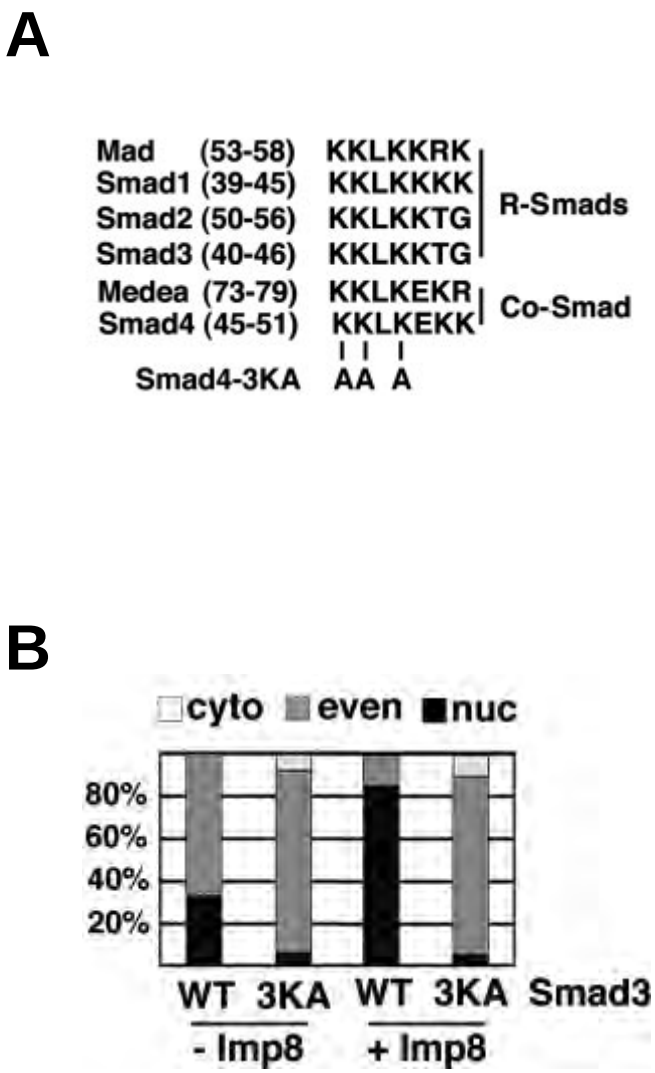
A
Mad (53-58) KKLKKRK
Smad1 (39-45) KKLKKKK
Smad2 (50-56) KKLKKTG
Smad3 (40-46) KKLKKTG
R-Smads
Medea (73-79) KKLKEKR
Smad4 (45-51) KKLKEKK
Co-Smad
Smad4-3KA AA A
B
cyto even nuc
80%
60%
40%
20%
WT 3KA WT 3KA Smad3
- Imp8
+ Imp8

Fig 2.4 The KKLK motif is required for Importin 8-mediated nuclear import of Smad3 (A) alignment of the KKLK motifs in Smads, and the 3KA mutations. (B) FLAG-tagged wild type or 3KA mutant Smad3 (^{40}KKLK to ^{40}AALA) was transfected into HeLa cells with or without Imp8. Cells were stained with anti-FLAG, and the percentages of cells exhibiting different staining patterns are shown (n>200).

CHAPTER III SPECIFIC NUCLEOPORIN REQUIREMENT FOR SMAD NUCLEAR TRANSLOCATION

Summary:

Here I identify a subset of nucleoporins that, in conjunction with Msk (*Drosophila* Imp7/8), specifically mediate activation-induced nuclear translocation of MAD (*Drosophila* Smad1) but not the constitutive import of proteins harboring a classic nuclear localization signal (cNLS) or the spontaneous nuclear import of Medea (*Drosophila* Smad4). Surprisingly, many of these nucleoporins, including Sec13, Nup75, Nup93, and Nup205, are scaffold nucleoporins considered important for the overall integrity of the nuclear pore complex (NPC) but not known to have cargo-specific functions. I demonstrate that the roles of these nucleoporins in supporting Smad nuclear import are separate from their previously assigned functions in NPC assembly. Furthermore, I uncovered novel pathway-specific functions of Sec13 and Nup93; both Sec13 and Nup93 are able to preferentially interact with the phosphorylated/activated form of MAD, and Nup93 acts to recruit the importin Msk to the nuclear periphery. These findings, together with the observation that Sec13 and Nup93 could interact directly with Msk, suggest their direct involvement in the nuclear import of MAD. Thus, I have delineated the nucleoporin requirement of MAD nuclear import, reflecting a unique trans-NPC mechanism.

Introduction:

Two critical elements in nuclear import are the transport receptors and the NPC. In the previous chapter, I described Msk (*Drosophila* Imp7/8) as the importin for Dpp activated MAD, but how the Msk-MAD complex translocates through the NPC has yet to be elucidated. How importins and the NPC function in a concerted manner in nuclear import is still highly debatable. Importins are capable of direct interaction with FG-nucleoporins, and this provides the foundation for current models of nuclear import (Radu et al., 1995; Pemberton and Paschal 2005; Terry et al., 2007). However, whether non-FG nucleoporins participate directly in the nuclear translocation process remained unknown.

Emerging evidence suggests specificity in NPC function. Genetic studies of yeast revealed redundancy among FG-nucleoporins but also showed that a subset of FG-nucleoporins are differentially employed by different importins (Strawn et al. 2004; Terry and Wente 2007). Mice with a deletion in the non-FG nucleoporin gene nup133 or nup155 developed distinct phenotypes affecting specific cell lineages, arguing for specific functions of these scaffold nucleoporins, although it is unclear whether the phenotypes were due to defects in the nuclear transport of particular cargoes or to something else (Lupu et al. 2008; Zhang et al. 2008).

In this chapter, I will characterize the nucleoporin requirements for Smad nuclear

translocation which were revealed in the same RNAi screen of the *Drosophila* gemone that uncovered importin Msk.

Results:

Identification of nucleoporins required for Msk-mediated nuclear import of MAD. Besides Msk, I further evaluated all the other potential hits from the RNAi screening by testing two non-overlapping dsRNAs to eliminate false-positive hits due to off-target RNAi. Among the confirmed hits were nucleoporins Nup75, Nup93, Sec13, Nup205, and Nup50 (**Fig. 3.1.A and B**). Moreover, the deficiency in MAD nuclear import caused by *sec13* or *nup93* RNAi was fully rescued by *sec13* or *nup93* cDNA, respectively, further confirming the specificity of our RNAi experiments (**Fig. 3.1.C**). As controls, we determined that RNAi of these nucleoporins did not affect the phosphorylation of MAD, which is a prerequisite for MAD nuclear import, or the expression level of Msk, so the decreased concentration of MAD in the nucleus was directly due to impaired nuclear import (**Fig. 3.1.D and E**). Sec13 is also a component of the COPII coat, but knockdown of other key players in COPII coat assembly, such as the GTPase Sar-1, did not affect the nuclear import of MAD, arguing that vesicle transport in general is not a requirement for the nuclear targeting of MAD (Haucke 2003) .

Nup75 and Sec13 are part of the vertebrate Nup107-160 subcomplex in the NPC

(Siniossoglou et al. 2000; Allen 2001; Lutzmann 2004), whereas Nup93 and Nup205 are components of the Nup53-93 complex (part of the Nup170 complex) (Lusk et al. 2002) (**Fig. 1.4**); both subcomplexes are evolutionarily conserved and are believed to serve general structural roles in NPC assembly (Siniossoglou et al. 2000;Walther et al. 2003). Thus, the requirement for these non-FG nucleoporins in the nuclear transport of a particular cargo is intriguing. We therefore focused on Sec13 and Nup93 as representatives for further analyses. Available antibodies could barely detect endogenous MAD in S2 or S2R+ cells in immunofluorescence experiments. Fortuitously, in an S2 cell line transfected with MAD driven by an inducible metallothionein promoter (Bunch, Grinblat, and Goldstein 1988), without induction, the leaky expression of MAD was sufficient for a phospho-Smad-specific antibody to detect a predominantly nuclear signal only in cells treated with Dpp (a *Drosophila* TGF-β family cytokine) (**Fig. 3.2**). In this setting, where there is only limited overexpression of MAD, knockdown of *sec13*, *nup93*, and *nup75* also significantly reduced nuclear versus cytoplasmic concentrations of phospho-MAD (**Fig. 3.2**, right). These data further support important roles for Sec13, Nup93, and Nup75 in MAD nuclear import in response to Dpp stimulation.

The dependence on Sec13 and Nup93 for MAD nuclear import raised the question of whether these nucleoporins function in concert with Msk or whether they

represent a separate mechanism. We previously found that overexpression of Msk could force the nuclear accumulation of MAD without the need for Dpp activation (Yao et al. 2008). Since such nuclear import is entirely Msk driven, we could directly test the nucleoporin requirement for Msk. RNAi against *sec13, nup93,* or *Nup75* inhibited the Msk-driven nuclear import of MAD (**Fig. 3.3**; see quantification on the right). Therefore, these non-FG nucleoporins are likely part of the same pathway as Msk, which imports MAD into the nucleus.

Sec13/Nup75/Nup93 are specifically utilized for the nuclear import of MAD. One important question is whether Sec13, Nup93, and Nup75 are uniquely required for MAD or are rather broadly involved in the nuclear import of many cargos. We tested the nuclear import of cNLS-GFP (two copies of GFP fused to a classic NLS). As expected, the nuclear import of cNLS-GFP was critically dependent on Impβ (Ketel in *Drosophila*) (Fig. **3.4.**A; see Fig. **3.4.B** for quantification). Depletion of Sec13, Nup93, or Nup75 had no effect on the nuclear localization of cNLS-GFP, while, in contrast, it strongly impaired the nuclear import of MAD (Fig. **3.4.A**; see Fig. **3.4.B** for quantification). The same conclusion was reached when we examined a cell line coexpressing GFP-MAD, Punt/Tkv, and RFP-cNLS so that we could monitor the localizations of GFP-MAD and RFP-cNLS concurrently (**Fig 3.5**). In contrast, knockdown of *nup54* (an FG-nucleoporin) significantly reduced the nuclear import of cNLS-GFP, as

previously reported, but had no adverse effect on the nuclear accumulation of MAD (Fig. **3A and B**) (Sabri et al. 2007). These observations are not likely due to differences in RNAi efficiency, since quantitative real-time PCR confirmed that knockdowns of *sec13*, *nup75*, *nup93*, and *nup54* were equally efficient in the two cell lines expressing GFP-MAD/Punt/Tkv (GFP-MAD+R) or cNLS-GFP (**Fig 3.4.D**). More interestingly, when GFP-MAD was fused to a cNLS, it became constitutively nuclear and was completely independent of Sec13, Nup93, or Nup75 for nuclear import but instead relied on Nup54 and Impβ (Fig. **3.4.A**;see Fig. **3.4.C** for quantification). Again, RNAi efficiencies in cells expressing cNLS-GFP-MAD or GFP-MAD+R were comparable (**Fig 3.4.E**). Thus, the cNLS was sufficient to switch MAD to a completely different route across the NPC. cNLS-cargoes are imported by Impα/Impβ independently of Msk/Imp7/8; thus, our results suggest that importins may dictate which nucleoporins to engage, and their modes of translocation through the NPC are likely different (Adam & Gerace 1991; Gorlich et al. 1994)

We further investigated the nucleoporin requirement of Medea, the *Drosophila* ortholog of Smad4, whose nuclear import is independent of either Msk or Impβ (Yao et al. 2008). Medea spontaneously undergoes nuclear accumulation upon inhibition of CRM-1 by Leptomycin B (LMB), without the need for Dpp stimulation (**Fig. 3.6.A**). RNAi of *sec13*, *nup75*, *nup93*,

or *nup54* had little effect on LMB-induced nuclear translocation of Medea (**Fig. 3.6.A**; see quantification on the right). Real-time PCR showed similar or more efficient knockdown of these nucleoporins in the FLAG-Medea-expressing cell line than in the GFP-MAD+R line (**Fig. 3.6.B**). Thus, the nucleoporin requirement for the basal-state Medea nuclear import is different from that for either MAD or cNLS-cargoes. Therefore, the results from three types of cargos strongly suggest that different import pathways utilize different sets of nucleoporins and that non-FG nucleoporins, such as Sec13, Nup93, and Nup75, are specific for Msk-mediated nuclear import.

Physical interactions of non-FG nucleoporins with MAD. In coimmunoprecipitation experiments, we readily detected an interaction of MAD with Sec13 in S2 cells (**Fig. 3.7.A**). More importantly, when the TGF-β receptor kinases Punt and Tkv were cotransfected to induce MAD phosphorylation, the binding of MAD to Sec13 was markedly enhanced (**Fig. 3.7.A**). Earlier studies of live cells indicated that TGF-β treatment accelerates the rate of Smad nuclear import, yet we previously found that the interaction between the transport factor Msk/Imp7/8 and Smads was rather constitutive (Schmierer et al. 2008; Xu et al. 2007). Our observations here thus suggest that perhaps association with Sec13 is a rate-limiting step favoring the translocation of activated/phosphorylated MAD into the nucleus. To further test whether a Sec13-MAD interaction could be detected

with endogenous proteins, we used anti-MAD and anti-Sec13 antibodies but found that neither could immunoprecipitate. However, when only Sec13 was overexpressed, we detected its interaction with endogenous MAD in Dpp-treated cells (**Fig. 3.7.B**). Likewise, when only MAD was overexpressed with the receptor kinases, we again readily detected the coimmunoprecipitation of MAD with endogenous Sec13 (**Fig. 3.7.C**).

We also observed an interaction between MAD and Nup93 in coimmunoprecipitation experiments, and phosphorylation of MAD also appeared to enhance its binding to Nup93, although the effect was not as strong as in the case of Sec13 (**Fig. 3.7.D**; compare to **Fig. 3.7.A**). Moreover, using purified recombinant proteins, we determined that MAD could interact directly with Sec13 or Nup93 (**Fig. 3.8.A and 3.8.B**). In such direct binding assays, an excess of Sec13 did not compete away the Nup93 interaction with MAD, suggesting that their association with MAD is not mutually exclusive (**Fig 3.8.C**). We also investigated whether Nup75 could contribute to the interaction between MAD and Sec13 or Nup93. After knocking down Nup75 (to less than 30% of its normal level, as measured by real-time reverse transcription-PCR (RT-PCR), we still detected similar levels of interaction between MAD and Sec13 or Nup93 in coimmunoprecipitation experiments (**Fig. 3.9.A and B**). Therefore, Nup75 does not appear to regulate the interaction of MAD with Sec13 or Nup93.

Physical interactions of non-FG nucleoporins with Msk. Importins are believed to interact mostly with FG-nucleoporins in mediating nuclear transport. Our observations thus raised an interesting question: whether importins such as Msk could also interact with non-FG structural nucleoporins. Indeed, we found that Sec13 interacted with endogenous Msk in coimmunoprecipitation experiments (**Fig. 3.10.A**). But Dpp treatment had no discernible effect on this interaction. Moreover, overexpression of Sec13 had a marginal impact on the interaction between Msk and MAD, so Sec13 is not likely to regulate the loading of phospho-MAD onto Msk (**Fig. 3.10.B**). We also detected coimmunoprecipitation between endogenous Msk and overexpressed Nup93 in a Dpp-independent manner (**Fig. 3.10.C**). Msk could bind directly to Sec13 or Nup93, as indicated by GST pulldown experiments (**Fig. 3.10.D**) using purified recombinant proteins. Interestingly, when Nup75 was knocked down to below 30% of its normal level (judging by real-time RT-PCR analysis), the coimmunoprecipitation between Msk and Sec13 or Nup93 was significantly decreased (**Fig. 3.10.E**). Therefore, even though Msk is capable of direct interaction with Sec13 and Nup93, in the context of the whole NPC, Nup75 may further facilitate such association.

These biochemical observations reinforced the RNAi data and suggest that Sec13 and Nup93 are directly involved in the nuclear import of MAD. The currently prevailing model is that importins interact mainly with the FG-nucleoporins to

transport cargoes through the NPC (Pemberton & Paschal 2005; Stewart 2007a; Terry et al. 2007). Our finding here that Msk binds directly to structural non-FG nucleoporins suggests a new mode of importin-NPC interaction that is important for the nuclear import of MAD.

Functional distinction between Sec13/Nup75 and other components of the Nup107-160 subcomplex. Nup75 and Sec13 are part of the Nup107-160 subcomplex (Walther et al. 2003). Non-FG nucleoporins of the Nup107-160 complex have been suggested to be critical for NPC assembly and integrity from yeast to mammals; thus, it is surprising that Sec13 and Nup75 are required for the nuclear import of specific cargos. A comprehensive analysis of the Nup107-160 complex showed that Nup107, Nup145, and Nup160, but not Seh1 or Nup133, were also required for MAD nuclear import (**Fig. 3.11.**A). The lack of effect on MAD nuclear import was not likely due to inefficient Seh1 or Nup133 depletion, since we tested two different RNAi constructs with similar results, and at least for *nup133* RNAi there was a strong phenotype in NPC assembly, as expected (**Fig. 3.11.B**).

The integrity of the NPC is commonly analyzed with the monoclonal antibody MAb414, which recognizes a subset of FG-nucleoporins and exhibits a predominantly nuclear rim pattern in yeast and vertebrate cells (**7**) (**Fig. 3.11.B**).

Somewhat surprisingly, the MAb414 staining pattern was unchanged after knockdown of *sec13* or *nup75*, but in the same cells, the nuclear translocation of MAD was clearly impaired (**Fig. 3.11.B**). In contrast, knockdown of other Nup107-160 members, including *nup107*, *nup133*, *nup145*, and *nup160*, resulted in a diffuse MAb414 pattern throughout the nuclei, indicating defects in NPC assembly, as expected (**Fig. 3.11.C**). It is known that RNAi against *nup107* or *nup133* results in concomitant loss of several other nucleoporins in the Nup107-160 complex, which might have contributed to the more severe defects in NPC integrity (Walther et al. 2003; Boehmer et al. 2003). Immunoblot analysis confirmed that *sec13* RNAi was highly robust, and knockdown of other Nup107-160 complex components did not cause concomitant loss of Sec13 (**Fig 3.11.D**). A normal MAb414 pattern does not necessarily indicate intact NPC assembly, so roles for Sec13 and Nup75 in NPC structure cannot be ruled out. However, our observations did distinguish Sec13/Nup75 from Nup107/Nup145/Nup160 in terms of their requirement in maintaining a normal MAb414 pattern.

Nup133 knockdown clearly affected the MAb414 pattern, as expected for a core component of Nup107-160, but remarkably, in the same cells, nuclear accumulation of GFP-MAD was largely intact (**Fig. 3.11.B**). This is compelling evidence that components of the Nup107-160 subcomplex individually serve

different functions in the process of MAD nuclear transport and NPC assembly. These observations strongly argue that Sec13 and Nup75 are important for the nuclear import of MAD not because they are part of the Nup107-160 complex but because they have unique individual functions.

The Nup53-93 complex is critically involved in the anchoring of the NPC to the nuclear envelope (Hawryluk-Gara, Shibuya, and Wozniak 2005). Previous studies of mammalian cells showed aberrant MAb414 staining upon *nup93* RNAi (Hawryluk-Gara et al. 2008). However, MAb414 staining seemed normal in S2R+ cells after *nup93* RNAi, even though the nuclear import of MAD was clearly inhibited in the same cells (**Fig. 3.11.B**). Even when we simultaneously knocked down *nup93* and *nup205*, the MAb414 staining pattern still remained normal (**Fig. 3.11.C**). Interestingly, depletion of Nup93 or Nup205 also failed to affect NPC formation in *Caenorhabditis elegans* (Galy, Mattaj, and Askjaer 2003). Therefore, we again observed differential dependence on Nup93 in the nuclear import of MAD and the assembly of the NPC.

Impact of RNAi against non-FG nucleoporins on nuclear envelope permeability. MAb414 is limited in its ability to detect changes in the NPC. We therefore used a dextran exclusion assay to examine the permeability of the nuclear envelope. We found that RNAi against *sec13* or *nup75* had only a minor

effect, whereas knockdown of *nup133* or *nup107* resulted in a significantly higher number of leaky nuclei (**Fig. 3.12.B**) (see **Fig 3.12.A** and Materials and Methods for scoring criteria). This again indicated functional differences between Sec13/Nup75 and other members of the Nup107-160 complex. Knockdown of *nup93* increased the leakiness of the nuclear envelope, in agreement with previous reports (**Fig. 3.12.B**) (Galy, Mattaj, and Askjaer 2003). But a leaky nuclear envelope *per se* does not necessarily lead to impaired MAD nuclear import, since RNAi against *nup133* did not affect the nuclear concentration of MAD. Although it is in the same subcomplex with Nup93, Nup205 did not appear to be critical for maintaining the permeability barrier (**Fig. 3.12.B**). Therefore, the defect in MAD nuclear import after RNAi against Sec13, Nup75, Nup93, or Nup205 was not due to a compromised NPC permeability barrier.

Nup93 regulates the subcellular localization of Msk. We further investigated how non-FG nucleoporins functionally interact with Msk. Confirming an earlier report, we found endogenous Msk concentrated around the nuclear rim, with some overlap with MAb414 staining (**Fig. 3.13.A**) (James et al. 2007). The immunofluorescence staining was highly specific, since *msk* RNAi abolished the signals (**Fig 3.13.B**). Activation of the Dpp pathway by Punt/Tkv did not change the distribution pattern of Msk (**Fig 3.13.C**). Interestingly, we detected a completely different Msk pattern after *nup93* knockdown: the prominent nuclear

rim pattern was absent, and Msk was distributed evenly in both the nucleus and the cytoplasm (**Fig. 3.13.D**). In contrast, RNAi against *nup75* or *sec13* did not alter Msk distribution, although nuclear import of MAD was inhibited just as strongly as in the case of *nup93* RNAi (**Fig. 3.13.D**). We found that even though knockdown of Nup133 disrupted the MAb414 pattern (**Fig. 3.11.B**), the distribution of Nup93 appeared to be unaffected, and indeed, Msk was still localized to the nuclear periphery after Nup133 knockdown (**Fig. 3.13.D**). Interestingly, even though Nup205 is part of the same subcomplex as Nup93, its knockdown did not affect Msk distribution but did cause much-reduced MAD nuclear import (**Fig. 3.13.D**). Thus, clearly the role of Nup93 in MAD nuclear import is very different from those of Sec13, Nup75, and Nup205. This again illustrates the distinct functional roles that non-FG nucleoporins play in MAD nuclear transport. The fact that knockdown of these non-FG nucleoporins affects different aspects of MAD nuclear translocation is also a strong argument against the possibility that the defect in MAD nuclear transport is due to general disruption of the NPC.

Mutational analysis of Msk further supported the idea that perinuclear localization of Msk is essential for its function as a Smad nuclear import factor. Removal of the C-terminal 290 amino acids of Msk abolished its function, since it could no longer rescue the *msk* RNAi phenotype, although the deletion mutant was still

capable of interacting with MAD (**Fig. 3.14.B**). In agreement with the inability to import MAD, this deletion mutant (Msk-dC; aa 1 to 761) was diffusely distributed and was no longer concentrated in the perinuclear space, in contrast to full-length Msk (**Fig. 3.14.A**). Thus, our data suggest that the localization of Msk to the perinuclear space is important for its ability to transport MAD into the nucleus.

Interestingly, when we examined the direct interaction between purified recombinant Msk and Nup93, we found that Msk-dC failed to interact with Nup93 (**Fig. 3.14.C**). Therefore, combining the RNAi and protein interaction data, we arrived at the hypothesis that Nup93 may recruit Msk to the nuclear periphery by binding to the C-terminal 290 amino acids of Msk. However, one caveat is that we cannot rule out the possibility that the Msk C terminus is required for interaction with another factor that directly anchors Msk to the nuclear periphery.

Distinct roles of FG-nucleoporins in the nuclear import of MAD. False-negative results due to cell lethality, RNAi inefficiency, or functional redundancy are potential pitfalls in RNAi screening. Our previous studies have suggested that the FG-nucleoporins Nup153 and Nup214 play roles in the nuclear import of Smads, but they were not scored as positive hits in our screening (Xu et al. 2007). However, upon close examination, we noticed that both *nup153* and *nup358* RNAi resulted in cell lethality. Therefore, we decided to revisit the

issue of whether FG-nucleoporins Nup153, Nup214, and Nup358 are important for the nuclear import of Smads. By moderating the RNAi efficiency (i.e., reducing the dsRNA concentration by half and shortening the duration of RNAi from 4 days to 3 days), we considerably improved the viability of the cells treated with *nup153* or *nup358* RNAi and found that, indeed, Nup153, Nup358, and also Nup214 were required for the nuclear import of MAD (**Fig. 3.15.A**; quantification in Fig. **3.15.B**). Importantly, by immunoblotting, we detected little change in the Nup358 level upon RNAi against *sec13*, *nup75*, or *nup93*, ruling out the possibility that the impaired MAD nuclear import observed earlier after RNAi against these non-FG nucleoporins was caused by co-depletion of Nup358 (Fig. **3.15.C**). Although there was a slight decrease in the level of Nup153 upon RNAi against *sec13*, *nup75*, or *nup93*, it was not likely significant enough to affect the nuclear import of MAD, since *nup133* RNAi also caused a similar change in the Nup153 level (Fig. **3.15.C**), with no impact on MAD nuclear transport (Fig.**3.15.B**). Therefore, the requirements for Nup153 and Nup358 in MAD nuclear import are separate from those for the non-FG nucleoporins Sec13, Nup75, and Nup93.

When MAD was fused to a cNLS, its nuclear import became independent of Nup214 and Nup153 but, interestingly, still required Nup358 (**Fig. 3.15.D**). These observations agree with the findings of a previous study on the requirement of

Nup358 for cNLS-dependent nuclear import (Sabri et al. 2007). The same study also found that Nup153 was important for cNLS-mediated nuclear import, but this was not confirmed here, probably because we had to knock down Nup153 only partially (Sabri et al. 2007). Thus, the notion of pathway-specific utilization of nucleoporins applies to FG-nucleoporins as well: Nup358 is involved broadly in the nuclear import of both MAD and the cNLS, while Nup214 may serve more specifically in the nuclear import of MAD. Again, we confirmed that the efficiencies of RNAi were similar in cells expressing cNLS-GFP-MAD and those expressing GFP-MAD+R. Furthermore, by double immunofluorescence staining, we found that *nup358* knockdown affected the perinuclear localization of Msk but RNAi against *nup153* or *nup214* had little effect (**Fig. 13.15.E**). In terms of disrupting the MAb414 pattern, *nup153* knockdown had a very severe effect, whereas RNAi against *nup358* or *nup214* had a weaker impact, consistent with a previous report (**Fig. 13.15.E**) (Sabri et al. 2007). These data suggest that different FG-nucleoporins play different roles in the nuclear import of MAD, in agreement with our observations with non-FG nucleoporins.

Materials and Methods

Plasmids

GFP-MAD, NLS-GFP-Mad, FLAG-MAD, FLAG-Sec13, FLAG-Nup93 and Msk-v5 were cloned into pSH vector under the control of metallothionein

promoter. Punt, Tkv, HA-Sec13 and HA-Nup93, Msk (full length)-HA and Msk(1-761aa)-HA were cloned into pMK33 vector with the metallothionein promoter. Sec13, Nup93 and Msk were cloned into pGEX4T1 for expression in *E. coli*.

Tissue culture, transfection, and conditional expression of cDNAs

Drosophila S2 and S2R+ cells were maintained in Schneider's *Drosophila* medium (Invitrogen) supplemented with 10% fetal bovine serum, penicillin (100 U/ml), and streptomycin (100 U/ml). Transient transfection was carried out using the Effectene reagent according to the manufacturer's protocol (Qiagen). All expression vectors are under the control of a metallothionein promoter, and expression was induced by $CuSO_4$ (at 0.5 mM for 3 h) (Bunch, Grinblat, and Goldstein 1988).

Immunofluorescence staining, confocal microscopy and image quantification.

Cells were seeded onto coverslips and were induced with $CuSO_4$ (0.5 mM, 3 h) to express various green fluorescent protein (GFP)- or FLAG-tagged proteins for evaluation of their subcellular localizations. Cells were fixed with 4% paraformaldehyde in phosphate-buffered saline (PBS), followed by permeabilization with 0.2% Triton X-100-PBS, and were stained with appropriate antibodies and 4',6-diamidino-2-phenylindole (DAPI) according to previously

published procedures (Xu et al. 2007). Prolong Gold (Invitrogen) was used for mounting, and the samples were analyzed by confocal microscopy. All confocal images were collected with a laser-scanning microscope (Leica DMIRE2) at the following wavelengths: UV (DAPI), 488 nm (Alexa Fluor 488 or GFP), 543 nm (Alexa Fluor 546 or red fluorescent protein [RFP]/DsRed2), and 633 nm (Alexa Fluor 633). For low- and high-magnification images, 63x/1.40-numerical-aperture and 100x/1.40-numerical-aperture oil immersion objectives were used. The captured images were processed with Leica confocal microscope software.

Confocal images collected at identical settings were analyzed by NIH ImageJ to measure signal intensities from the nucleus and the cytoplasm. The ratio of the nuclear signal intensities to the cytoplasmic signal intensities was calculated. In each case, at least three separate fields (magnification, x60) were quantified. Provided that stable cell lines were used, usually there were more than 50 GFP-positive cells in each field. The standard error (SE) was calculated based on the average of the nuclear/cytoplasmic signal ratios from at least three different fields.

RNAi and rescue experiments.

The whole-genome RNAi screening was carried out at the *Drosophila* RNAi Screening Center (DRSC) at Harvard Medical School (www.flyrnai.org) by

following the format described in the Chapter II. The images were acquired and analyzed by automated confocal microscopy (Evotech Opera high-content screening system; Perkin-Elmer). The nuclear/cytoplasmic signal ratio was measured using algorithms accompanying the Opera system (Acapella). The design of RNAi constructs was based on recommendations by DRSC, and the sequence information is available through the DRSC web page (www.flyrnai.org) by specific amplicon numbers: DRSC23929 and DRSC11340 for *msk*; DRSC06947 and DRSC28056 for *nup75*; DRSC14144 and DRSC36009 for *sec13*; DRSC19344 and DRSC39780 for *nup93*; DRSC19432 and DRSC32816 for *nup205*; DRSC06827 and DRSC26470 for *nup50*; DRSC17039 for *punt*; DRSC00861 for *tkv*; DRSC03328 for *ketel*; DRSC07282 for *nup54*; DRSC16150 for *nup133*; DRSC01999 for *nup107*; DRSC14209 for *nup145*; DRSC1997 for *nup160*; DRSC19904 for *nup153*; DRSC04421 for *nup214*; DRSC14410 for *nup358*. DNA amplicons corresponding to different regions of targeted genes were generated by PCR and were used for *in vitro* transcription (MEGAscript; Applied Biosystems) to synthesize double-stranded RNA (dsRNA). RNAi in S2R+ cells using the soaking method has been described previously (Xu et al. 2007). In general, 5 µg of dsRNA was used for each well in a 24-well plate, and incubated with cells for 4 days. But for Nup153 and Nup358 RNAi, 2.5 µg of dsRNA was used for 3 days in order to minimize cell lethality.

In RNAi rescue experiments, S2R+ cells (0.2 x 10^6/well in a 24-well plate) were first treated with 5 μg dsRNA targeting the 3' UTR of either *sec13* or *nup93* for 2 days and were then transfected with the rescue plasmids (HA-Sec13 and HA-Nup93, driven by the inducible metallothionein promoter) using Effectene. After another 2 days, the cells were induced by $CuSO_4$ (0.5 mM, 3 h) to express GFP-MAD/Punt/Tkv and the rescue constructs and were then processed for immunostaining and imaging.

Nuclear envelope permeability assay

S2R+ cells were resuspended at 2 x 10^6 to 4 x 10^6 cells/ml in ice-cold hypotonic buffer (10 mM HEPES [pH 7.5], 2 mM $MgCl_2$, 25 mM KCl, 2 mM dithiothreitol [DTT], and 200 mM sucrose) supplemented with protease inhibitors. After a 10-min incubation on ice, the cell membrane was disrupted by a Dounce homogenizer (60 strokes, type A pestle). Broken and intact cells were pelleted by centrifugation (1,000 x *g*, 5 min) and resuspended in transport buffer (20 mM HEPES [pH 7.5], 110 mM potassium acetate [KOAc], 2 mM magnesium acetate [$Mg(OAc)_2$], 5 mM sodium acetate [NaOAc], 0.5 mM EGTA, 250 mM sucrose, 2 mM DTT) containing 0.2 mg/ml 70-kDa Texas red-labeled dextran (Invitrogen), 0.25 mg/ml 500-kDa fluorescein isothiocyanate (FITC)-labeled dextran (Sigma), and 0.2 mg/ml Cascade blue-labeled 3-kDa dextran (Invitrogen). After incubation at room temperature for 5 min, the nuclei were directly imaged without being

fixed by confocal microscopy. Only nuclei that were permeable to the 3-kDa dextran (indicating a lysed cell membrane) but not the 500-kDa dextran (suggesting no gross damage to the nuclear envelope during Dounce homogenization) were scored for leakiness toward the 70-kDa dextran.

Protein-protein interactions

For co-immunoprecipitation, S2 or S2R+ cells were lysed in 50 mM Tris-Cl (pH 7.4), 150 mM NaCl, 1 mM EDTA, 0.5% NP-40, and 2 mM DTT supplemented with protease inhibitors. Cell extracts were incubated with an anti-FLAG or antihemagglutinin (anti-HA) antibody conjugated to agarose beads (Sigma) at 4°C for 16 h, and the beads were washed in the lysis buffer three times before immunoblot analysis.

Recombinant *Drosophila* Sec13, Nup93, and Msk were produced in *Escherichia coli* as glutathione *S*-transferase (GST) fusion proteins and were purified using glutathione-Sepharose 4B beads (GE Healthcare). GST-Msk was digested by thrombin (Novagen) to remove the GST moiety. GST-Sec13 (10 μg) or GST-Nup93 (1 μg) on beads was incubated with recombinant Msk (0.1 μg/μl) at 4°C for 16 h in 20 mM Tris Cl (pH 7.5)-200 mM NaCl-5% glycerol. The beads were washed in the same buffer three times, and the bound proteins were analyzed by immunoblotting. For interaction with MAD, phosphorylated FLAG-MAD was

first affinity purified by anti-FLAG agarose beads (Sigma) from stable S2 cells expressing FLAG-MAD and Punt/Tkv. FLAG-MAD was eluted from the anti-FLAG beads by a 3x FLAG peptide in a buffer containing 25 mM Tris Cl (pH 8.0), 250 mM NaCl, 0.05% NP-40, 5% glycerol, and 1 mM DTT. The purified recombinant FLAG-MAD (0.2 µg/µl) in this buffer was incubated at 4°C for 16 h with GST-Sec13 (10 µg) or GST-Nup93 (1 µg) bound to the glutathione-Sepharose beads. The beads were washed 3 times with 20 mM Tris Cl (pH 8.0), 250 mM NaCl, 0.05% NP-40, and 5% glycerol, and the bound proteins were subjected to immunoblot analysis.

For testing of the Nup93-Msk interaction, S2 cells (~8 x 10^6) expressing Msk-HA or HA-tagged Msk with a C-terminal deletion (Msk-dC-HA) were purified by an anti-HA affinity matrix (Roche) in 25 mM Tris Cl (pH 8.0), 250 mM NaCl, 0.05% NP-40, 5% glycerol, and 1 mM DTT with protease inhibitors and phosphatase inhibitors. Bound Msk-HA or Msk-dC-HA was then eluted from the beads with HA peptides and was incubated with purified GST-Nup93 (1 µg) on glutathione-Sepharose beads at 4°C for 16 h. The beads were washed three times in the same buffer before immunoblot analysis.

For testing of the effect of *nup75* RNAi on the Msk-nucleoporin interaction, S2 cells were transfected with 4 µg dsRNA targeting *nup75* using Dharmafect 4

(Thermo Fisher Scientific) and were incubated for 2 days. The same cells were then transfected with the expression vectors using Effectene (Qiagen). Forty-eight hours later, cells were induced with $CuSO_4$ (0.5 mM, 3 h) to express the constructs and were lysed in 20 mM Tris Cl (pH 8.0), 150 mM NaCl, 0.5% NP-40, 5% glycerol, 2 mM DTT, protease inhibitors, and phosphatase inhibitors. The cell extracts were incubated with anti-FLAG-agarose beads (Sigma) at 4°C for 16 h, and the beads were washed in the lysis buffer three times before immunoblot analysis.

Antibodies

The polyclonal anti-MAD antibody was raised against the N-terminal 160-amino-acid (160-aa) fragment. Rabbit anti-Msk was a gift from L. Perkins (Harvard Medical School), and anti-Sec13 was a gift from B. Fontoura (University of Texas Southwestern Medical School) and W. Hong (IMCB, Singapore). The other antibodies used in the study were anti-phospho-Smad1/5/8 (also recognizing phospho-MAD) (Cell Signaling), MAb414 (Covance), anti-GFP (Zymed), anti-FLAG, and anti-HA (Sigma).

Quantitative real-time RT PCR

Total RNA was isolated by RNeasy spin columns (Qiagen) and was reverse transcribed using the iScript cDNA synthesis kit (Bio-Rad). Real-time PCR was

conducted using the iQ SYBR green kit (Bio-Rad), and the threshold values for Rp49 were used as internal standards for quantification. *dad* forward primer: GAAGCGACTGCCCACTTG, reverse primer: CGGTGTTGGGGATTCTGT; *rp49* forward primer: CGGATCGATATGCTAAGCTGT, reverse primer GC GCTTGTTCGATCCGTA; *nup75* forward primer: TGCTGGACAGGTTCCGG TGCT, reverse primer: TGGCCCGCGAACCCAACT; *sec13* forward primer: GG GCCAATGGATCCGCATCAAC, reverse primer: GCGCCTGTTGTTGGTGCT GTTG; *nup93* forward primer: CCAGCGCCTGACGAACGAGAC, reverse primer: CACGCCCTTAGAGCCGAGCAG; *nup54* forward primer: TTGGA GCCGCCACAGGAACTTC, reverse primer: GCTGCTCCAAATCCGCCGAA AC; *ketel* forward primer: CATCGAAAGCCAGGAGGCCACTG, reverse primer: GGCTCCAGGTGTCCTCGTCATCG.

Fig 3.1

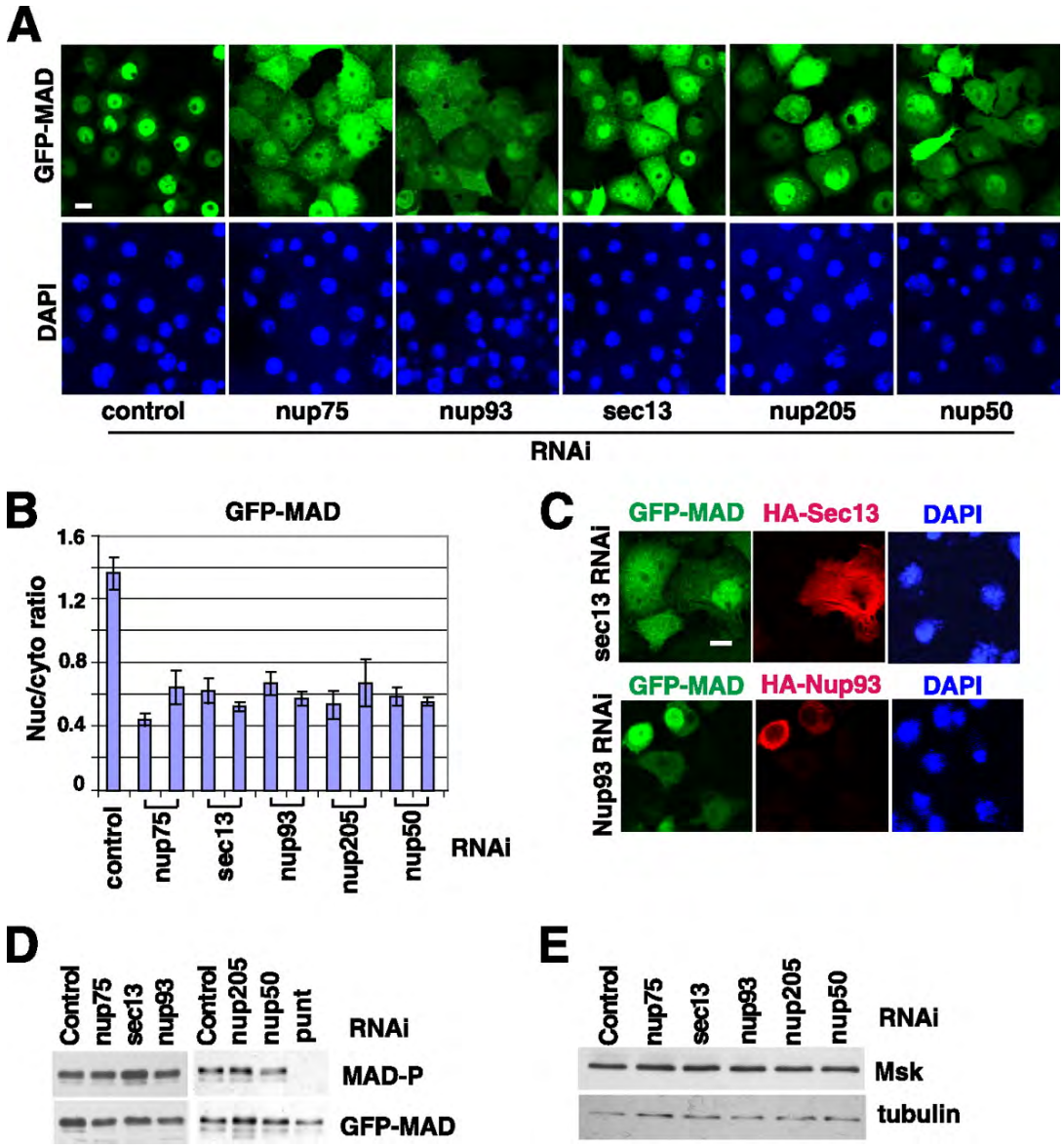
A
GFP-MAD
DAPI
control
nup75
nup93
sec13
nup205
nup50
RNAi
B
GFP-MAD
Nuc/cyto ratio
1.6
1.2
0.8
0.4
0
control
nup75
sec13
nup93
nup205
nup50
RNAi
C
GFP-MAD
HA-Sec13
DAPI
sec13 RNAi
GFP-MAD
HA-Nup93
DAPI
Nup93 RNAi
D
Control
nup75
sec13
nup93
Control
nup205
nup50
punt
RNAi
MAD-P
GFP-MAD
E
Control
nup75
sec13
nup93
nup205
nup50
RNAi
Msk
tubulin

Fig 3.1 Nucleoporin requirement for nuclear accumulation of activated MAD. (A) S2R+ cells inducibly expressing GFP-MAD and Punt/Tkv (GFP-MAD+R) were treated with the indicated RNAi, and the distribution patterns of GFP-MAD are shown. Nuclei were stained with DAPI. Bar, 10 μM. (B) Two different dsRNA constructs against each nucleoporin hit were tested as described for panel A. The GFP-MAD signals in the nucleus and cytoplasm were quantified, and the ratios were plotted. Data are means ±SEs from ≥3 fields. (C) GFP-MAD+R cells were treated with dsRNAs targeting the 3' UTR of *sec13* or *nup93*, followed by transfection of HA-Sec13 or HA-Nup93 cDNAs. The distributions of GFP-MAD (green) and the rescue constructs (red) are shown. (D and E) GFP-MAD+R cells were subjected to the indicated RNAi, and the cell extracts were analyzed by immunoblotting with the indicated antibodies.

Fig 3.2

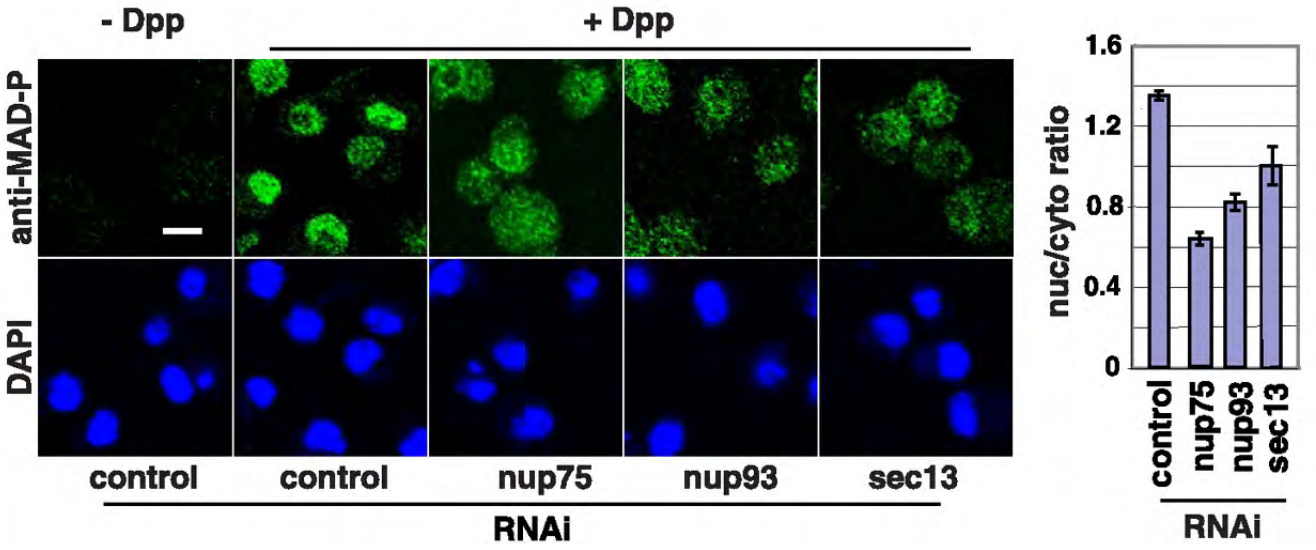
- Dpp
+ Dpp
anti-MAD-P
DAPI
control
control
nup75
nup93
sec13
RNAi
nuc/cyto ratio
1.6
1.2
0.8
0.4
0
control
nup75
nup93
sec13
RNAi

Fig 3.2 Sec13, Nup75 and Nup93 are required for nuclear import of endogenous MAD upon Dpp stimulation. (Left) S2 cells were treated with the indicated RNAi, and the phospho-MAD distribution pattern after Dpp treatment (10^{-9} M, 1 h) was detected by a phospho-MAD-specific antibody. Bar, 10 μM. (Right) Nuclear/cytoplasmic ratios of phospho-MAD signals are plotted; data are means ±SEs for ≥3 fields ($P < 0.05$ in all cases).

Fig 3.3

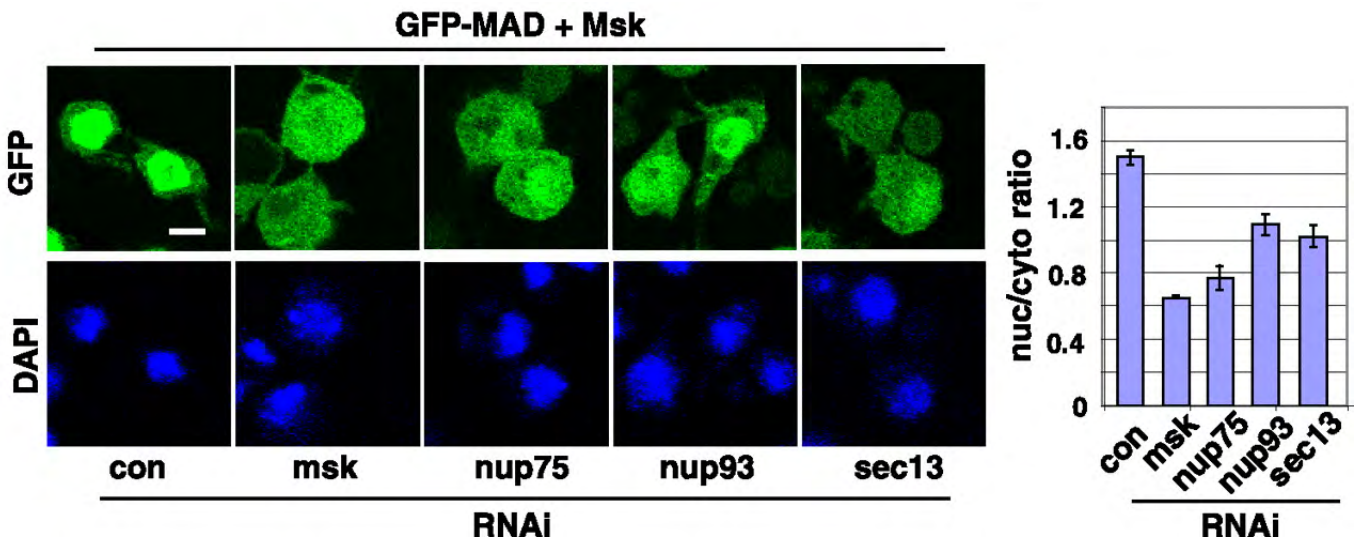
GFP-MAD + Msk
GFP
DAPI
con
msk
nup75
nup93
sec13
RNAi
nuc/cyto ratio
1.6
1.2
0.8
0.4
0
con
msk
nup75
nup93
sec13
RNAi

Fig 3.3 S ec13, Nup75 and Nup93 are part of the Msk-dependent nuclear import machinery for activated MAD. (Left) S2R+ cells transfected with GFP-MAD and Msk were subjected to the indicated RNAi, and the distribution patterns of GFP-MAD are shown. Bar, 10 μM. (Right) Nuclear and cytoplasmic GFP signals were quantified, and the ratios are plotted; data are means ±SEs for ≥3 fields ($P < 0.005$ in all cases).

Fig 3.4

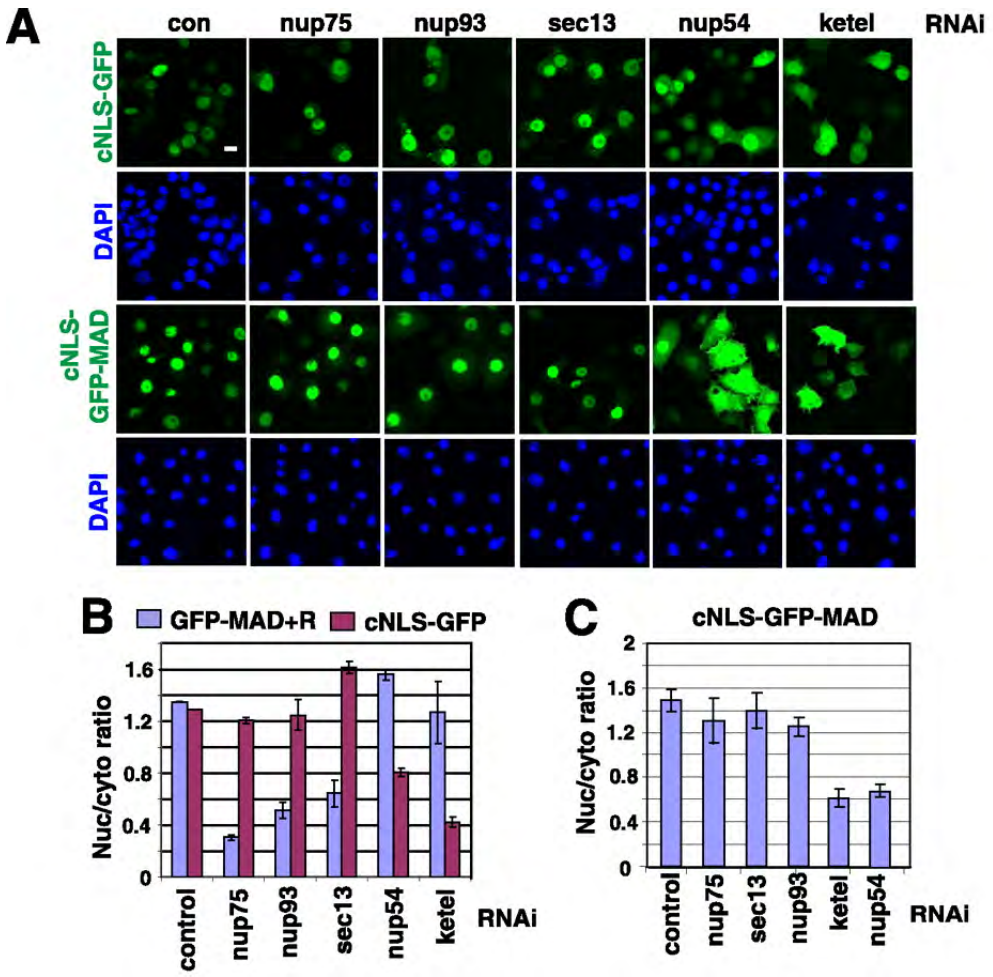
A
con
nup75
nup93
sec13
nup54
ketel
RNAi
cNLS-GFP
DAPI
cNLS-GFP-MAD
DAPI
B
GFP-MAD+R
cNLS-GFP
Nuc/cyto ratio
1.6
1.2
0.8
0.4
0
control
nup75
nup93
sec13
nup54
ketel
RNAi
C
cNLS-GFP-MAD
Nuc/cyto ratio
2
1.6
1.2
0.8
0.4
0
control
nup75
sec13
nup93
ketel
nup54
RNAi

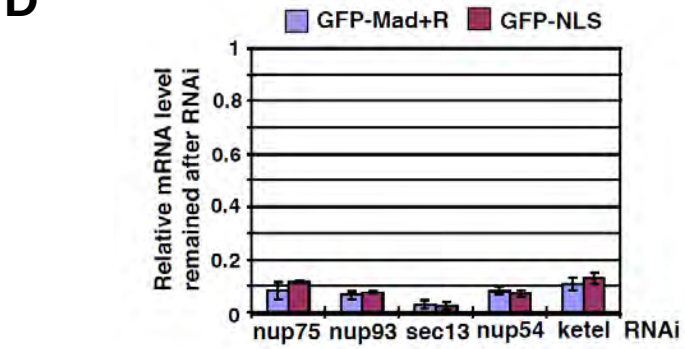
D
GFP-Mad+R
GFP-NLS
Relative mRNA level remained after RNAi
1
0.8
0.6
0.4
0.2
0
nup75
nup93
sec13
nup54
ketel
RNAi

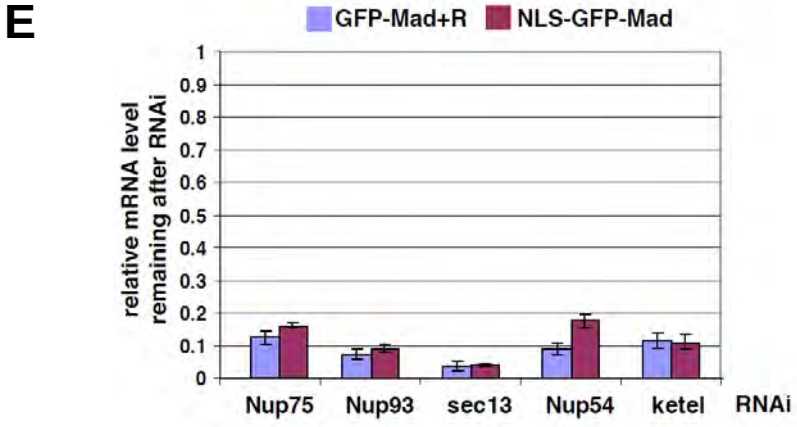
E
GFP-Mad+R
NLS-GFP-Mad
relative mRNA level remaining after RNAi
1
0.9
0.8
0.7
0.6
0.5
0.4
0.3
0.2
0.1
0
Nup75
Nup93
sec13
Nup54
ketel
RNAi

Fig 3.4 Sec13, Nup93, and Nup75 are required specifically for the nuclear import of MAD but not for cNLS-dependent nuclear import. (A) The indicated RNAi experiments were carried out in three S2R+ cell lines inducibly expressing cNLS-GFP (2 copies of GFP fused with a cNLS[PKKKRKVED]), GFP-MAD+R, or cNLS-GFP-MAD. Only images for cNLS-GFP or cNLS-GFP-MAD are shown. Bar, 10 μM. (B and C) The nuclear/cytoplasmic ratio of the GFP signal was quantified and plotted. Data are means ±SEs for ≥3 fields. Compared to activation-induced nuclear translocation of GFP-MAD, constitutive nuclear import of cNLS-GFP-MAD depended on different nucleoporins. (D) S2R+ stable cell lines inducibly expressing GFP-MAD and Punt/Tkv (GFPMAD+R) or NLS-GFP were harvested after indicated RNAi. Total RNA was extracted and analyzed for nucleoporin mRNA levels using quantitative real-time RT-PCR. Shown are the levels of nucleoporin mRNA relative to that in control knockdown cells (mean ± S.E.). Rp45 (ribosomal protein) was used as the standard for normalization. (E) Similar experiments as in (D) comparing stable cell lines inducibly expressing GFP-MAD+R or NLS-GFP-MAD mean ± S.E.).

Fig 3.5

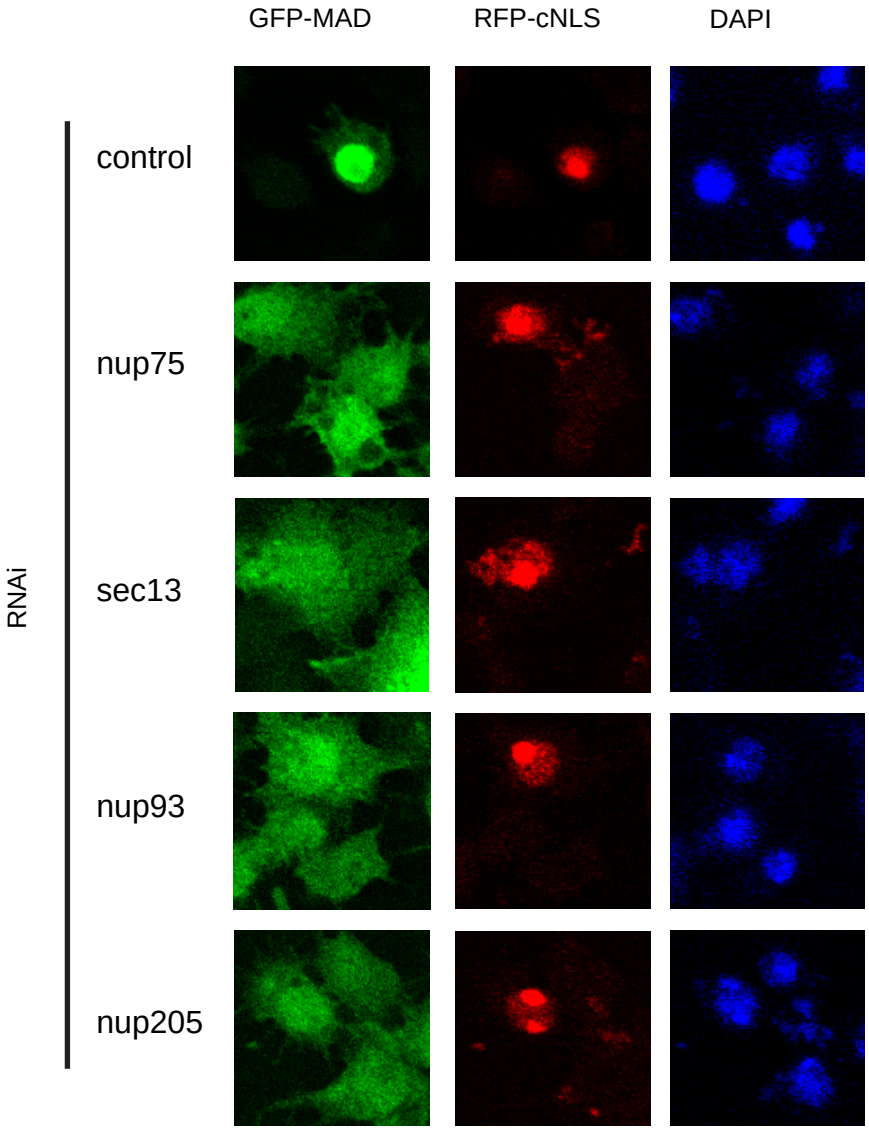

Fig 3.5 Sec13, Nup93, and Nup75 are not required for cNLS-dependent nuclear import in cell lines concurrently expressing activated GFP-MAD and RFP-cNLS. GFP-MAD+R cells were subjuected to indicated RNAi for 2 days, followed by transfection of RFP-cNLS and incubation for another 2 days. All proteins were inducibly expressed in media containing 0.5 mM $CuSO_4$ for 3 h. Green signal indicates the GFP-MAD localization, red signal indicates the RFP-cNLS localization. Nuclei were marked using DAPI (blue).

Fig 3.6

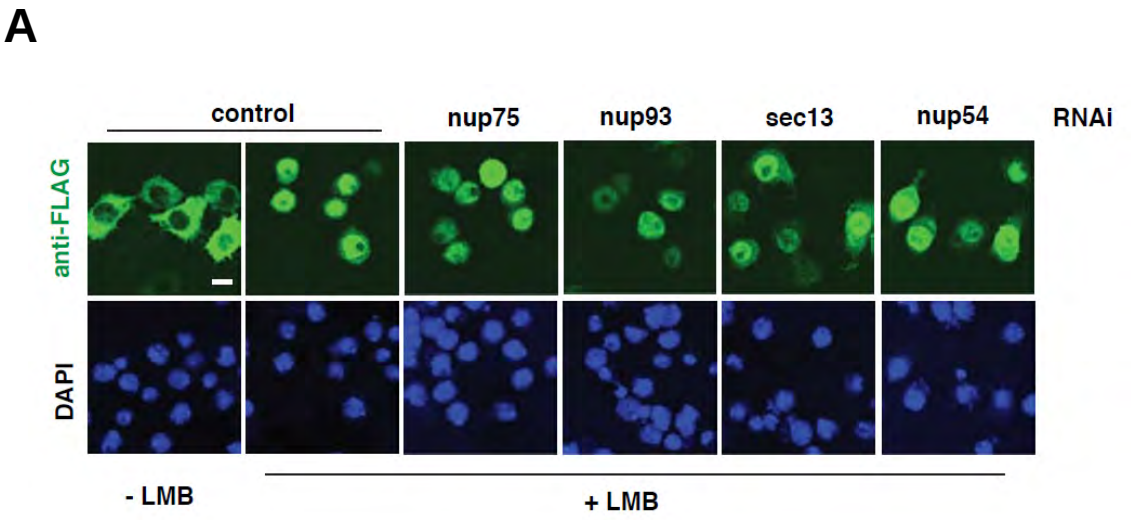
A
control
nup75
nup93
sec13
nup54
RNAi
anti-FLAG
DAPI
- LMB
+ LMB

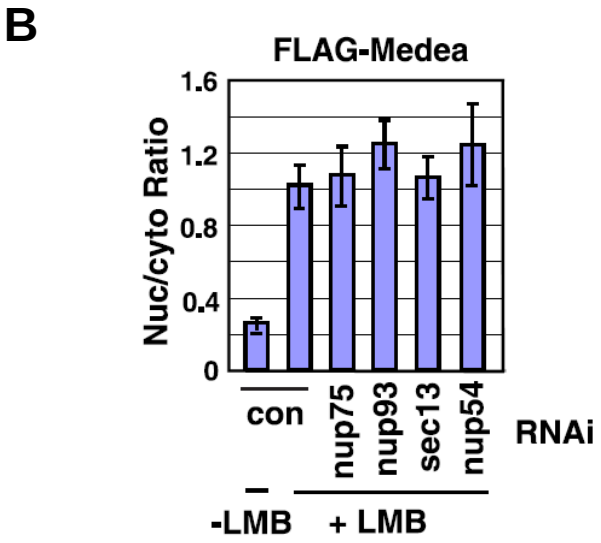
B
FLAG-Medea
Nuc/cyto Ratio
1.6
1.2
0.8
0.4
0
con
nup75
nup93
sec13
nup54
RNAi
-LMB
+ LMB

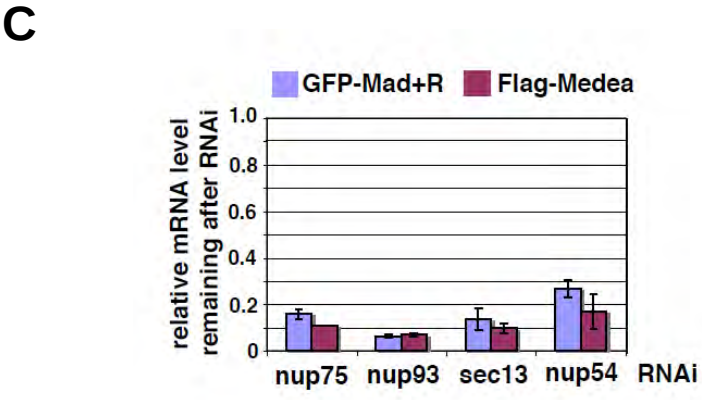
C
GFP-Mad+R
Flag-Medea
relative mRNA level remaining after RNAi
1.0
0.8
0.6
0.4
0.2
0
nup75
nup93
sec13
nup54
RNAi

Fig 3.6 Sec13, Nup93, and Nup75 are not required for Medea nuclear import driven by LMB treatment. (A) S2R+ cells inducibly expressing FLAG-Medea were subjected to the indicated RNAi, and after treatment with leptomycin B (LMB) (10 ng/ml for 1 h), the distribution pattern of FLAG-Medea was detected by immunofluorescence staining with an anti-FLAG antibody. Bar, 10 μM. (B) The nuclear/cytoplasmic ratio of the FLAG-Medea signal was quantified. Data are means ±SEs for≥3 fields. (C) Comparable RNAi efficiencies in GFP -MAD+R and FLAG-Medea cell lines shown in quantitative real-time PCR.

Fig 3.7

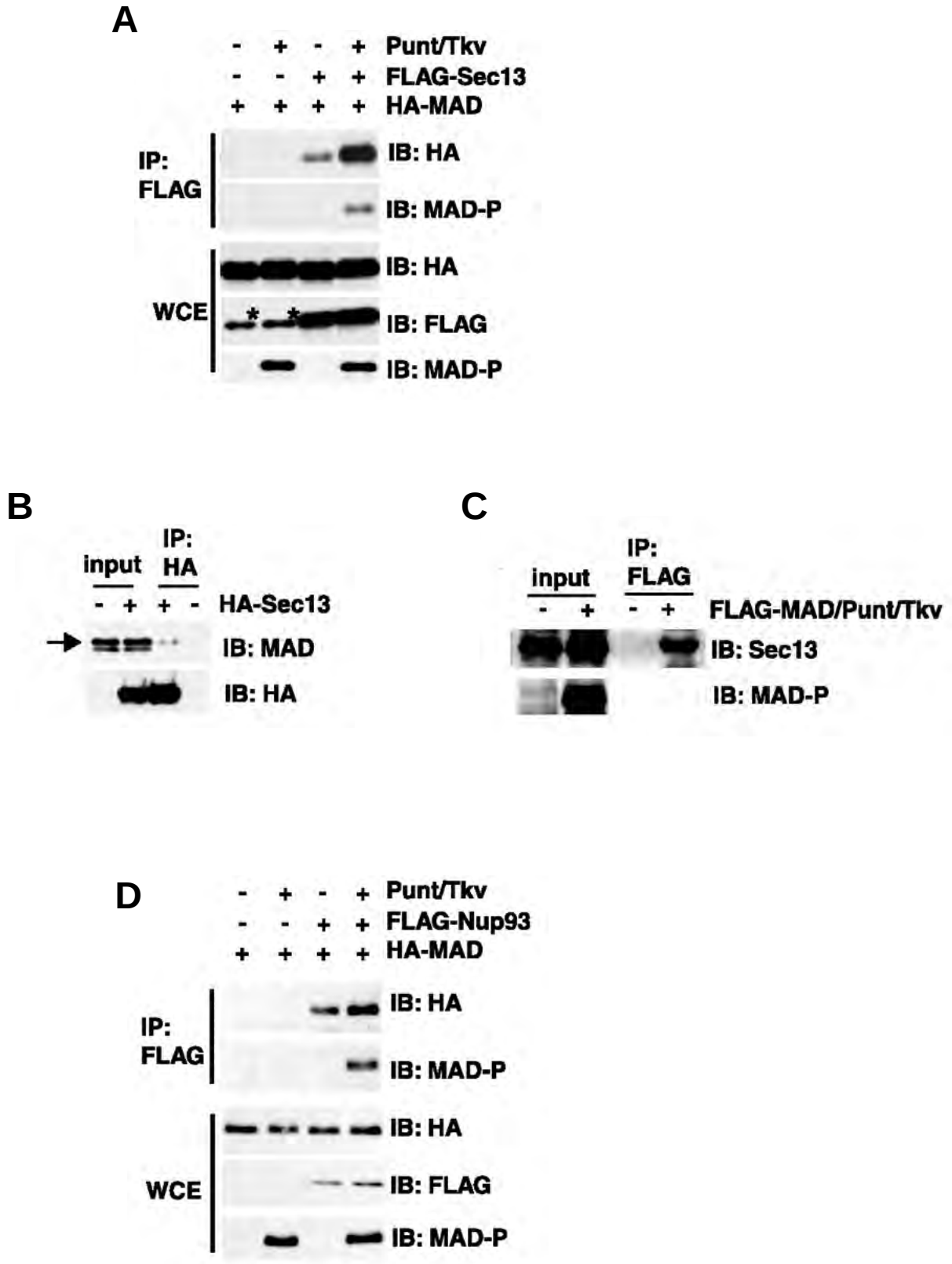
A
- + - + Punt/Tkv
- - + + FLAG-Sec13
+ + + + HA-MAD
IP: FLAG
IB: HA
IB: MAD-P
WCE
IB: HA
IB: FLAG
IB: MAD-P
B
input
IP: HA
- + + - HA-Sec13
IB: MAD
IB: HA
C
input
IP: FLAG
- + - + FLAG-MAD/Punt/Tkv
IB: Sec13
IB: MAD-P
D
- + - + Punt/Tkv
- - + + FLAG-Nup93
+ + + + HA-MAD
IP: FLAG
IB: HA
IB: MAD-P
WCE
IB: HA
IB: FLAG
IB: MAD-P

Fig 3.7 S ec13 and Nup93 co-immunoprecipitated with MAD. (A) Sec13 preferentially interacts with phosphorylated MAD. The indicated expression vectors were transfected into S2 cells, together with Punt/Tkv to phosphorylate MAD. The whole-cell extracts (WCE) were immunoprecipitated (IP) with anti-FLAG, and the bound proteins were analyzed by immunoblotting (IB) with the indicated antibodies. The asterisk marks a protein comigrating with Sec13 that cross-reacts with the anti-FLAG antibody. (B) S2 cells transfected with HA-Sec13 only were treated with Dpp, and the cell lysate was subjected to immunoprecipitation with anti-HA. The bound proteins were examined by IB using anti-MAD. The arrow points to endogenous MAD. (C) Cell extracts from S2 cells transfected with FLAG-MAD and Punt/Tkv only were immunoprecipitated with anti-FLAG, and the bound proteins were examined by IB with anti-Sec13. (D) Experiments similar to those described for panel A were carried out to examine the Nup93-MAD interaction.

Fig 3.8

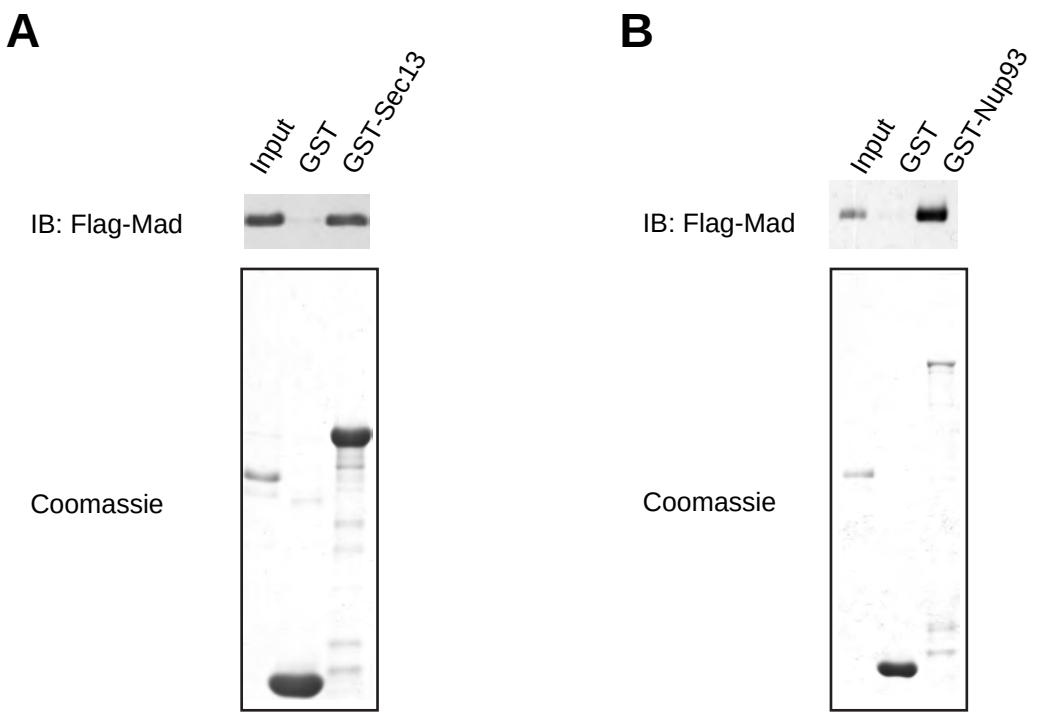
A
Input
GST
GST-Sec13
IB: Flag-Mad
Coomassie
B
Input
GST
GST-Nup93
IB: Flag-Mad
Coomassie

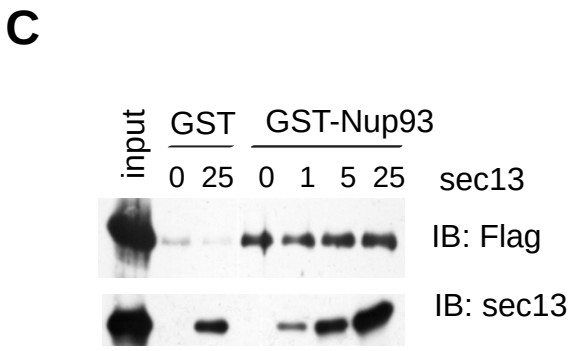
C
input
GST
GST-Nup93
0 25 0 1 5 25
sec13
IB: Flag
IB: sec13

Fig 3.8 Sec13 and Nup93 directly interact with activated MAD. (A and B) GST pulldown assays to test direct protein interactions using purified recombinant FLAG-MAD (after phosphorylation by Punt/Tkv) and GST-Sec13 or GST-Nup93, with GST serving as the control. The bound proteins were analyzed by IB with anti-FLAG antibodies (upper panels). The input proteins were stained with Commassie Blue (lower panels). (C) Sec13 did not compete away the Nup93 binding to MAD. FLAG-MAD were loaded to GST-Nup93 prior to the addition of Sec13 at indicated amout. The GST part of Sec13 was removed by Thrombin digestion before incubation with FLAG-MAD bound GST-Nup93 beads. The bound proteins were analyzed by IB with anti-FLAG and anti-Sec13 antibodies.

Fig 3.9

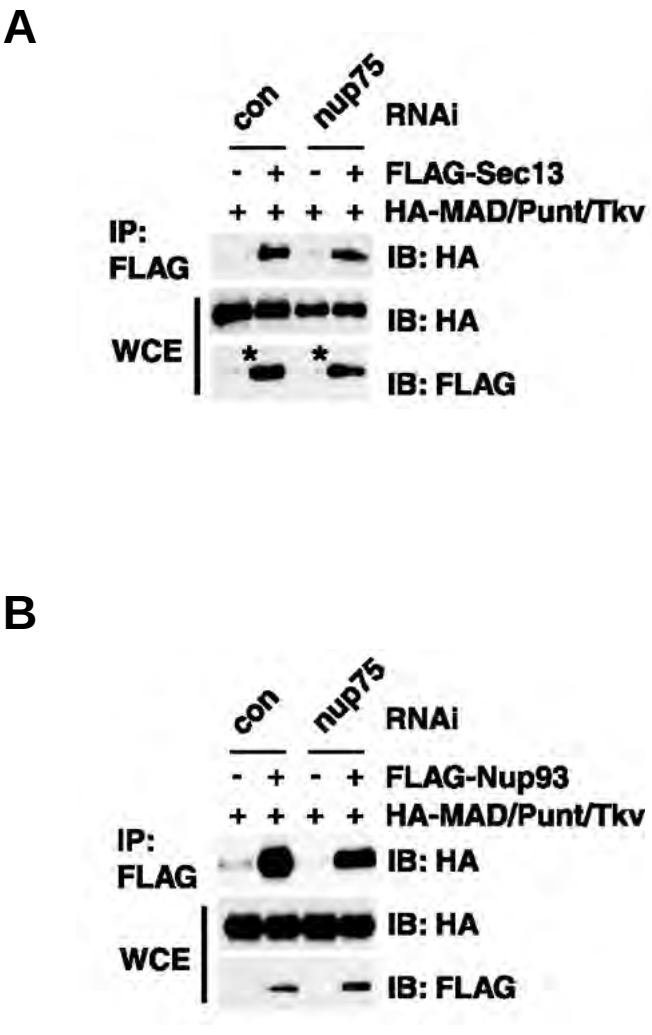
A
con
nup75
RNAi
- + - +
FLAG-Sec13
+ + + +
HA-MAD/Punt/Tkv
IP:
FLAG
IB: HA
WCE
IB: HA
IB: FLAG
B
con
nup75
RNAi
- + - +
FLAG-Nup93
+ + + +
HA-MAD/Punt/Tkv
IP:
FLAG
IB: HA
WCE
IB: HA
IB: FLAG

Fig 3.9 Nup75 depletion does not affect the interaction of MAD with Sec13 or Nup93. (A and B) S2 cells were treated with the indicated RNAi and were transfected with the indicated plasmids. The cell extracts were subjected to IP with anti-FLAG in order to test interactions between MAD and Sec13 or Nup93. Quantitative real-time PCR confirmed that Nup75 knockdown was 70%. The asterisks indicate a band cross-reacting with anti-FLAG.

Fig 3.10

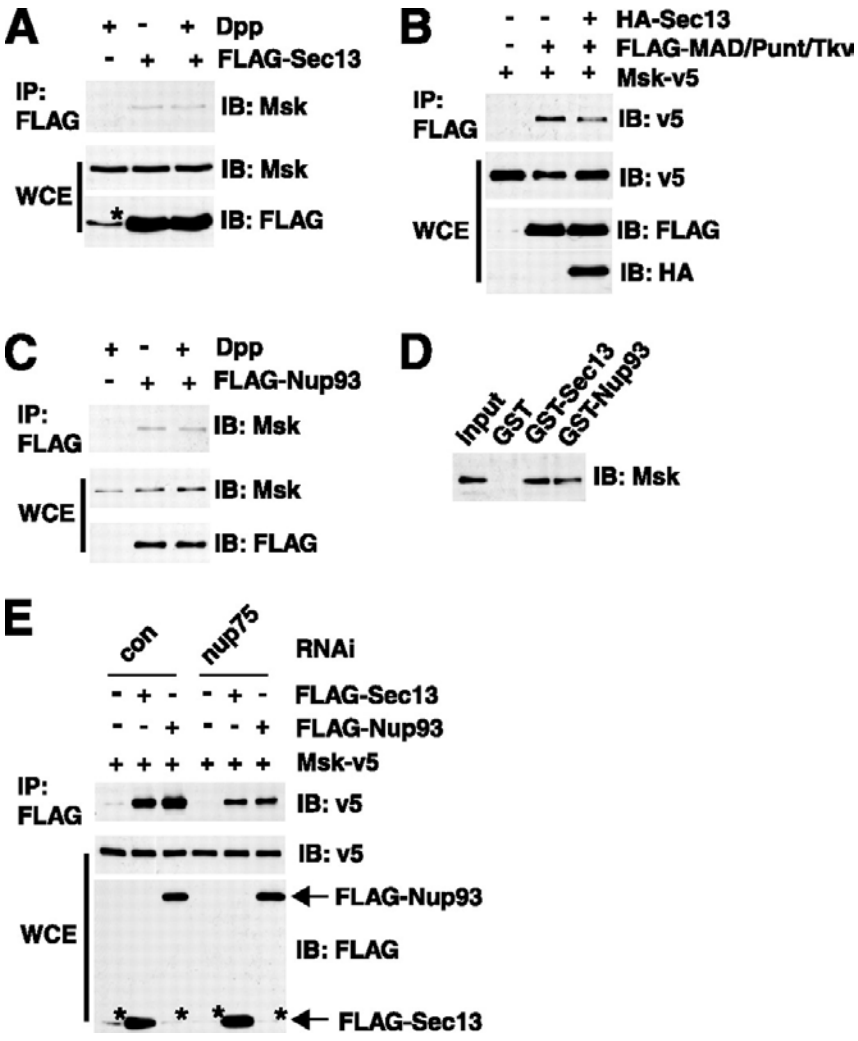
A
+ - + Dpp
- + + FLAG-Sec13
IP: FLAG
IB: Msk
WCE
IB: Msk
*
IB: FLAG
B
- - + HA-Sec13
- + + FLAG-MAD/Punt/Tkv
+ + + Msk-v5
IP: FLAG
IB: v5
WCE
IB: v5
IB: FLAG
IB: HA
C
+ - + Dpp
- + + FLAG-Nup93
IP: FLAG
IB: Msk
WCE
IB: Msk
IB: FLAG
D
Input
GST
GST-Sec13
GST-Nup93
IB: Msk
E
con
nup75
RNAi
- + - - + - FLAG-Sec13
- - + - - + FLAG-Nup93
+ + + + + + Msk-v5
IP: FLAG
IB: v5
IB: v5
WCE
FLAG-Nup93
IB: FLAG
* * * * FLAG-Sec13

Fig 3.10 Physical interaction between Msk and Sec13 or Nup93. (A) S2 cells were transfected with FLAG-Sec13, and the lysate was used for immunoprecipitation (IP) with anti-FLAG. The endogenous Msk was detected by immunoblotting (IB). (B) Sec13 overexpression did not significantly affect the Msk-MAD interaction. S2 cells were transfected with the indicated expression vectors. The whole-cell extracts (WCE) were immunoprecipitated with anti-FLAG, and the bound proteins were analyzed by IB as indicated. (C) FLAG-Nup93 was expressed in S2 cells, and anti-FLAG immunoprecipitation was used to detect its interaction with endogenous Msk. (D) GST pulldown experiment testing direct interactions between purified recombinant Msk and GST-Sec13 or GST-Nup93, with GST as the control. Proteins bound to GST beads were analyzed by IB with anti-Msk. (E) S2 cells were subject to the indicated RNAi and were then transfected with the indicated expression vectors. IP was carried out to test for interactions between Msk-V5 and FLAG-Sec13 or FLAG-Nup93. RNAi knockdown of Nup75 resulted in decreased Sec13-Msk and Nup93-Msk interactions. Quantitative real-time PCR confirmed that Nup75 knockdown was 70%. The asterisk indicates a band cross-reacting with anti-FLAG.

Fig 3.11

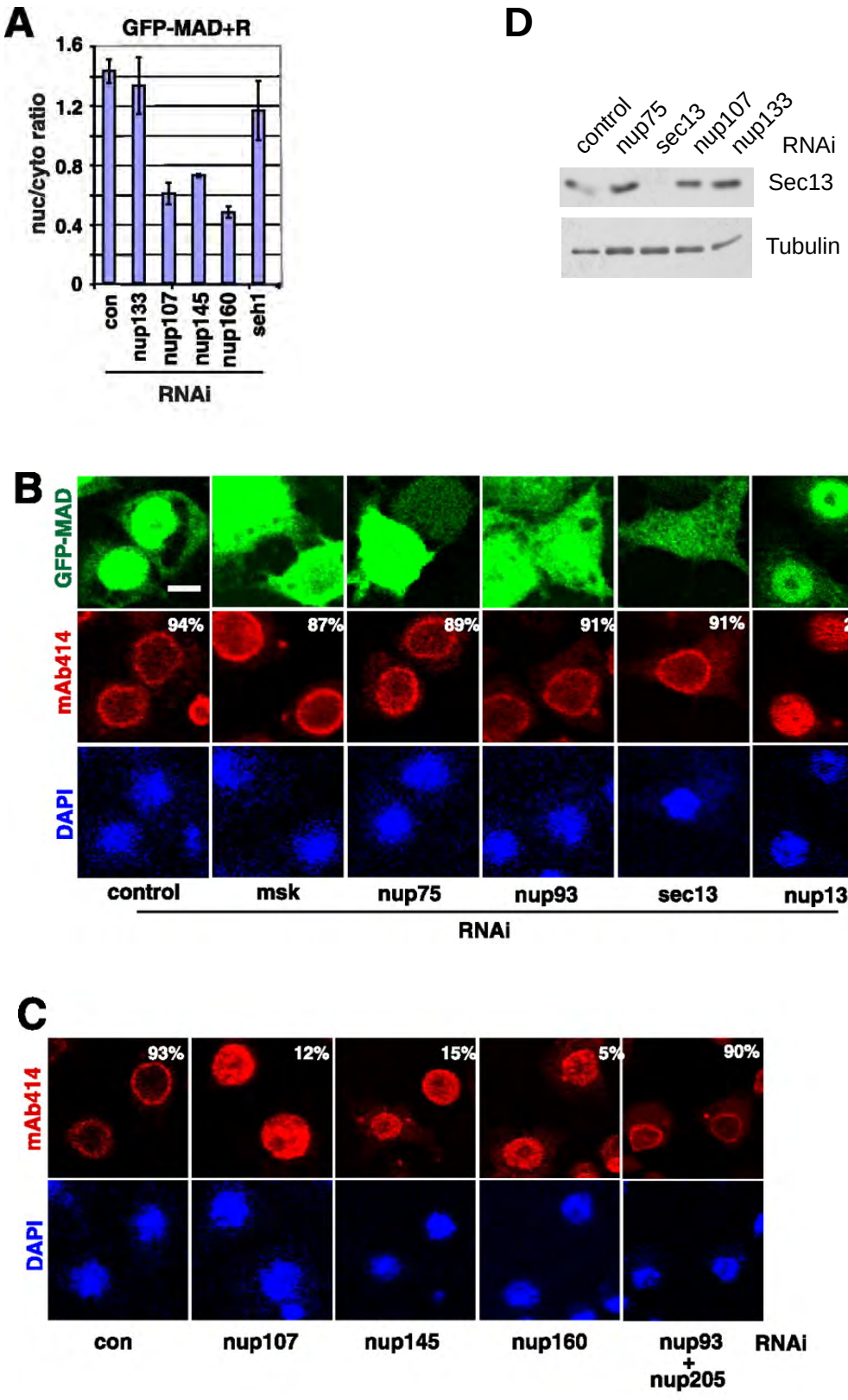
A
GFP-MAD+R
nuc/cyto ratio
1.6
1.2
0.8
0.4
0
con
nup133
nup107
nup145
nup160
seh1
RNAi
D
control
nup75
sec13
nup107
nup133
RNAi
Sec13
Tubulin
B
GFP-MAD
mAb414
DAPI
94%
87%
89%
91%
91%
20%
control
msk
nup75
nup93
sec13
nup133
RNAi
C
mAb414
DAPI
93%
12%
15%
5%
90%
con
nup107
nup145
nup160
nup93 + nup205
RNAi

Fig 3.11 Impact of RNAi against non-FG nucleoporins on MAb414 pattern (A) GFP-MAD+R cells were treated with the indicated RNAi, and the quantification of the nuclear/cytoplasmic concentration of GFP-MAD is plotted. Data are means ±SEs for ≥3 fields. (B) GFP-MAD+R cells were treated with the indicated RNAi and were then induced to express GFP-MAD and Punt/Tkv. The cells were stained with MAb414, and the images for GFP-MAD (green), MAb414 (red), and DAPI (blue) were captured by confocal microscopy. The percentages of cells exhibiting a normal MAb414 staining pattern (50 cells scored) are shown. Bar, 5 μM. (C) GFP-MAD+R cells were treated with the indicated RNAi and were immunostained with MAb414 (red). The percentages of cells exhibiting a normal MAb414 staining pattern (50 cells scored) are shown. (D) GFP-MAD+R cells were subjected to indicated RNAi and were immuneblotted with anti-Sec13 and anti-Tubulin.

Fig 3.12

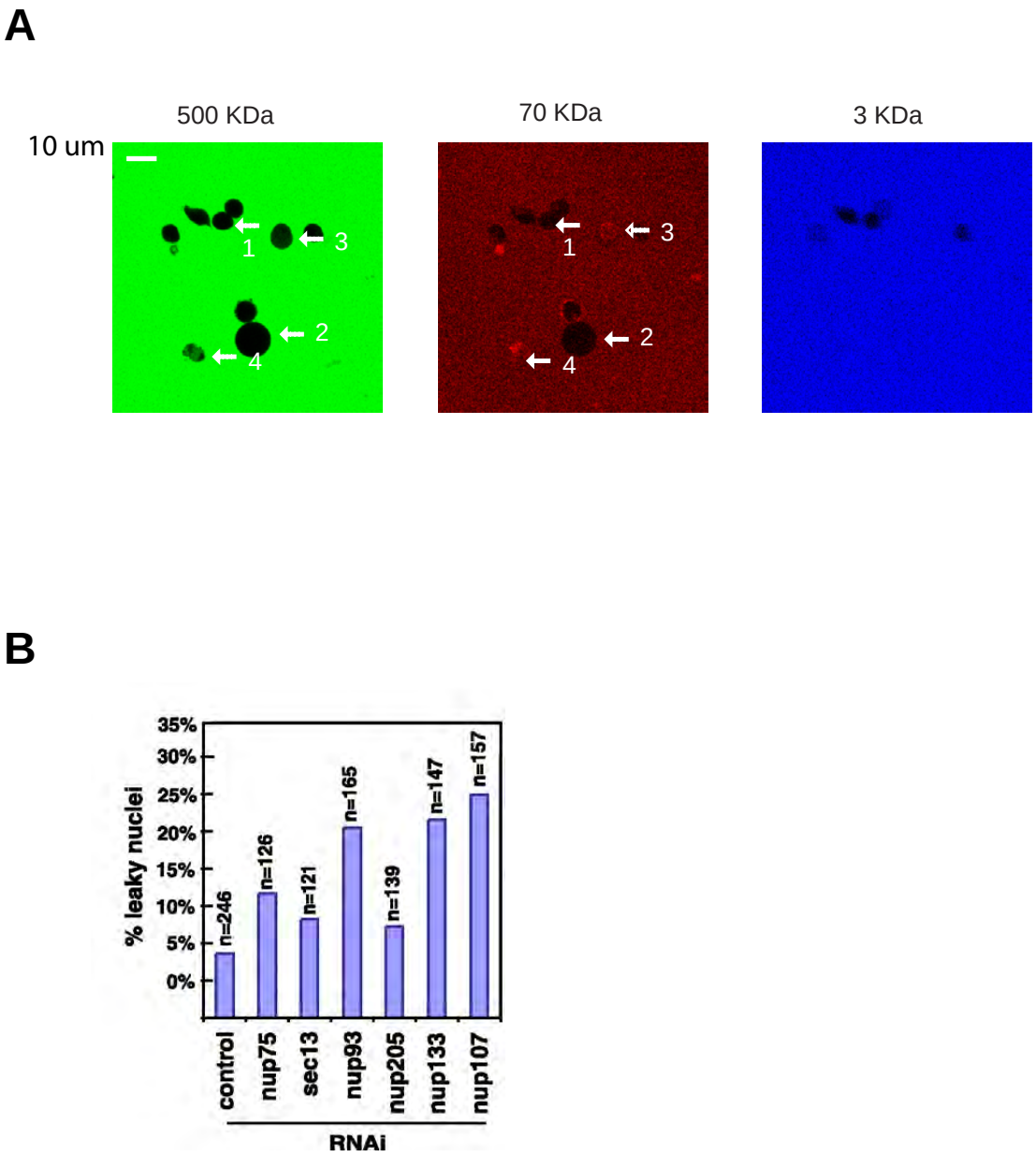
A
500 KDa
70 KDa
3 KDa
10 um
1
2
3
4
1
2
3
4
B
% leaky nuclei
35%
30%
25%
20%
15%
10%
5%
0%
n=246
n=126
n=121
n=165
n=139
n=147
n=157
control
nup75
sec13
nup93
nup205
nup133
nup107
RNAi

Fig 3.12 Impact of RNAi against non-FG nucleoporins on nuclear envelope permeability. (A) Permeability scales: 1) intact cell and nuclear membrane, 2) permeabilized cell membrane but intact nuclear envelope, 3) leaky nuclear envelope, 4) complete permeablized nuclear envelope. 500-kDa dextran in green, 70-kDa dextran in red, 3-kDa dextran in blue. **(B)** GFP-MAD+R cells were treated with the indicated RNAi, and the permeability of the nuclear envelope was tested by dextran exclusion assays. The percentages of nuclei permeable to the 70-kDa but not the 500-kDa dextran are plotted.

Fig 3.13

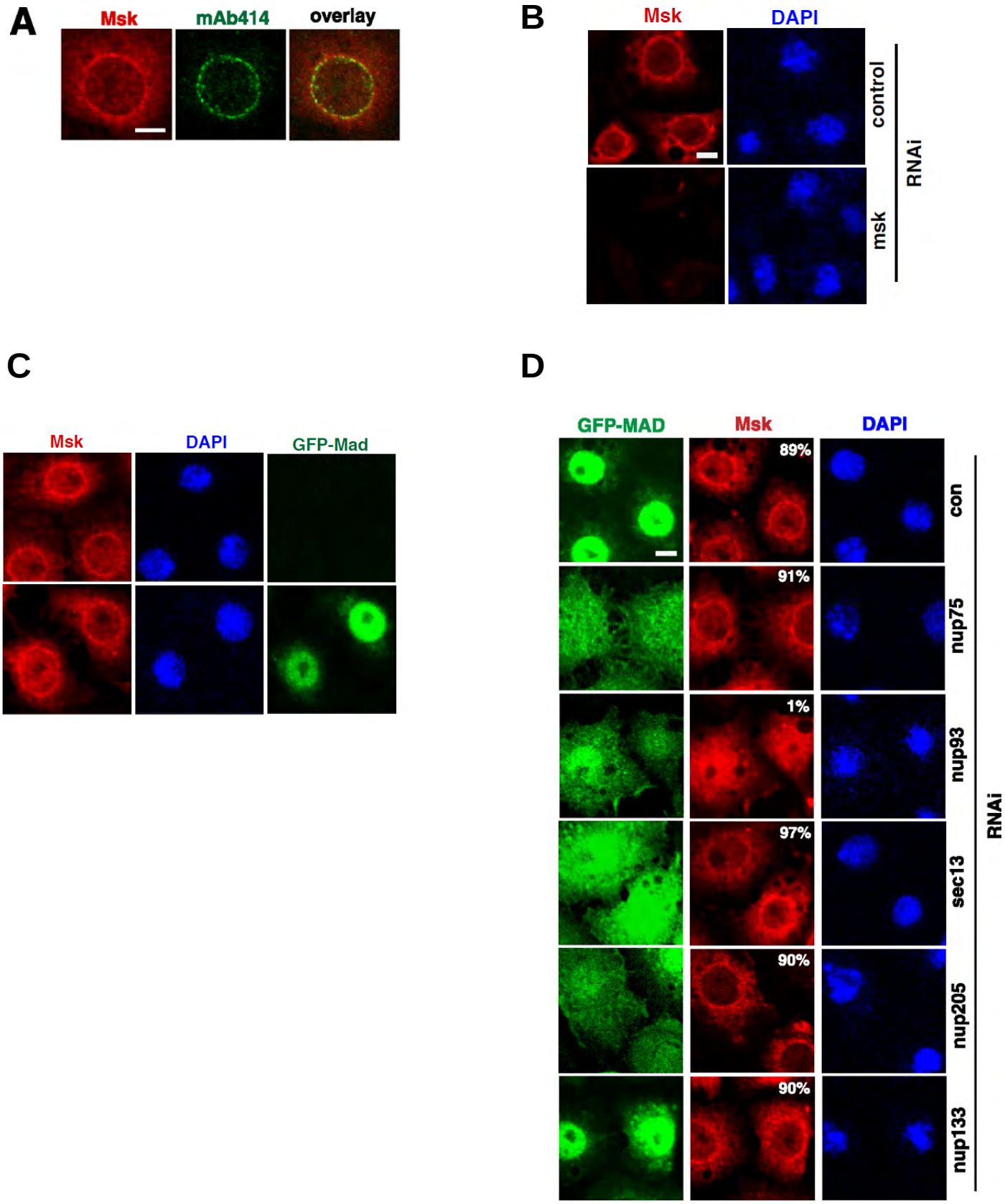
A
Msk
mAb414
overlay
B
Msk
DAPI
control
msk
RNAi
C
Msk
DAPI
GFP-Mad
- Punt/Tkv
+ Punt/Tkv
D
GFP-MAD
Msk
DAPI
89%
91%
1%
97%
90%
90%
con
nup75
nup93
sec13
nup205
nup133
RNAi

Fig 3.13 The perinuclear localization of Msk depends on Nup93. (A) Double immunofluorescence staining of endogenous Msk (red) and NPC (green; by MAb414) in S2R+ cells. (B) S2R+ cells treated with indicated RNAi were immunostained with anti-Msk (Red). The anti-Msk staining was highly specific. The nuclei were marked with DAPI (blue). (C) GFP-MAD+R cells with or without CuSO4 induction to express GFP-MAD and Punt/Tkv were immunostained with anti-Msk (red). The Msk pattern did not change noticeably after GFP-MAD phosphorylation by Punt/Tkv and nuclear accumulation. (D) GFP-MAD+R cells were treated with the indicated RNAi, and after induction of GFP-MAD/Punt/Tkv expression, the cells were stained with anti-Msk (red). Shown are confocal images of GFP-MAD (green), endogenous Msk (red), and DAPI (blue). The percentages of cells exhibiting a nuclear rim pattern of Msk staining (50cells scored) are shown.

Fig 3.14

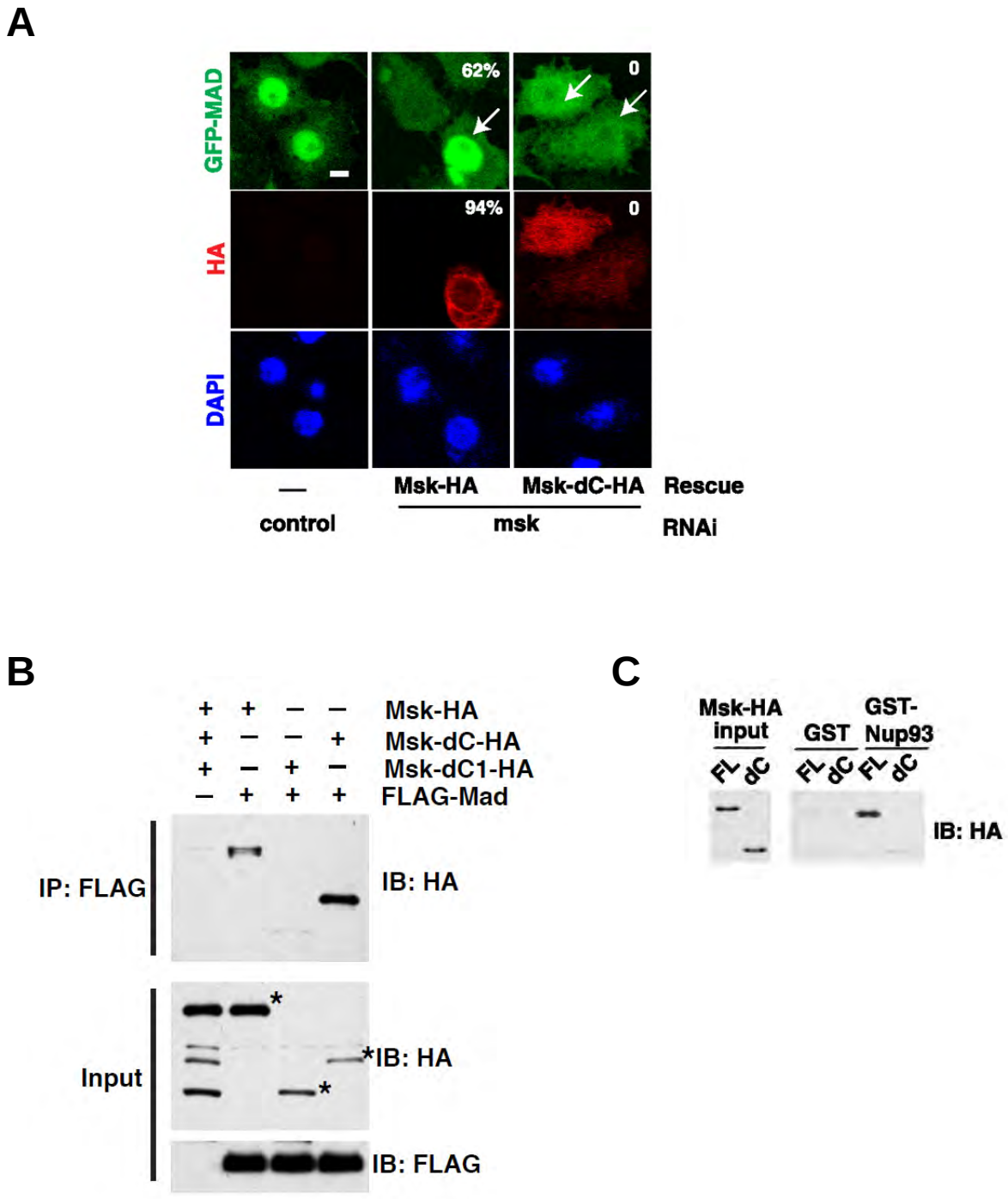
A
GFP-MAD
HA
DAPI
62%
0
94%
0
—
Msk-HA
Msk-dC-HA
Rescue
control
msk
RNAi
B
+ + — — Msk-HA
+ — — + Msk-dC-HA
+ — + — Msk-dC1-HA
— + + + FLAG-Mad
IP: FLAG
IB: HA
Input
*IB: HA
IB: FLAG
C
Msk-HA input
GST
GST-Nup93
FL dC FL dC FL dC
IB: HA

Fig 3.14 The perinuclear localization of Msk is dependent on its C-terminal region and correlates with its ability to import MAD into the nucleus. (A) GFP-MAD+R cells were subjected to RNAi targeting the 5' UTR of Msk and were then transfected with rescue vectors (arrows) expressing HA-tagged full-length Msk or HA-tagged Msk with a C-terminal deletion (Msk-dC; aa 1 to 761). Confocal images of GFP-MAD (green), Msk-HA or Msk-dC-HA (red), and DAPI (blue) are shown. The percentages of cells with normal GFP-MAD nuclear import (green) (50 cells scored) or exhibiting a nuclear rim pattern of Msk staining (red) (50 cells scored) are shown. Bars, 5 μM. (B) MAD interaction with full length and Msk truncation mutants. S2 cells were transiently transfected with indicated vectors (all inducibly expressed). Upon expression, the cell extracts were subject to immunoprecipitation (IP) using anti-FLAG-conjugated agarose beads. The bound proteins were examined by indicated immunoblottings (IB). The positions of full length, Msk-dC (aa1-761) andMsk-dC1 (aa1-600) are marked (*). Msk-dC interacted more strongly with MAD in comparison to full length Msk, while Msk-dC1 interacted much more weakly. (C) Recombinant full-length Msk-HA (FL) and Msk-dC-HA (dC) were purified and tested for direct interaction with GST-Nup93.

Fig 3.15

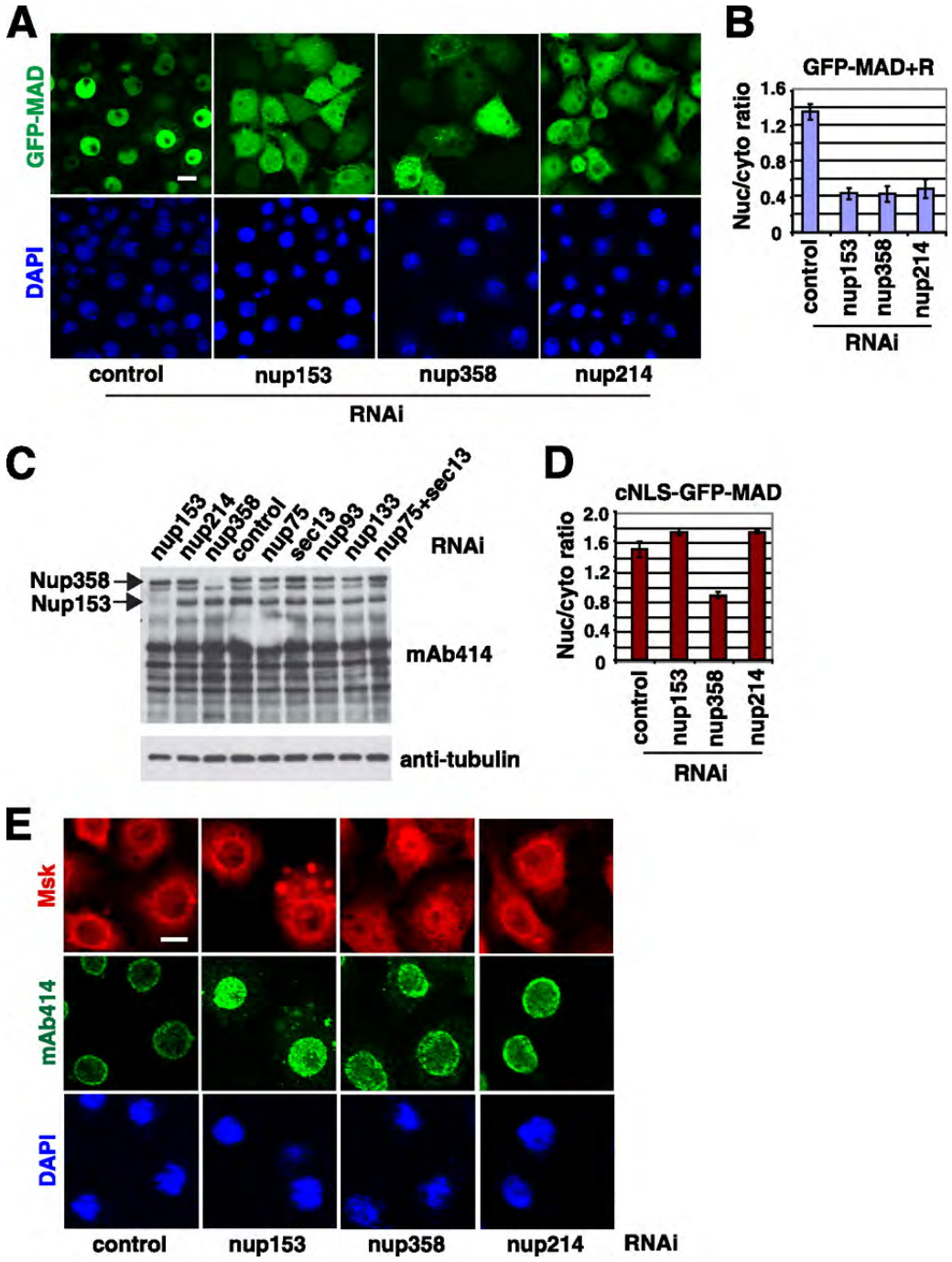
A
GFP-MAD
DAPI
control
nup153
nup358
nup214
RNAi
B
GFP-MAD+R
Nuc/cyto ratio
1.6
1.2
0.8
0.4
0
control
nup153
nup358
nup214
RNAi
C
nup153
nup214
nup358
control
nup75
sec13
nup93
nup133
nup75+sec13
RNAi
Nup358
Nup153
mAb414
anti-tubulin
D
cNLS-GFP-MAD
Nuc/cyto ratio
2.0
1.6
1.2
0.8
0.4
0
control
nup153
nup358
nup214
RNAi
E
Msk
mAb414
DAPI
control
nup153
nup358
nup214
RNAi

Fig 3.15 FG-nucleoporins Nup153, Nup214, and Nup358 serve different functions for the transport of MAD into the nucleus. (A) GFPMAD+R cells were treated with the indicated RNAi and were induced to express GFP-MAD and Punt/Tkv. The distribution patterns of GFP-MAD (green) and DAPI (blue) are shown. Bar, 10 μM. (B) Quantification of the nuclear/cytoplasmic ratio of GFP-MAD signals in panelA. Data are means ±SEs for 3 fields. (C) GFP-MAD+R cells were treated with the indicated RNAi, and the cell extracts were analyzed by immunoblotting with MAb414 and antitubulin. (D) Quantification of the nuclear/cytoplasmic ratio of cNLS-GFP-MAD in cells treated with the indicated RNAi. Data are means ±SEs for 3 fields. (E) S2R+ cells were treated with the indicated RNAi, and the cells were double stained with MAb414 (green) and anti-Msk (red). Bar, 5 μM.

CHAPTER IV: GENETIC INTERACTION BETWEEN MISSHAPEN AND MAD

Summary

The level of TGF-β/BMP signaling through Smad is tightly regulated to ensure proper embryonic patterning and homeostasis. Previously, we showed that Smad activation by TGF-β/BMP is blocked by a highly conserved novel phosphorylation event in the α-helix 1 region of Smad (T312 in *Drosophila* MAD). Through RNAi screening of the kinome, we also uncovered Misshapen (Msn), a member of the Ste20 family of MAP kinase kinase kinase kinase (MAP4K) that is required for T312 phosphorylation of MAD. Here, we describe that targeted expression of an active form of Msn in the wing imaginal disc abrogated MAD activation by Dpp (*Drosophila* BMP). More importantly, reducing the function of endogenous Msn by RNAi in the developing wing resulted in extra vein tissues and this phenotype was suppressed by the loss of one copy of either *mad* or *dpp*. All these data suggest that Msn is a negative regulator of the Dpp/MAD pathway *in vivo*. Therefore, we have uncovered a novel Smad inhibition mechanism that is likely to have important implications in development and diseases.

Introduction:

To identify cross-talk signals that control TGF-β/BMP signaling through regulating phosphorylation status of R-Smads, we systematically searched for novel phosphorylation sites within Smads in *Drosophila* S2 cells. Indeed, we identified a single phosphorylation event in the α-helix 1 region of Smad (T312 in *Drosophila* MAD) that effectively blocks TGF-β/BMP-induced R-Smad phosphorylation at the C-terminus (Kaneko et al. 2011). We also identified the kinase Msn that directly phosphorylates this conserved site in Smads (Kaneko et al. 2011). Here I will address the biological relevance of Msn kinase to Dpp signaling *in vivo*.

A well-established model for studying Dpp signaling *in vivo* is *Drosophila* wing disc (Garcia-Bellido 2009). *Drosophila* wing disc is the precursor organ for the adult wing and arises as an epithelial, sac-like structure at the end of embryogenesis. Key players for patterning the disc are the morphogens Wingless (Wg, along the Dorsal Ventral axis) and Dpp (along the Anterior Posterior axis). Dpp is expressed in the developing wing disc in a narrow stripe of cells in the anterior compartment along the AP compartment boundary. Because it is a secreted ligand, Dpp moves from its source of production into the more lateral areas, forming a concentration gradient and exerting a long-range organizing effect in both compartments. Dpp negatively regulates the expression of the

transcriptional repressor Brinker (Brk), creating a gradient of brk expression that is reciprocal to the Dpp gradient. Brk regulates in a concentration dependent manner the nested expression domains of the genes *sal* and *omb*, which position the longitudinal veins L2 and L5 along the AP axis of the wing.

Dpp/MAD promotes vein differentiation during larval and pupal stages of wing development, as well as wing growth (Martín-Castellanos and Edgar 2002). Loss-of-function mutations at the ligand, receptor or transcription factor of the Dpp signaling pathway resulted in vein deformation and reduced wing size. Conversely, overexpression of Dpp, activated Tkv receptor or degradation-resistant MAD caused increased vein formation (Eivers et al. 2009; Sander et al. 2010). These observations made *Drosophila* wing an excellent model system to study Dpp signaling *in vivo*.

Results:

Ectopic Msn Activity Suppresses MAD Activation *in vivo*

Dpp signaling plays critical roles in development of the imaginal discs in *Drosophila*. Using this model, we tested whether ectopically activated Msn could disrupt Dpp activation of MAD *in vivo*. A constitutively active kinase can be generated by engineering a myristoylation sequence (MGNCLT, derived from the *Drosophila* Src kinase Src42A) to the N-terminus of Msn (myr-Msn). We

therefore generated transgenic flies containing UAS-driven myr-Msn (HA-tagged) and targeted its expression specifically to the wing imaginal disc using the A9-Gal4 driver. Myr-HA-Msn expression was greatest in the dorsal compartment of the wing discs, so we quantified the pC-ter-MAD signal in this segment to evaluate the level of MAD activation by Dpp (**Fig.4.1.A**; anti-HA staining). In the positive control experiment, A9-driven *in vivo* RNAi against *mad* strongly reduced pC-ter-MAD signal in the third instar wing disc (**Fig. 4.1.B** and **Fig. 4.2.A**). Expression of myr-Msn also resulted in a greatly diminished pC-ter-MAD immunostaining signal compared with the negative control (**Fig. 4.1.A** and **Fig 4.2.A**). As expected from the diminished pC-ter-MAD signal, the endogenous mRNA level of dad was significantly reduced in the wing discs with ectopic myr-Msn expression (**Fig. 4.2.B**). These results are consistent with the observations in S2 cells and demonstrate in vivo that activated Msn is an inhibitor of MAD function.

Many A9-Gal4; UAS-myr-msn flies developed to adulthood, but with severe morphological defects in the wing (**Fig. 4.3**, 8 out of 10 adult wings scored). Most notably these wings lost cross vein structure and were grossly deformed (**Fig. 4.3**). The overall phenotypes in the wing somewhat resemble those of an A9-Gal4-driven mad RNAi transgenic line (**Fig. 4.3**). These experiments demonstrated in vivo that activated Msn is a potent inhibitor of MAD function.

Depletion of Msn by RNAi enhanced MAD C-terminal phosphorylation *in vivo*

To more rigorously investigate functional interactions between Msn and MAD/Dpp in vivo, we studied two *Drosophila* lines carrying UAS-msn RNAi constructs. We investigated whether depleting endogenous Msn had specific effect on the pattern of C-terminal phosphorylated MAD in the wing imaginal disc. In third instar wing discs, the stripes of cells with peak pC-ter-MAD signal in the dorsal and ventral compartments of the wing pouch are typically equal in length (**Fig. 4.4.A**). However, upon A9-Gal4-driven RNAi against msn, the dorsal segment of cells with peak pC-ter-MAD expanded significantly in length along the D/V axis (**Fig. 4.4.A**). The expansion was only obvious in the dorsal compartment, which correlates with the knowledge that the A9 promoter drives expression more strongly to the dorsal compartment (**Fig. 4.1.A**) (Haerry et al. 1998). The results are consistent in both msn RNAi lines and the conclusion was confirmed by counting the pixel numbers and calculating the dorsal/ventral ratio of the length (**Fig. 4.2.B**).

Depletion of Msn by RNAi induces extra vein formation

We also investigated whether depleting endogenous Msn had specific effect on

vein formation of the adult wings. Again we used the A9-Gal4 driver to target msn RNAi to the wing. In the UAS-sh-msn-1 line we frequently observed extra vein tissues in the adult wing (**Fig. 4.5.A**, 80%, n = 40). These extra veins are mostly in parallel to and confined between the L2-L5 veins in the adult wings (**Fig. 4.5.A**). This phenotype was also observed in the second line UAS-sh-msn-2 although with a lower penetrance (47%, n=30), probably due to weaker RNAi efficiency. Interestingly, extra vein is a phenotype observed in transgenic flies with MAD or Dpp overexpression, suggesting that msn RNAi may result in ectopic activation of the MAD/Dpp pathway which would be consistent with our model (Eivers et al. 2009; Sander et al. 2010; Sotillos & De Celis 2005).

Extra vein formation caused by Msn RNAi was rescued by *mad* and *dpp* hypomorphic alleles

We further investigated whether weakening MAD/Dpp pathway activity could suppress the msn RNAi phenotype. We first examined the hypomorphic mad^{k00237} allele and verified that flies with the mad^{k00237}/+ genotype by itself had no abnormality in the adult wings. When we crossed A9-Gal4; UAS-sh-msn-1 into the mad^{k00237}/+ background, the loss of one copy of mad suppressed the “extra vein” phenotype (from 80% down to 35%, n = 48, **Fig. 4.5.B**). We also examined a recessive lethal allele dpp^{hr4} (Wharton, Ray, and Gelbart 1993). The dpp^{hr4}/+ line exhibited some abnormalities in the posterior cross-vein and other parts of the

wing, but the vein phenotype is very different from that in the msn RNAi lines (**Fig. 4.5.B**). Again, when we crossed A9-Gal4; UAS-sh-msn-1 into the dpp^{hr4}/+ background, the extra vein phenotype was strongly suppressed (from 80% down to 7%, n = 60, **Fig. 4.5.B**). The vein phenotype associated with the dpp^{hr4}/+ genotype itself was still present (**Fig. 4.5.B**). These observations from the genetic rescue experiments strongly argue that the msn RNAi phenotype in the wing is attributable to enhanced MAD/Dpp activity.

Therefore, from both the vein phenotype and the change in pattern of C-terminal phosphorylated MAD, our experimental evidence is consistent with the notion that Msn is indeed a negative regulator of MAD/Dpp signaling *in vivo*.

Experimental Procedures

Antibodies

The pT312-MAD antibody was raised against the peptide CNRNS[pT]IENTRRHIG. The sera were first absorbed by beads conjugated with the non-phospho peptide, and then affinity purified using the phospho-peptide. pC-ter-Smad1, pC-ter-Smad2 and HA antibodies were from Cell Signaling. Anti-FLAG was purchased from Sigma-Aldrich.

Drosophila transgenic studies

cDNA encoding HA-tagged myr-Msn was cloned into the UASp-pPW vector at its attR1 and attR2 sites through recombination and used to generate the transgenic line UAS-myr-msn (Genetic Services). The following UAS-driven RNAi strains were acquired from the Vienna *Drosophila* RNAi Center: mad shRNA (transformant# 12635), UAS-sh-msn-1 (transformant# 101517), UAS-pp2a-1 and -2 (transformant# 4971 and 4972). UAS-sh-msn-2 was obtained from the *Drosophila* RNAi Screening Center (DRSC) at Harvard Medical School (Trip# JF03219). The A9-Gal4 (Bloomington *Drosophila* Stock Center) was used for driving transgene expression in the wing disc.

In msn RNAi rescue experiments, A9-GAL4 male flies were crossed with FM7a;TW24/TW1; DTS91/CyO (Bloomington Stock Center) female flies. The female progenies with the genotype A9-GAL4/FM7a,TWZ4; +/CyO were crossed with UAS-sh-msn-1 (on the 2nd chromosome) male flies. The male progenies with the genotype A9-GAL4/Y; UAS-sh-msn-1/CyO were crossed with female mad^{k00237}/CyO; hs-mad/TM3,dpp^{hr4}/CyO (from Dr. Stuart Newfeld, Arizona State Univ.), or w^{1118}, respectively. Straight wing female progenies were collected for wing vein pattern imaging. The dissected wings were mounted in halocarbon oil and imaged by a Nikon Eclipes E600 microscope.

Immunofluorescence staining of third instar larvae imaginal discs

The third instar larvae wing discs were dissected and fixed directly in 4% paraformaldehyde/PBS at RT for 30 minutes. The discs were permeabilized in 0.1% Triton X-100/PBS 2 times, 30 minutes each, followed by incubation in 0.1% Triton X-100/PBS/0.5%BSA/2% normal horse serum for 2h. Anti-phospho-SMAD1/5/8 (Cell Signaling, also recognizes phosphor-MAD) was used at 1:300 dilution and anti-HA (Sigma, clone 6E2) was used at 1:200 dilution for overnight incubation at 4 °C. After washing 4 times in 0.1% Triton X-100/PBS, discs were incubated with secondary antibodies: Alex488 anti-rabbit and Alex633 anti-mouse at dilution of 1:1000 for 2h, followed by washing in 0.1% Triton X-100/PBS and mounting in PBS/vectorshield (DAPI included) 1:1. Confocal images of the discs were obtained using Leica DMIRE2. For measuring the length of stripes with peak pC-ter-MAD signal, pixel counts were taken at 16 different locations for each strip along the D/V axis. The ratio of dorsal/ventral stripe length was calculated and statistical significance was determined by t test

Fig 4.1

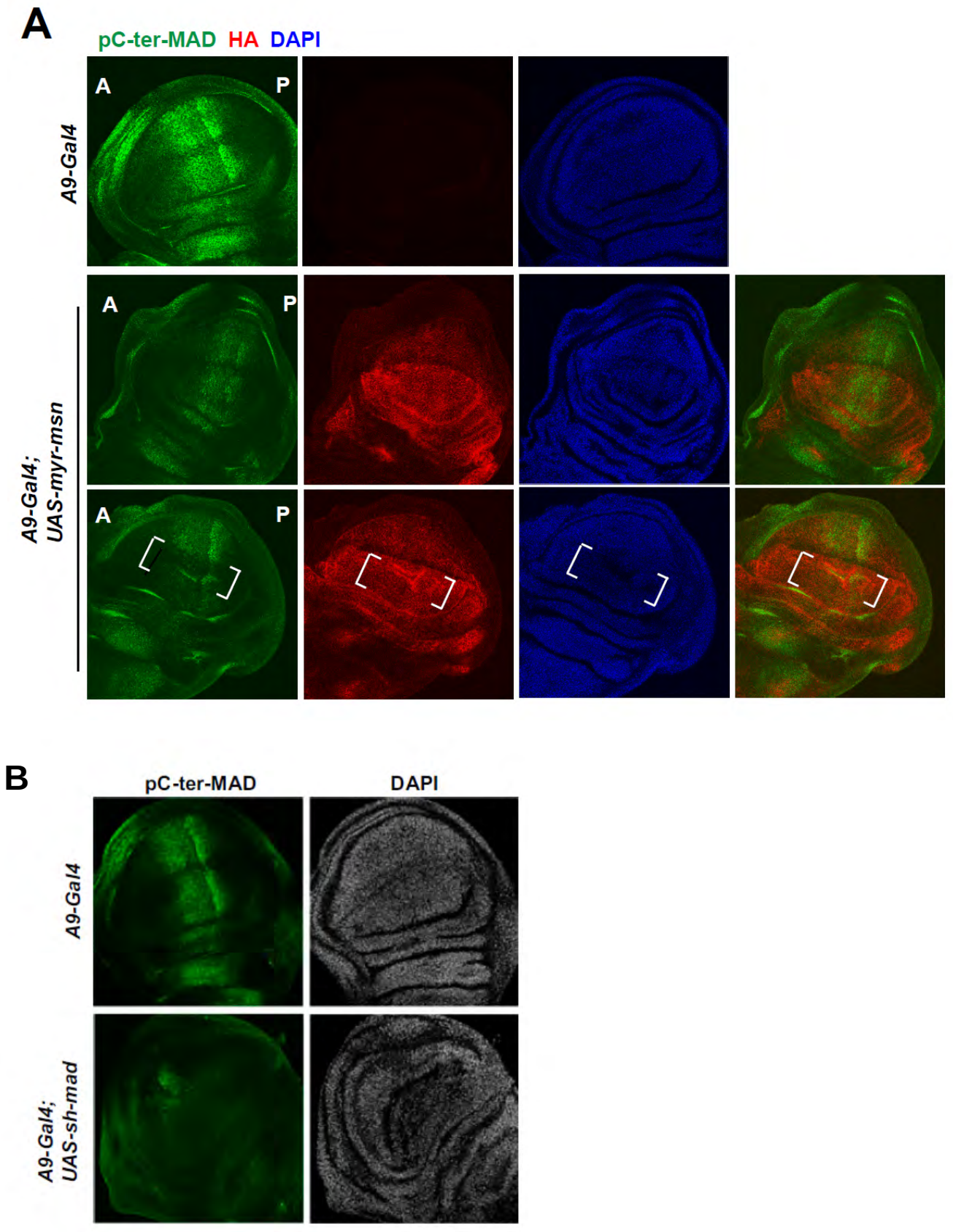
A
pC-ter-MAD HA DAPI
A9-Gal4
A9-Gal4;
UAS-myr-msn
A
P
B
pC-ter-MAD
DAPI
A9-Gal4
A9-Gal4;
UAS-sh-mad

Fig 4.1 E ctopically activated Msn suppresses Dpp/MAD signaling in wing imaginal discs. (A) Third instar wing imaginal discs were double-immunostained with pC-ter-MAD (green) and HA (red). The nuclei were stained by DAPI (blue). The orientation of the wing disc is marked as “A”: anterior; “P”: posterior, and the brackets indicate the dorsal compartment of the wing pouch. (B) Wing imaginal discs from indicated transgenic lines were immunostained with the pC-ter-MAD antibody, and the nuclei were marked by DAPI.

Fig 4.2

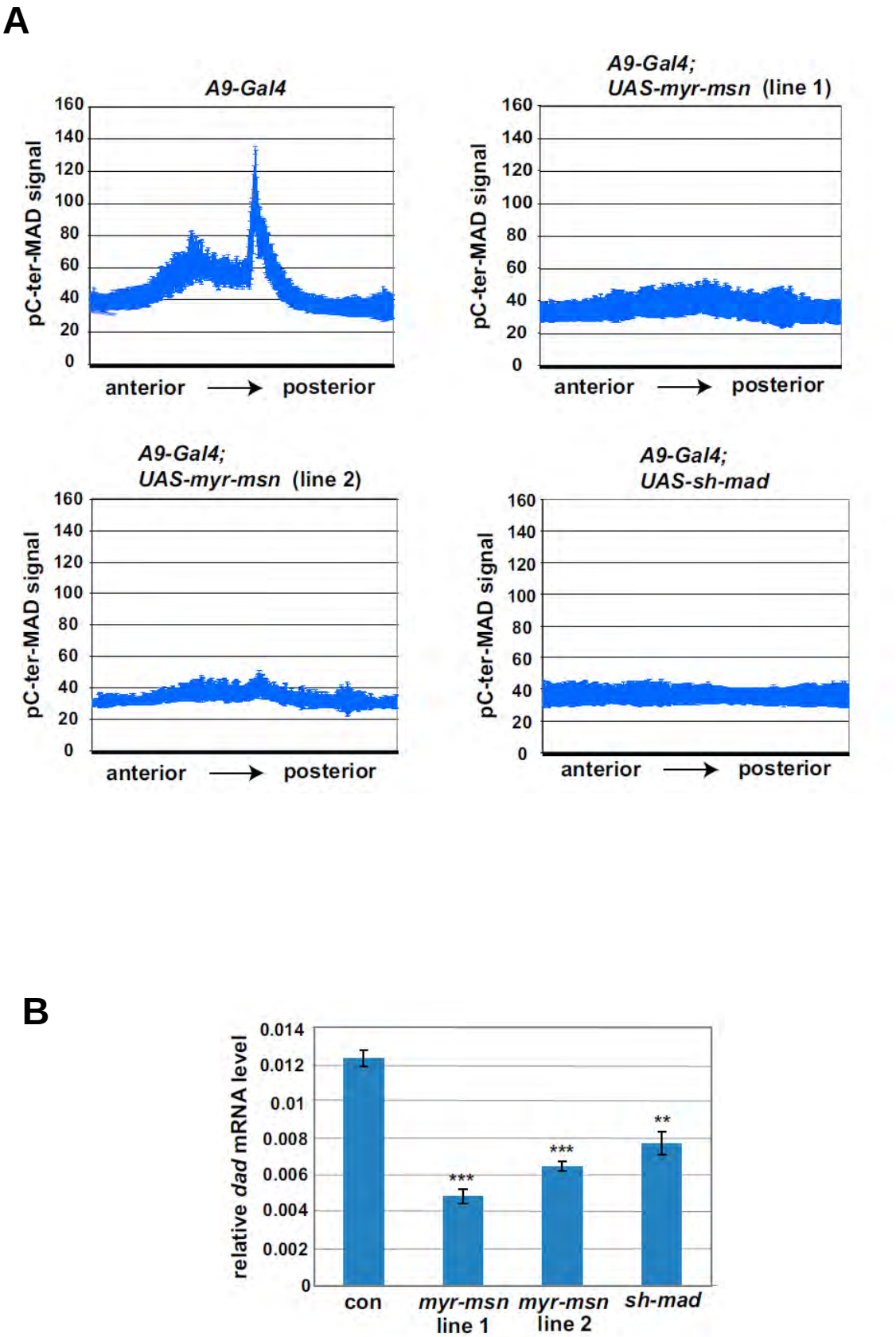
A
A9-Gal4
A9-Gal4;
UAS-myr-msn (line 1)
A9-Gal4;
UAS-myr-msn (line 2)
A9-Gal4;
UAS-sh-mad
pC-ter-MAD signal
0
20
40
60
80
100
120
140
160
anterior
posterior
B
relative dad mRNA level
0
0.002
0.004
0.006
0.008
0.01
0.012
0.014
***
***
**
con
myr-msn line 1
myr-msn line 2
sh-mad

Fig 4.2 Quantification of the effect of Msn overexpression on Dpp/MAD signaling in wing imaginal discs. (A) Confocal images of wing discs immunostained with pC-ter-MAD were analyzed by line scan along the anteroposterior axis to measure the level of pC-ter-MAD staining. The mean ± SD of the values are plotted for the indicated transgenic lines. (B) The mRNA levels of dad in the wing discs from the indicated transgenic lines were measured by qPCR, using rp49 as the internal standard (mean ± SD. ***P < 0.001; **P < 0.01.)

Fig 4.3

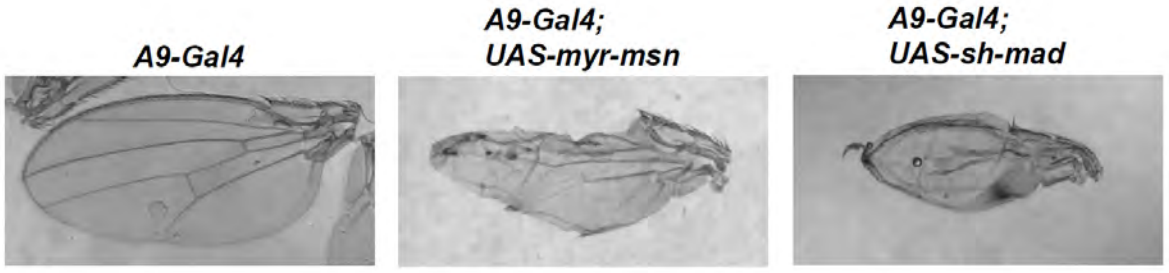

Fig 4.3 E ctopic activated Msn causes morphological defects in the wing. Images of adult wings from indicated control and transgenic flies.

Fig 4.4

A

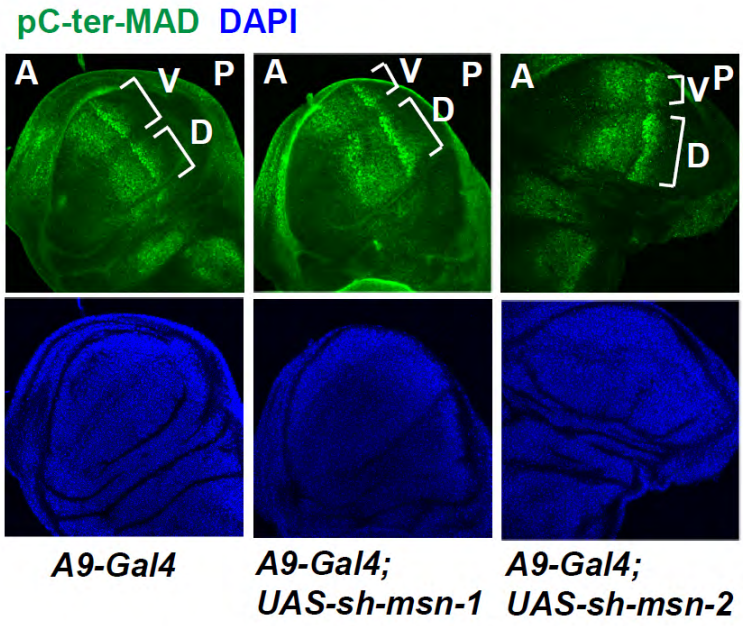
pC-ter-MAD DAPI
A
V
P
D
A9-Gal4
A9-Gal4; UAS-sh-msn-1
A9-Gal4; UAS-sh-msn-2

B

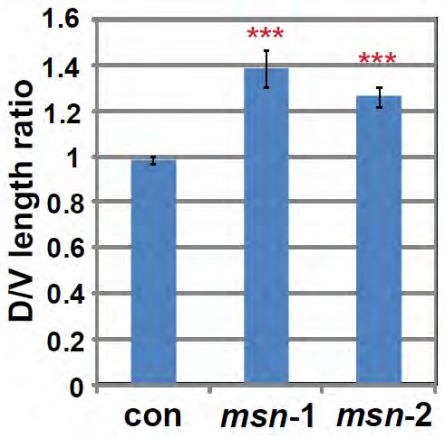
D/V length ratio
1.6
1.4
1.2
1
0.8
0.6
0.4
0.2
0
***
***
con
msn-1
msn-2

Fig 4.4 Depletion of Msn by RNAi enhanced MAD C-terminal phosphorylation *in vivo* (A) Third instar wing discs from the indicated transgenic lines were immunostained with pC-ter-MAD (green) and DAPI (blue). The brackets mark the dorsal and ventral segments of cells with the peak pC-ter-MAD signal. A: anterior; P: posterior; D: dorsal and V: ventral. (B) The dorsal (D) and ventral (V) segments of cells exhibiting the peak pC-ter-MAD signal were measured along the D-V axis by pixel counting. Plotted are the ratios of dorsal/ventral segment length in control and the two msn RNAi lines. *** : $p < 0.001$, $n>22$ in each case.

Fig 4.5

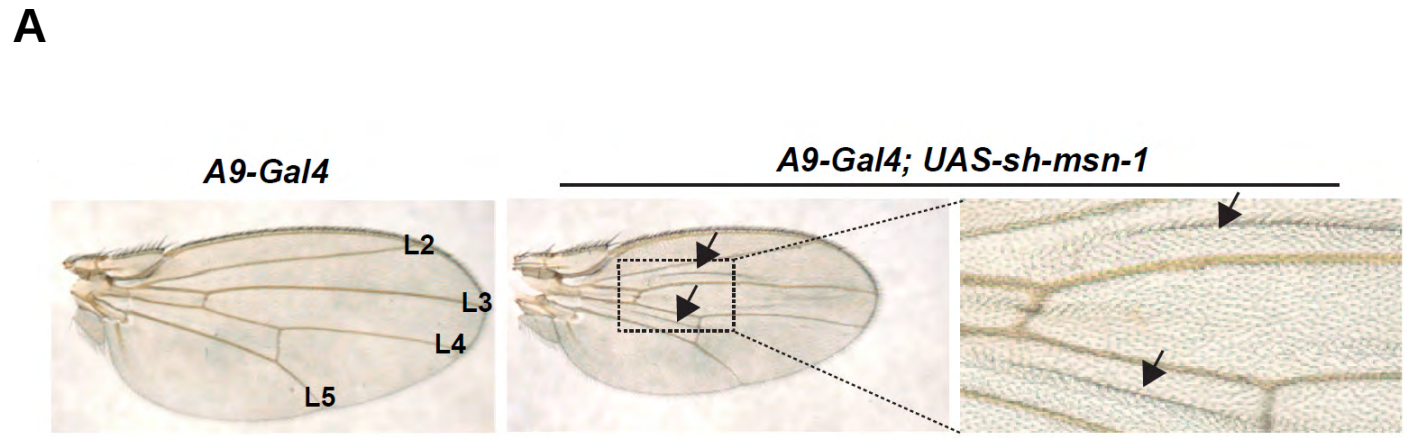
A
A9-Gal4
A9-Gal4; UAS-sh-msn-1
L2
L3
L4
L5

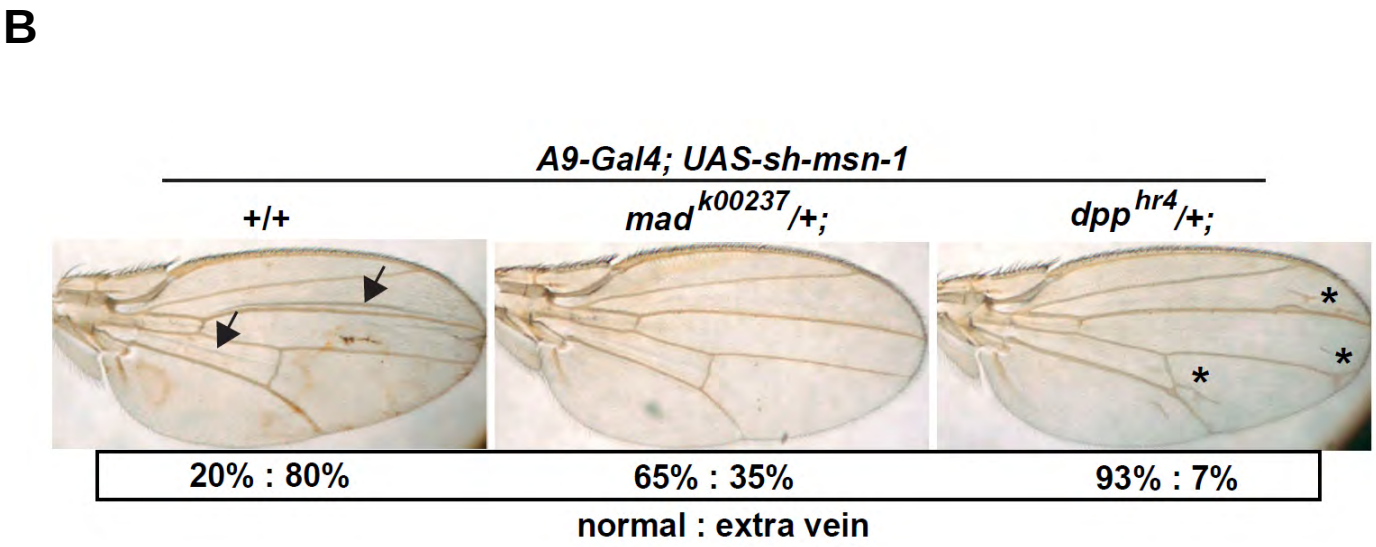
B
A9-Gal4; UAS-sh-msn-1
+/+
mad k00237 /+;
dpp hr4 /+;
20% : 80%
65% : 35%
93% : 7%
normal : extra vein

Fig 4.5 Endogenous Msn negatively regulates Dpp/MAD signaling *in vivo*. (A) The adult wing vein patterns in control and msn RNAi transgenic lines. The arrows point to the extra vein tissues observed upon msn RNAi in the developing wing. (B) The extra vein phenotype was suppressed by the loss of one copy of either *mad* or *dpp*. The percentages of wings exhibiting normal or extra veins are shown in each case. The arrows point to the extra vein and the stars indicate the vein abnormalities found in the dpp^{hr4}/+ line.

CHAPTER V: GENERAL DISCUSSION

5.1 Msk and nuclear import of activated R-Smads

Genome-wide RNAi screening in this study offers a genetic approach to uncover new elements in TGF-β signal transduction. Here we identify and validate with *in vivo* evidence that Msk and its mammalian orthologues Imp7 and 8 are critical components in transporting TGF-β–activated Smads into the nucleus. Biochemical evidence further suggests that Msk/Imp7/8 directly import activated R-Smads as cargoes.

Although there appears to be some discrepancy between these new findings and our previous reports that importins are dispensable for the nuclear import of Smads, these observations can be reconciled (Xu et al. 2002; Xu 2003). Our present and previous studies, based on different approaches, may have revealed different nuclear import mechanisms used by basal and activated Smads to enter the nucleus. There are important differences comparing Smad import with or without TGF-β stimulation. Unphosphorylated Smads are monomers, but phosphorylated Smads are assembled into complexes with Smad4 and are thus much larger in size (Wu et al. 2001; Chacko et al. 2004). Moreover, as phospho-Smads accumulate in the nucleus they have to move across the nuclear pore against an ascending concentration gradient of Smads already in the nucleus,

whereas unphosphorylated Smads never reach a higher concentration in the nucleus than in the cytoplasm. Thus, importing phospho-Smad complexes and unphosphorylated Smad monomers may entail different mechanisms, with or without the participation of importins. Indeed, our RNAi data in both *Drosophila* and mammalian cells suggest that nuclear import of the two forms of Smads is very different regarding the requirement of Msk/Imp7/8. This type of differential requirement for import factors is not unique to Smads. In fact, STATs (signal transducers and activators of transcription) in the interferon pathway are another example in which the latent STATs are imported by an importin-independent mechanism, whereas the phosphorylated STATs depend on importins to accumulate in the nucleus (Meyer et al. 2002). It is also interesting to note that phospho-Smads were still detected in the nucleus upon RNAi-mediated knockdown of Msk/Imp7/8. Although we cannot rule out the trivial explanation that this may be due to incomplete depletion of the targeted proteins, this observation may also suggest additional import mechanisms for activated Smads. We recognize that our previous finding of importin-independent nuclear import of Smads was largely based on an *in vitro* reconstituted nuclear import assay (Xu et al. 2002; Xu 2003). Although this *in vitro* system is widely accepted, it may not fully recapitulate nuclear import of activated Smads in cells (Adam et al. 1992). Based on our RNAi data, regarding the requirement of importins, the conclusion drawn from the *in vitro* import assay may not apply to phospho-Smads in intact

cells.

However, the current study does not necessarily contradict the previous suggestions that direct Smad–nucleoporin interaction is critical for nuclear import of Smads (Xu et al. 2002; Sapkota et al. 2007). Our data showed that Msk/Imp7/8 interact with Smads regardless of their phosphorylation status; thus, additional factors must be involved to explain why only TGF-β/BMP–activated Smads can accumulate in the nucleus. Because basal state Smads are actively exported out of the nucleus (Inman et al. 2002; Xu et al. 2002; Kurisaki et al. 2006), it is possible that retaining only phospho-Smads in the nucleus requires blocking Smad nuclear export, a scenario that has been demonstrated for Smad4 (Chen et al. 2005). This hypothesis would be consistent with findings in live cells, in which TGF-β signaling led to reduced mobility of Smad2 in the nucleus (Schmierer and Hill 2005). Because Msk, Imp7, and Imp8 are shown to be critical for targeting phospho-Smads into the nucleus, it is conceivable that regulatory inputs to this nuclear import factor would impact TGF-β signaling. Although we did not notice any changes in subcellular localization of Msk or Imp7/8 in response to TGF-β in cultured cells (Xu et al. 2007), during *Drosophila* embryonic development, Msk distribution changed between cytoplasm and nucleus in a dynamic fashion (Lorenzen et al. 2001). Moreover, Msk is phosphorylated on tyrosine residues with yet-unknown functional consequences (Lorenzen et al. 2001). If and how

Msk localization is regulated and by what signals are completely open questions at present. A number of mitogen-induced phosphorylation events in the linker region of Smad have been suggested to inhibit TGF-β–induced nuclear translocation of Smads in Xenopus and mammalian cells (Kretzschmar et al. 1997; Kretzschmar et al. 1999; Grimm and Gurdon 2002;Sapkota et al. 2007). Because part of the Imp7/8 binding was mapped to the linker region of Smad3, it will be interesting to determine if linker phosphorylation would affect the interaction between Smads and Imp7/8 and hence the rate of nuclear import. It is also worth noting that Msk has been genetically implicated in the nuclear import of activated ERK in *Drosophila*. Such convergence on the same molecule for nuclear import raises the possibility of cross-talk between MAP kinase and TGF-β pathways at the level of nuclear translocation of key signal transducers.

We demonstrated that R-Smads interaction with Imp7/8 involved the MH1 and linker region. Consistent with this observation, we identified a Lys-rich KKLK motif in MH1 domain that was required for Imp8-driven nuclear import of Smad3. Such a structural element is conserved in R-Smads and Smad4 and indeed is required for nuclear import of Smad4 (Yao et al. 2008). However, the KKLK motif is not sufficient to facilitate nuclear import of a heterologous protein (Yao et al. 2008). In addition, while the KKLK motif is present in Smad2 and Medea, these two Smads are not directly imported by Imp8/Msk (Yao et al. 2008). These

findings indicate the requirement of other structural elements in nuclear import of Smads. These structural elements are likely to reside within the MH1 and the linker region since the C-terminal MH2 domains of Smad2 and Smad3 are almost identical. Smad2 interaction with Imp8 was also significantly weaker when compared with Smad3 (Yao et al. 2008), indicating that other structural elements but not the KKLK motif are more critical in mediating the Smads interaction with Imp8. Indeed, mutating KKLK to AALA did not affect Smad4 interaction with Imp8. Then what is the function of the KKLK motif in the Imp8-mediated nuclear import of Smads? One possibility is that the KKLK motif is critical for Smad import at the steps after Imp8 association. Alternatively, the Imp8-Smad interaction involves the KKLK and other domains, but the KKLK sequence is required for an interaction with Imp8 that would generate an import-competent configuration. It is also possible that another factor binding the KKLK motif is crucial for nuclear import of Smads.

5.2 Nucleoporins and nuclear transport of activated Smads

In this study we also identified a distinct nucleoporin cohort, including both non-FG nucleoporins and FG-nucleoporins, that represents a unique trans-NPC mechanism for signal-activated MAD. Such specificity in nucleoporin utilization may reflect different demands of constitutive and signal-induced nuclear import events. Most unexpectedly, several non-FG nucleoporins, including Sec13, Nup93,

Nup75, and Nup205, appear to act in concert with Msk to selectively transport MAD, but not the cNLS-cargo or basal-state Medea, into the nucleus (Chen and Xu 2010). This is the first indication that beyond their involvement in the general assembly of the NPC, non-FG nucleoporins could play discrete roles in specific nuclear transport pathways. We further identified the distinct functions served by two non-FG scaffold nucleoporins, Sec13 and Nup93, that are critical and specific for the nuclear import of MAD. Our findings suggest a novel functional interplay between the MAD nuclear import machinery and the NPC.

Sec13 is part of the Nup107-160 complex, and Nup93 is part of the Nup53-93 complex; both are scaffolds of the NPC. We emphasize that our findings are not in conflict with the established roles of Sec13 and Nup93 in general NPC assembly but broaden the functions of these non-FG nucleoporins to specific nuclear import pathways. It was somewhat surprising that depletion of Nup75 and Sec13 had little impact on MAb414 staining and nuclear envelope permeability, in contrast to the more severe phenotypes exhibited by the knockdown of other components in the Nup107-160 complex (i.e., *nup145*, *nup107*, and *nup160*). We could hardly detect Sec13 after RNAi, so the lack of impact on MAb414 staining could not be attributed to incomplete depletion of Sec13. Therefore, our observations suggest that knocking down individual components of the Nup107-160 complex could lead to different phenotypes regarding MAD nuclear import, the MAb414 staining

pattern, and the permeability of the NPC, arguing that each nucleoporin in the Nup107-160 complex serves distinct functions.

The challenging question ahead is how these non-FG nucleoporins mediate the nuclear import of MAD. Interestingly, Sec13 has been shown to dynamically transit between the cytoplasm and the nucleus, and endogenous Sec13 is partitioned among the NPC, the intranuclear space, and the endoplasmic reticulum (ER) (Enninga, Levay, and Fontoura 2003). With our observation that Sec13 preferentially interacts with phosphorylated/activated MAD, it is possible that Sec13 could act as an active trafficker rather than as a stationary component of the NPC to mediate the nuclear import of MAD. Whether phosphorylated MAD reaches the NPC via random diffusion or is guided by particular factors remains an open question and it will be interesting to investigate whether Sec13 might be involved.

Msk has a characteristic nuclear rim localization pattern that we show here is important for its ability to transport MAD into the nucleus. Two of the nucleoporins that are required for MAD nuclear import, Nup93 and Nup358, appear to be responsible for targeting Msk to the nuclear periphery. Deletion of the C-terminal region of Msk disrupted its nuclear rim distribution and also significantly weakened the Msk-Nup93 interaction. It is unclear whether the

same C-terminal deletion of Msk would affect the Msk-Nup358 interaction as well. Thus, the question remains, between Nup93 and Nup358, which one is more directly responsible for recruiting Msk to the nuclear periphery. Interestingly, Impβ is also concentrated to the nuclear periphery, like Msk, but such localization has been shown to depend on Nup153 instead of Nup93 and Nup358 (Sabri et al. 2007). Therefore, different importins are apparently recruited to the NPC through distinct nucleoporins, another direct indication that various nuclear import pathways operate through different modes of interaction with the NPC.

As exemplified by Sec13, Nup93, and Nup358, the nucleoporins implicated in MAD nuclear import serve distinct functions at different stages of the import process. While our data clearly suggest that Sec13 and Nup93 play roles distinct from those of the other components of the Nup107-160 or Nup53-93 complex, we do not suggest that they function in isolation from the other nucleoporins. Nor can we at this point rule out a possible requirement for other nucleoporins in the nuclear import of MAD. Nevertheless, the direct physical interaction between Sec13/Nup93 and MAD or Msk, as well as the very selective impact of Sec13 and Nup93 RNAi on the nuclear import of MAD, but not other cargoes, is consistent with our interpretation that Sec13 and Nup93 are directly involved in the nuclear import of MAD.

Our genetic dissection of the Smad nuclear import pathway has important implications for the model of NPC structure and function. The findings in this study depart from the current dogma that puts only FG-nucleoporins at the center of the NPC-importin interplay. The diversity in trans-NPC routes and the pathway-specific involvement of non-FG nucleoporins need to be incorporated into models of NPC function in nuclear transport. It is increasingly clear that there are multiple distinct routes through the NPC that are taken by different importin/cargo complexes. The question, then, is how the NPC can accommodate these different passages. X-ray crystal structure analysis and electron microscopy have suggested that the Nup107-160 complex assumes a Y-shaped topography, raising speculations that such a porous assembly may leave room for additional trans-NPC passages besides the central tunnel, which is densely populated by FG-nucleoporins (Boehmer et al. 2003). It is also plausible that non-FG nucleoporins regulate the transport when cargoes are translocated through the peripheral transport route in the central tunnel that has recently been identified (**Fig 1.6 D**) (Ma and Yang 2010; Yamada et al. 2010). One could also speculate that maybe the NPC can assume different configurations upon receiving different importin/cargo complexes to enable the translocation process.

5.3 Biological Implications of Smad Inhibition by Msn Kinases

The Smad inhibition mechanism uncovered here identifies Msn kinases as new

modulators controlling the magnitude of TGF-β/BMP signaling. The physiological importance of Msn in developmental processes such as dorsal closure and planar polarity has been documented in *Drosophila* and vertebrates, but the direct Msn targets relevant to these processes remain unclear (Paricio et al. 1999; Su et al. 1998; Xue et al. 2001). Our finding that Smad is a substrate of Msn may help understand phenotypes exhibited by animals with Msn loss-of-function mutations. For example, Dpp is also a major regulator of dorsal closure in *Drosophila* embryonic development, so the dorsal closure defects observed in *msn* mutant animals may be partly attributable to dysregulation of Dpp signaling (Su et al. 1998; Xue et al. 2001; Harden 2002). Msn has been suggested to be an upstream activator of the MAP kinase JNK, by activating the intermediate MAP3Ks and MAP2Ks, although the direct target of Msn in this case was not clear (Su et al. 1997; Su et al. 1998; Garlena et al. 2010). In mammalian cells, a recent RNAi screen has identified MAP4K4 as an inhibitor of adipogenesis, mTOR signaling and insulin responses (Tang et al. 2006; Tesz et al. 2007; Guntur et al. 2009). In separate RNAi screens, MAP4K4 was found to promote tumor cell motility (Collins et al. 2006) and MINK1 was identified as a mediator of Ras induced cell growth arrest (Nicke et al. 2005). More recently, TNIK was reported to be an activator of Wnt target genes by interacting with and phosphorylating the transcription factor TCF4 (Mahmoudi et al. 2009; Shitashige et al. 2010). Therefore, the Msn kinases are critical signaling nodes that in parallel to

repressing Smad may impact multiple pathways, giving rise to complex pathophysiological outcomes.

The underlying molecular mechanism that activates Msn catalytic function remains largely unknown. Addressing this question is critical for understanding the physiological context that stimulates Msn-mediated Smad inhibition. Interestingly we found that Msn is activated when targeted to the cell membrane by a myristoylation sequence (Kaneko et al. 2011). Perhaps membrane association facilitates phosphorylation/activation of Msn kinases by a membrane-bound kinase or interaction with certain membrane-bound proteins that turn on the Msn kinase activity. Our observations present a stepping-stone to further dissect the upstream regulatory inputs that are imposed on Msn. The biological outcomes of TGF-β/BMP are critically dependent on the cellular contexts.

This current study uncovered a negative impact on Smad from the Msn kinases. Understanding the molecular control of this Smad inhibition pathway will advance our knowledge on TGF-β/BMP integration with other signals during embryonic patterning as well as in diseases such as cancer.

5.4 Conclusions and Remaining Questions:

Using nuclear translocation of MAD as the readout in a systemic RNAi screen in

Drosophila, I have identified two critical elements required in nuclear import of Dpp-activated MAD: the importin Msk and a unique subset of nucleoporins, including Nup75, Sec13, Nup93, Nup205 and Nup50 (Xu et al. 2007; Chen and Xu 2010). While this systemic approach is powerful in gene function studies and gene discovery, the RNAi screening associates with inherent limitations. In particular, off-target effects with the use of long dsRNAs in *Drosophila* cells can contribute to a higher rate of false positives. Fortunately, the long dsRNA library DRSC 2.0 collection that we used for the screen has improved dsRNA designs to minimize the prevalence of OTEs. We also used a second independent dsRNA to eliminate OTEs in validation of a potential hit. Moreover, random errors that cannot be prevented lead to non-specific phenotypes in particular wells and contribute to a higher rate of false positives or false negatives. They arise through occasional malfunctions of liquid-handling robotics, random loss of cells during the processing steps or changes in concentrations due to evaporation in certain wells and occasional defects in tissue-culture plates.

Until recently, systemic RNAi screening in *Drosophila* has been limited to a cell culture approach, even though transgenic RNAi libraries had been assembled in Vienna *Drosophila* RNAi Center and *Drosophila* RNAi Screening Center at Harvard Medical School. These libraries contain transgenic fly strains with an RNAi hairpin under UAS-Gal4 control. Although genome-wide screens *in vivo*

with these libraries will be far more labor-intensive and time-consuming than the cell-based approaches, they will provide the opportunity to examine a wide of complex phenotypes in the whole animal or in a particular development stage in a particular tissue. Additionally, these transgenic RNAi lines can be used in rapid validating *in vivo* the involvement of candidate genes identified in cell-based RNAi screens. For example, in the Chapter IV, I examined the in *vivo* function of Msn kinase in Dpp signaling in *Drosophila* wings by using UAS-msn RNAi transgenic flies. Similar experiments can be applied to the nucleoporins that I identified in the screen to further investigate their biological relevance to Dpp signaling. Specific functions of both FG and non-FG nucleoporins have been implicated in cancers and cell differentiation (Xu and Powers 2009; Lupu et al. 2008; Xianqin Zhang et al. 2008). Whether this unique subset of nucleoporins that regulate activated MAD nuclear import will impact Dpp signaling in *Drosophila* development, oncogenesis or cell differentiation is currently an open question.

Collectively, my findings delineated unique importin and nucleoprins for Smad nuclear import pathway, suggesting a novel trans-NPC route (Xu et al. 2007; Chen and Xu 2010). One appealing model is that Msk is positioned by Nup93 and Nup358 to the vicinity of NPC, and perhaps Sec13 engages phosphorylated MAD and, through its own trafficking ability, delivers MAD to Msk. The MAD-Msk import complex then translocate across the NPC by taking the peripheral transport

route where the MAD-Msk import complex interact with both non-FG nucleoporins and FG nucleoprins. This new knowledge has revealed novel molecular mechanisms involved with nuclear transport and TGF-β signaling and in the future, will broaden our understanding of the role of TGF-β in development as well as in disease such as cancer.

References:

Adam, S. A, and L. Gerace. 1991. “Cytosolic proteins that specifically bind nuclear location signals are receptors for nuclear import.” *Cell* 66(5): 837-47.

Affolter, M., and K. Basler. 2007. “The Decapentaplegic morphogen gradient: from pattern formation to growth regulation.” *Nature Reviews Genetics* 8 (9): 663–674.

Akey, C. W., and D. S. Goldfarb. 1989. “Protein import through the nuclear pore complex is a multistep process.” *The Journal of Cell Biology* 109(3): 971.

Alarcón, C., A. I. Zaromytidou, Q. Xi, S. Gao, J. Yu, S. Fujisawa, A. Barlas, A. N. Miller, K. Manova-Todorova, and M. J. Macias. 2009. “Nuclear CDKs Drive Smad Transcriptional Activation and Turnover in BMP and TGF-β Pathways.” *Cell* 139(4) (November): 757-769.

Alber, F., S. Dokudovskaya, L. M. Veenhoff, W. Zhang, J. Kipper, D. Devos, A. Suprapto, et al. 2007. “The molecular architecture of the nuclear pore complex.” *Nature* 450(7170) (November): 695-701.

Allen, N. P. C. 2001. “Proteomic Analysis of Nucleoporin Interacting Proteins.” *Journal of Biological Chemistry* 276(31) (May): 29268-29274.

Aragon, E., N. Goerner, A.-I. Zaromytidou, Q. Xi, A. Escobedo, J. Massague, and M. J. Macias. 2011. “A Smad action turnover switch operated by WW domain readers of a phosphoserine code.” *Genes & Development* 25 (June 17): 1275-1288.

Armknecht, S., M. Boutros, A. Kiger, K. Nybakken, B. Mathey-Prevot, and N. Perrimon. 2005. “High-throughput RNA interference screens in Drosophila tissue culture cells.” *Methods Enzymol* 392: 55-73.

Batut, J., M. Howell, and C. S. Hill. 2007. “Kinesin-Mediated Transport of Smad2 Is Required for Signaling in Response to TGF-β Ligands.” *Developmental Cell* 12(2) (February): 261-274.

Boehmer, T., J. Enninga, S. Dales, G. Blobel, and H. Zhong. 2003. “Depletion of a single nucleoporin, Nup107, prevents the assembly of a subset of nucleoporins into the nuclear pore complex.” *Proceedings of the National Academy of Sciences* 100(3): 981.

Brickner, J. H., and P. Walter. 2004. “Gene recruitment of the activated INO1 locus to the nuclear membrane.” *PLoS Biology* 2(11): e342.

Brohawn, S. G., N. C. Leksa, E. D. Spear, K. R. Rajashankar, and T. U. Schwartz. 2008. “Structural evidence for common ancestry of the nuclear pore complex and vesicle coats.” *Science* 322(5906): 1369.

Bunch, T. A, Y. Grinblat, and L. S Goldstein. 1988. “Characterization and use of the Drosophila metallothionein promoter in cultured Drosophila melanogaster cells.” *Nucleic Acids Res.* 16(3): 1043-61.

Capelson, M., Y. Liang, R. Schulte, W. Mair, U. Wagner, and M. W. Hetzer. 2010. “Chromatin-Bound Nuclear Pore Components Regulate Gene Expression in Higher Eukaryotes.” *Cell* 140(3) (February): 372-383.

Casolari, J. M. 2005. “Developmentally induced changes in transcriptional program alter spatial organization across chromosomes.” *Genes & Development* 19(10) (May): 1188-1198.

Chacko, B. M., B. Y. Qin, A. Tiwari, G. Shi, S. Lam, L. J. Hayward, M. De Caestecker, and K. Lin. 2004. “Structural Basis of Heteromeric Smad Protein Assembly in TGF-β Signaling.” *Molecular Cell* 15(5): 813–823.

Chen, H. B., J. G. Rud, K. Lin, and L. Xu. 2005. “Nuclear Targeting of Transforming Growth Factor-β-activated Smad Complexes.” *Journal of Biological Chemistry* 280(22) (March): 21329-21336.

Chen, X., and L. Xu. 2010. “Specific Nucleoporin Requirement for Smad Nuclear Translocation.” *Molecular and Cellular Biology* 30 (June 14): 4022-4034.

Chuderland, D., A. Konson, and R. Seger. 2008. “Identification and Characterization of a General Nuclear Translocation Signal in Signaling Proteins.” *Molecular Cell* 31 (September): 850-861.

Clemens, J.C., C.A. Worby, N. Simonson-Leff, M. Muda, T. Maehama, B.A. Hemmings, and J.E. Dixon. 2000. “Use of double-stranded RNA interference in Drosophila cell lines to dissect signal transduction pathways.” *Proceedings of the National Academy of Sciences* 97(12): 6499.

Collins, C. S., J. Hong, L. Sapinoso, Y. Zhou, Z. Liu, K. Micklash, P. G. Schultz, and G. M. Hampton. 2006. “A small interfering RNA screen for modulators of tumor cell motility identifies MAP4K4 as a promigratory kinase.” *Proceedings of the National Academy of Sciences of the United States of America* 103(10): 3775.

Cronshaw, J. M., A. N. Krutchinsky, W. Zhang, B. T. Chait, and M. J. Matunis. 2002. “Proteomic analysis of the mammalian nuclear pore complex.” *The Journal of Cell Biology* 158(5): 915.

Dai, F., X. Lin, C. Chang, and X. H. Feng. 2009. “Nuclear Export of Smad2 and Smad3 by RanBP3 Facilitates Termination of TGF-β Signaling.” *Developmental Cell* 16(3) (March): 345-357.

Dean, K. A., O. von Ahsen, D. Görlich, and H. M. Fried. 2001. “Signal recognition particle protein 19 is imported into the nucleus by importin 8 (RanBP8) and transportin.” *Journal of Cell Science* 114(19): 3479.

Devos, D., S. Dokudovskaya, F. Alber, R. Williams, B. T. Chait, A. Sali, and M. P. Rout. 2004. “Components of Coated Vesicles and Nuclear Pore Complexes Share a Common Molecular Architecture.” *PLoS Biology* 2(12): e380.

Devos, D., S. Dokudovskaya, R. Williams, F. Alber, N. Eswar, B. T. Chait, M. P. Rout, and A. Sali. 2006. “Simple fold composition and modular architecture of the nuclear pore complex.” *Proceedings of the National*

Academy of Sciences of the United States of America 103(7): 2172.

ten Dijke, P., M. J. Goumans, F. Itoh, and S. Itoh. 2002. “Regulation of cell proliferation by Smad proteins.” *Journal of Cellular Physiology* 191(1) (April): 1-16.

Dupont, S., A. Mamidi, M. Cordenonsi, M. Montagner, L. Zacchigna, M. Adorno, G. Martello, et al. 2009. “FAM/USP9x, a Deubiquitinating Enzyme Essential for TGFβ Signaling, Controls Smad4 Monoubiquitination.” *Cell* 136(1) (January): 123-135. doi:10.1016/j.cell.2008.10.051.

Dziembowski, A., A. P. Ventura, B. Rutz, F. Caspary, C. Faux, F. Halgand, O. Laprévote, and B. Séraphin. 2004. “Proteomic analysis identifies a new complex required for nuclear pre-mRNA retention and splicing.” *The EMBO Journal* 23(24): 4847–4856.

Eivers, E., L. C. Fuentealba, V. Sander, J. C. Clemens, L. Hartnett, and E. M. De Robertis. 2009. “Mad Is Required for Wingless Signaling in Wing Development and Segment Patterning in Drosophila.” Ed. M. H. Sham. *PLoS ONE* 4(8) (August): e6543.

Enninga, J., A. Levay, and B. Fontoura. 2003. “Sec13 shuttles between the nucleus and the cytoplasm and stably interacts with Nup96 at the nuclear pore complex.” *Molecular and Cellular Biology* 23(20): 7271.

Fassati, A., D. Görlich, I. Harrison, L. Zaytseva, and J. M. Mingot. 2003. “Nuclear import of HIV-1 intracellular reverse transcription complexes is mediated by importin 7.” *The EMBO Journal* 22(14): 3675–3685.

Feldherr, C. M., and D. Akin. 1997. “The location of the transport gate in the nuclear pore complex.” *Journal of Cell Science* 110(24): 3065.

Freedman, N. D., and K. R. Yamamoto. 2004. “Importin 7 and importin-alpha/importin-beta are nuclear import receptors for the glucocorticoid receptor.” *Molecular Biology of the Cell* 15(5): 2276.

Frey, S., and D. Görlich. 2007. “A Saturated FG-Repeat Hydrogel Can Reproduce the Permeability Properties of Nuclear Pore Complexes.” *Cell* 130(3) (August): 512-523.

Frey, S., and D. Görlich. 2009. “FG/FxFG as well as GLFG repeats form a selective permeability barrier with self-healing properties.” *The EMBO Journal* 28(17): 2554–2567.

Fuentealba, L. C., E. Eivers, A. Ikeda, C. Hurtado, H. Kuroda, E. M. Pera, and E. M. De Robertis. 2007. “Integrating Patterning Signals: Wnt/GSK3 Regulates the Duration of the BMP/Smad1 Signal.” *Cell* 131(5) (November): 980-993.

Galy, V., O. Gadal, M. Fromont-Racine, A. Romano, A. Jacquier, and U. Nehrbass. 2004. “Nuclear retention of unspliced mRNAs in yeast is mediated by perinuclear Mlp1.” *Cell* 116(1): 63–73.

Galy, V., I. W. Mattaj, and P. Askjaer. 2003. “Caenorhabditis elegans Nucleoporins Nup93 andNup205 Determine the Limit of Nuclear Pore ComplexSize

Exclusion In Vivo." *Molecular Biology of the Cell* 14: 5104-5115.

Gao, S., C. Alarcón, G. Sapkota, S. Rahman, P. Y. Chen, N. Goerner, M. J. Macias, H. Erdjument-Bromage, P. Tempst, and J. Massagué. 2009. "Ubiquitin Ligase Nedd4L Targets Activated Smad2/3 to Limit TGF-β Signaling." *Molecular Cell* 36(3) (November): 457-468.

Garcia-Bellido, A. 2009. "The cellular and genetic bases of organ size and shape in Drosophila." *The International Journal of Developmental Biology* 53 (8-9-10): 1291-1303.

Garlena, R. A., R. L. Gonda, A. B. Green, R. M. Pileggi, and B. Stronach. 2010. "Regulation of mixed-lineage kinase activation in JNK-dependent morphogenesis." *Journal of Cell Science* 123(18): 3177.

Goldfarb, D. S., J. Gariepy, G. Schoolnik, and R. D. Kornberg. 1986. "Synthetic peptides as nuclear localization signals." *Nature* 322(6080): 641-4.

Görlich, D., M. Dabrowski, F. R. Bischoff, U. Kutay, P. Bork, E. Hartmann, S. Prehn, and E. Izaurralde. 1997. "A novel class of RanGTP binding proteins." *The Journal of Cell Biology* 138(1): 65.

Gorlich, D., N. Pante, U. Kutay, U. Aebi, and F. R. Bischoff. 1996. "Identification of different roles for RanGDP and RanGTP iin nuclear protein import." *The EMBO Journal* 15(20): 5584-5594.

Gorlich, D., S. Prehn, R. A Laskey, and E. Hartmann. 1994. "Isolation of a protein that is essential for the first step of nuclear protein import." *Cell* 79(5): 767-78.

Grimm, O. H., and J. B. Gurdon. 2002. "Nuclear exclusion of Smad2 is a mechanism leading to loss of competence." *Nature Cell Biology* 4(7) (June): 519-522.

Guntur, K. V. P., A. Guilherme, L. Xue, A. Chawla, and M. P. Czech. 2009. "Map4k4 Negatively Regulates Peroxisome Proliferator-activated Receptor (PPAR) Protein Translation by Suppressing the Mammalian Target of Rapamycin (mTOR) Signaling Pathway in Cultured Adipocytes." *Journal of Biological Chemistry* 285(9) (December): 6595-6603.

Guo, X., A. Ramirez, D. S Waddell, Z. Li, X. Liu, and X. F. Wang. 2008. "Axin and GSK3β control Smad3 protein stability and modulate TGFβ signaling." *Genes & Development* 22: 106-120.

Haerry, T. E., O. Khalsa, M. B. O'Connor, and K. A. Wharton. 1998. "Synergistic signaling by two BMP ligands through the SAX and TKV receptors controls wing growth and patterning in Drosophila." *Development* 125 (20): 3977.

Harden, N. 2002. "Signaling pathways directing the movement and fusion of epithelial sheets: lessons from dorsal closure in Drosophila." *Differentiation* 70(4-5): 181–203.

Haucke, V. 2003. "Vesicle budding: a coat for the COPs." *Trends in Cell Biology* 13(2): 59–60.

Hawryluk-Gara, L. A., E. K. Shibuya, and R. W. Wozniak. 2005. “Vertebrate Nup53 interacts with the nuclear lamina and is required for the assembly of a Nup93-containing complex.” *Molecular Biology of the Cell* 16(5): 2382.

Hsia, K. C., P. Stavropoulos, G. Blobel, and A. Hoelz. 2007. “Architecture of a Coat for the Nuclear Pore Membrane.” *Cell* 131(7) (December): 1313-1326.

Hutten, S., S. Wälde, C. Spillner, J. Hauber, and R. H. Kehlenbach. 2009. “The nuclear pore component Nup358 promotes transportin-dependent nuclear import.” *Journal of Cell Science* 122(8): 1100.

Imoto, S. 2003. “Regulation of Transforming Growth Factor- Signaling by Protein Inhibitor of Activated STAT, PIASy through Smad3.” *Journal of Biological Chemistry* 278(36) (June): 34253-34258.

Inman, G. J., F. J. Nicolás, and C. S. Hill. 2002. “Nucleocytoplasmic shuttling of Smads 2, 3, and 4 permits sensing of TGF-β receptor activity.” *Molecular Cell* 10(2): 283–294.

Jäkel, S., W. Albig, U. Kutay, F. R. Bischoff, K. Schwamborn, D. Doenecke, and D. Görlich. 1999. “The importin-β/importin 7 heterodimer is a functional nuclear import receptor for histone H1.” *The EMBO Journal* 18(9): 2411–2423.

James, B. P., T. A. Bunch, S. Krishnamoorthy, L. A. Perkins, and D. L. Brower. 2007. “Nuclear Localization of the ERK MAP Kinase Mediated by Drosophila αPS2βPS Integrin and Importin-7.” *Molecular Biology of the Cell* 18(10): 4190.

Jeudy, S., and T. U. Schwartz. 2007. “Crystal Structure of Nucleoporin Nic96 Reveals a Novel, Intricate Helical Domain Architecture.” *Journal of Biological Chemistry* 282(48) (September): 34904-34912.

Jin, Q., W. Ding, and K. M. Mulder. 2007. “Requirement for the Dynein Light Chain km23-1 in a Smad2-dependent Transforming Growth Factor-beta Signaling Pathway.” *Journal of Biological Chemistry* 282(26) (April): 19122-19132.

Jin, Q., G. Gao, and K. M. Mulder. 2009. “Requirement of a dynein light chain in TGFβ Smad3 signaling.” *Journal of Cellular Physiology* 221(3): 707–715.

Joseph, J., and M. Dasso. 2008. “The nucleoporin Nup358 associates with and regulates interphase microtubules.” *FEBS letters* 582(2): 190–196.

Joseph, J., S. T. Liu, S. A. Jablonski, T. J. Yen, and M. Dasso. 2004. “The RanGAP1-RanBP2 complex is essential for microtubule-kinetochore interactions in vivo.” *Current Biology* 14(7): 611–617.

Kalverda, B., H. Pickersgill, V. V. Shloma, and M. Fornerod. 2010. “Nucleoporins Directly Stimulate Expression of Developmental and Cell-Cycle Genes Inside the Nucleoplasm.” *Cell* 140(3) (February): 360-371.

Kamiya, Y., K. Miyazono, and K. Miyazawa. 2008. “Specificity of the inhibitory

effects of Dad on TGF-[beta] family type I receptors, Thickveins, Saxophone, and Baboon in Drosophila." *FEBS letters* 582(17): 2496–2500.

Kaneko, S., X. Chen, P. Lu, X. Yao, T. G. Wright, M. Rajurkar, K.-i. Kariya, J. Mao, Y. T. Ip, and L. Xu. 2011. "Smad inhibition by the Ste20 kinase Misshapen." *Proceedings of the National Academy of Sciences* 108(27) (June): 11127-11132.

Kang, Y., C. R. Chen, and J. Massagué. 2003. "A Self-Enabling TGF-β Response Coupled to Stress Signaling:: Smad Engages Stress Response Factor ATF3 for Id1 Repression in Epithelial Cells." *Molecular Cell* 11(4): 915–926.

Kretzschmar, M., J. Doody, and J. Massague. 1997. "Opposing BMP and EGF signalling pathways converge on the TGF-β family mediator Smad1." *Nature* 389(6651): 618–622.

Kretzschmar, M., J. Doody, I. Timokhina, and J. Massagué. 1999. "A mechanism of repression of TGF-β/Smad signaling by oncogenic Ras." *Genes & Development* 13(7): 804.

Kuersten, S., M. Ohno, and I. W. Mattaj. 2001. "Nucleocytoplasmic transport: Ran, beta and beyond." *Trends in Cell Biology* 11(12): 497–503.

Kundu, S., P. J. Horn, and C. L. Peterson. 2007. "SWI/SNF is required for transcriptional memory at the yeast GAL gene cluster." *Genes & Development* 21(8) (April): 997-1004.

Kurisaki, A., S. Kose, Y. Yoneda, C. H. Heldin, and A. Moustakas. 2001. "Transforming Growth Factor-beta Induces Nuclear Import of Smad3 in an Importin-beta 1 and Ran-dependent Manner." *Molecular Biology of the Cell* 12(4): 1079.

Kurisaki, A., K. Kurisaki, M. Kowanetz, H. Sugino, Y. Yoneda, C. H. Heldin, and A. Moustakas. 2006. "The mechanism of nuclear export of Smad3 involves exportin 4 and Ran." *Molecular and Cellular Biology* 26(4): 1318.

Lewis, A., R. Felberbaum, and M. Hochstrasser. 2007. "A nuclear envelope protein linking nuclear pore basket assembly, SUMO protease regulation, and mRNA surveillance." *The Journal of Cell Biology* 178(5): 813.

Lim, R. Y. H., B. Fahrenkrog, J. Koser, K. Schwarz-Herion, J. Deng, and U. Aebi. 2007. "Nanomechanical Basis of Selective Gating by the Nuclear Pore Complex." *Science* 318(5850) (October): 640-643.

Lim, R. Y. H., N. P. Huang, J. K\öser, J. Deng, K. H. Lau, K. Schwarz-Herion, B. Fahrenkrog, and U. Aebi. 2006. "Flexible phenylalanine-glycine nucleoporins as entropic barriers to nucleocytoplasmic transport." *Proceedings of the National Academy of Sciences* 103(25): 9512.

Lorenzen, J. A., S. E. Baker, F. Denhez, M. B. Melnick, D. L. Brower, and L. A. Perkins. 2001. "Nuclear import of activated D-ERK by DIM-7, an importin family member encoded by the gene moleskin." *Development*

128(8): 1403.

Lupu, F., A. Alves, K. Anderson, V. Doye, and E. Lacy. 2008. “Nuclear Pore Composition Regulates Neural Stem/Progenitor Cell Differentiation in the Mouse Embryo.” *Developmental Cell* 14(6) (June): 831-842.

Lusk, C. P., T. Makhnevych, M. Marelli, J. D. Aitchison, and R. W. Wozniak. 2002. “Karyopherins in nuclear pore biogenesis: a role for Kap121p in the assembly of Nup53p into nuclear pore complexes.” *The Journal of Cell Biology* 159(2): 267.

Lutzmann, M., R. Kunze, K. Stangl, P. Stelter, K. F. Toth, B. Böttcher, and E. Hurt. 2004. “Reconstitution of Nup157 and Nup145N into the Nup84 Complex.” *Journal of Biological Chemistry* 280(18) (December): 18442-18451.

Ma, J., and W. Yang. 2010. “Three-dimensional distribution of transient interactions in the nuclear pore complex obtained from single-molecule snapshots.” *Proceedings of the National Academy of Sciences* 107(16): 7305.

Mahmoudi, T., V. S.W. Li, S. S. Ng, N. Taouatas, R. G. J. Vries, S. Mohammed, A. J Heck, and H. Clevers. 2009. “The kinase TNIK is an essential activator of Wnt target genes.” *The EMBO Journal* 28(21): 3329–3340.

Martín-Castellanos, C., and B. A. Edgar. 2002. “A characterization of the effects of Dpp signaling on cell growth and proliferation in the Drosophila wing.” *Development* 129(4): 1003.

Massagué, J. 2000. “How cells read TGF-beta signals.” *Nature Reviews Molecular Cell Biology* 1(3): 169–178.

Mattaj, I. W., and L. Englmeier. 1998. “Nucleocytoplasmic Transport: The Soluble Phase.” *Annu. Rev. Biochem.* 67: 265-306.

Meyer, T., A. Begitt, I. Lödige, M. van Rossum, and U. Vinkemeier. 2002. “Constitutive and IFN-gamma-induced nuclear import of STAT1 proceed through independent pathways.” *EMBO J.* 21(3): 344-54.

Miao, L., and K. Schulten. 2009. “Transport-Related Structures and Processes of the Nuclear Pore Complex Studied through Molecular Dynamics.” *Structure* 17(3) (March): 449-459.

Miles, W. O., E. Jaffray, S. G. Campbell, S. Takeda, L. J. Bayston, S. P. Basu, M. Li, et al. 2008. “Medea SUMOylation restricts the signaling range of the Dpp morphogen in the Drosophila embryo.” *Genes & Development* 22(18) (September): 2578-2590.

Moustakas, A., and C. H. Heldin. 2009. “The regulation of TGFβ signal transduction.” *Development* 136(22) (October): 3699-3714.

Nakao, A., M. Afrakhte, A. Moren, T. Nakayama, J. L. Christian, R. Heuchel, S. Itoh, et al. 1997. “Identification of Smad7, a TGF-β-inducible antagonist of TGF-β signalling.” *Nature* 389: 631-635.

Nicholls, R. E., and W. M. Gelbart. 1998. “Identification of Chromosomal Regions Involved in decapentaplegic Function in Drosophila.” *Genetics*

149: 203-215.

Nicke, B., J. Bastien, S. J. Khanna, P. H. Warne, V. Cowling, S. J. Cook, G. Peters, et al. 2005. “Involvement of MINK, a Ste20 family kinase, in Ras oncogene-induced growth arrest in human ovarian surface epithelial cells.” *Molecular Cell* 20(5): 673–685.

Nicolás, F. J., K. De Bosscher, B. Schmierer, and C. S. Hill. 2004. “Analysis of Smad nucleocytoplasmic shuttling in living cells.” *Journal of Cell Science* 117(18): 4113.

Paricio, N., F. Feiguin, M. Boutros, S. Eaton, and M. Mlodzik. 1999. “The Drosophila STE20-like kinase misshapen is required downstream of the Frizzled receptor in planar polarity signaling.” *The EMBO Journal* 18(17): 4669–4678.

Pemberton, L. F., and B. M. Paschal. 2005. “Mechanisms of Receptor-Mediated Nuclear Import and Nuclear Export.” *Traffic* 6(3): 187–198.

Perrimon, N., and B. Mathey-Prevot. 2006. “Applications of High-Throughput RNA Interference Screens to Problems in Cell and Developmental Biology.” *Genetics* 175(1) (October): 7-16.

Peters, R. 2009. “Translocation through the nuclear pore: Kaps pave the way.” *Bioessays* 31(4): 466–477.

Pichler, A., A. Gast, J. S. Seeler, A. Dejean, and F. Melchior. 2002. “The nucleoporin RanBP2 has SUMO1 E3 ligase activity.” *Cell* 108(1): 109–120.

Pierreux, C. E., F. J Nicolas, and C. S. Hill. 2000. “Transforming growth factor beta-independent shuttling of Smad4 between the cytoplasm and nucleus.” *Molecular and Cellular Biology* 20(23): 9041.

Radu, A., G. Blobel, and M. S. Moore. 1995. “Identification of a protein complex that is required for nuclear protein import and mediates docking of import substrate to distinct nucleoporins.” *Proceedings of the National Academy of Sciences* 92(5): 1769.

Raftery, L. A., V. Twombly, K. A. Wharton, and W. M. Gelbart. 1995. “Genetic Screens to Identify Elements of the decapentaplegic Signaling Pathway in Drosophila.” *Genetics* 139: 241-254.

Reverter, D., and C. D. Lima. 2005. “Insights into E3 ligase activity revealed by a SUMO–RanGAP1–Ubc9–Nup358 complex.” *Nature* 435(7042) (June): 687-692.

Rout, M. 2003. “Virtual gating and nuclear transport: the hole picture.” *Trends in Cell Biology* 13(12) (December): 622-628.

Sabri, N., P. Roth, N. Xylourgidis, F. Sadeghifar, J. Adler, and C. Samakovlis. 2007. “Distinct functions of the Drosophila Nup153 and Nup214 FG domains in nuclear protein transport.” *The Journal of Cell Biology* 178(4): 557.

Sander, V., E. Eivers, R. H. Choi, and E. M. De Robertis. 2010. “Drosophila

Smad2 opposes Mad signaling during wing vein development." *PLoS One* 5(4): e10383.

Sapkota, G., C. Alarcón, F. M. Spagnoli, A. H. Brivanlou, and J. Massagué. 2007. "Balancing BMP Signaling through Integrated Inputs into the Smad1 Linker." *Molecular Cell* 25(3) (February): 441-454.

Schmid, M., G. Arib, C. Laemmli, J. Nishikawa, T. Durussel, and U. K. Laemmli. 2006. "Nup-PI: the nucleopore-promoter interaction of genes in yeast." *Molecular Cell* 21(3): 379–391.

Schmierer, B., and C. S. Hill. 2005. "Kinetic analysis of Smad nucleocytoplasmic shuttling reveals a mechanism for transforming growth factor β-dependent nuclear accumulation of Smads." *Molecular and Cellular Biology* 25(22): 9845.

Schmierer, B., A. L. Tournier, P. A. Bates, and C. S. Hill. 2008. "Mathematical modeling identifies Smad nucleocytoplasmic shuttling as a dynamic signal-interpreting system." *Proceedings of the National Academy of Sciences* 105(18): 6608.

Shi, Y., and J. Massague. 2003. "Mechanism of TGF-beta Signaling from Cell Membrane to the Nucleus." *Cell* 113: 685-700.

Shitashige, M., R. Satow, T. Jigami, K. Aoki, K. Honda, T. Shibata, M. Ono, S. Hirohashi, and T. Yamada. 2010. "Traf2- and Nck-Interacting Kinase Is Essential for Wnt Signaling and Colorectal Cancer Growth." *Cancer Research* 70(12) (June): 5024-5033.

Siniossoglou, S., M. Lutzmann, H. Santos-Rosa, K. Leonard, S. Mueller, U. Aebi, and E. Hurt. 2000. "Structure and assembly of the Nup84p complex." *The Journal of Cell Biology* 149(1): 41.

Sotillos, S., and J. F. De Celis. 2005. "Interactions between the Notch, EGFR, and decapentaplegic signaling pathways regulate vein differentiation duringDrosophila pupal wing development." *Developmental Dynamics* 232(3) (March): 738-752.

Stewart, M. 2007a. "Molecular mechanism of the nuclear protein import cycle." *Nature Reviews Molecular Cell Biology* 8: 195-208.

Stewart, M. 2007b. "Ratcheting mRNA out of the Nucleus." *Molecular Cell* 25(3) (February): 327-330.

Strambio-De-Castillia, C., M. Niepel, and M. P. Rout. 2010. "The nuclear pore complex: bridging nuclear transport and gene regulation." *Nature Reviews Molecular Cell Biology* 11(7): 490–501.

Strawn, L. A., T. Shen, N. Shulga, D. S. Goldfarb, and S. R. Wente. 2004. "Minimal nuclear pore complexes define FG repeat domains essential for transport." *Nature Cell Biology* 6(3): 10–206.

Su, Y. C, J. E Treisman, and E. Y Skolnik. 1998. "The Drosophila Ste20-related kinase misshapen is required for embryonic dorsal closure and acts through a JNK MAPK module on an evolutionarily conserved signaling

pathway.” *Genes & development* 12(15): 2371.

Su, Y. C., J. Han, S. Xu, M. Cobb, and E. Y. Skolnik. 1997. “NIK is a new Ste20-related kinase that binds NCK and MEKK1 and activates the SAPK/JNK cascade via a conserved regulatory domain.” *The EMBO Journal* 16(6): 1279–1290.

Tang, X., A. Guilherme, A. Chakladar, A. M. Powelka, S. Konda, J. V. Virbasius, S. Nicoloro, J. Straubhaar, and M. P. Czech. 2006. “An RNA interference-based screen identifies MAP4K4/NIK as a negative regulator of PPARγ, adipogenesis, and insulin-responsive hexose transport.” *Proceedings of the National Academy of Sciences of the United States of America* 103(7): 2087.

Terry, L. J., and S. R. Wente. 2007. “Nuclear mRNA export requires specific FG nucleoporins for translocation through the nuclear pore complex.” *The Journal of Cell Biology* 178(7): 1121.

Terry, L. J., E. B. Shows, and S. R. Wente. 2007. “Crossing the Nuclear Envelope: Hierarchical Regulation of Nucleocytoplasmic Transport.” *Science* 318 (5855) (November): 1412-1416.

Tesz, G. J., A. Guilherme, K. V. P. Guntur, A. C. Hubbard, X. Tang, A. Chawla, and M. P. Czech. 2007. “Tumor Necrosis Factor α (TNFα) Stimulates Map4k4 Expression through TNFα Receptor 1 Signaling to c-Jun and Activating Transcription Factor 2.” *Journal of Biological Chemistry* 282 (27) (May): 19302-19312.

Therizols, P., C. Fairhead, G. G Cabal, A. Genovesio, J. C. Olivo-Marin, B. Dujon, and E. Fabre. 2006. “Telomere tethering at the nuclear periphery is essential for efficient DNA double strand break repair in subtelomeric region.” *The Journal of Cell Biology* 172(2): 189.

Towbin, B. D., P. Meister, and S. M. Gasser. 2009. “The nuclear envelope—a scaffold for silencing?” *Current Opinion in Genetics & Development* 19(2) (April): 180-186.

Tsuneizumi, K., T. Nakayama, Y. Kamoshida, T. B. Kornberg, J. L. Christian, and T. Tabata. 1997. “Daughters against dpp modulates dpp organizing activity in Drosophila wing development.” *Nature* 389: 627.

Varelas, X., R. Sakuma, P. Samavarchi-Tehrani, R. Peerani, B. M. Rao, J. Dembowy, M. B. Yaffe, P. W. Zandstra, and J. L. Wrana. 2008. “TAZ controls Smad nucleocytoplasmic shuttling and regulates human embryonic stem-cell self-renewal.” *Nature Cell Biology* 10(7) (June): 837-848.

Vetter, I. R., A. Arndt, U. Kutay, D. Görlich, and A. Wittinghofer. 1999. “Structural View of the Ran-Importinβ Interaction at 2.3Å Resolution.” *Cell* 97(5): 635–646.

Wälde, S., and R. H. Kehlenbach. 2010. “The Part and the Whole: functions of nucleoporins in nucleocytoplasmic transport.” *Trends in Cell Biology* 20(8)

(August): 461-469.

Walther, T. C., A. Alves, H. Pickersgill, I. Loïodice, M. Hetzer, V. Galy, B. B. Hülsmann, et al. 2003. “The conserved Nup107-160 complex is critical for nuclear pore complex assembly.” *Cell* 113(2): 195–206.

Wente, S. R., and M. P. Rout. 2010. “The Nuclear Pore Complex and Nuclear Transport.” *Cold Spring Harbor Perspectives in Biology* 2(10) (July): a000562-a000562.

Wharton, K. A., R. P. Ray, and W. M. Gelbart. 1993. “An activity gradient of decapentaplegic is necessary for the specification of dorsal pattern elements in the Drosophila embryo.” *Development* 117(2): 807.

Wu, J. W., M. Hu, J. Chai, J. Seoane, M. Huse, C. Li, D. J. Rigotti, et al. 2001. “Crystal Structure of a Phosphorylated Smad2: Recognition of Phosphoserine by the MH2 Domain and Insights on Smad Function in TGF-β Signaling.” *Molecular Cell* 8(6): 1277–1289.

Xu, L. 2003. “Distinct Domain Utilization by Smad3 and Smad4 for Nucleoporin Interaction and Nuclear Import.” *Journal of Biological Chemistry* 278(43) (August): 42569-42577.

Xu, L. 2006. “Regulation of Smad activities.” *Biochimica et Biophysica Acta (BBA)-Gene Structure and Expression* 1759(11-12): 503–513.

Xu, L., Y. Kang, S. Col, and J. Massagué. 2002. “Smad2 nucleocytoplasmic shuttling by nucleoporins CAN/Nup214 and Nup153 feeds TGFβ signaling complexes in the cytoplasm and nucleus.” *Molecular Cell* 10(2): 271–282.

Xu, L., X. Yao, X. Chen, P. Lu, B. Zhang, and Y. T. Ip. 2007. “Msk is required for nuclear import of TGF-beta/BMP-activated Smads.” *The Journal of Cell Biology* 178(6): 981.

Xu, S., and M. A. Powers. 2009. Nuclear pore proteins and cancer. In *Seminars in Cell & Developmental Biology*, 20:620–630.

Xue, Y., X. Wang, Z. Li, N. Gotoh, D. Chapman, and E. Y. Skolnik. 2001. “Mesodermal patterning defect in mice lacking the Ste20 NCK interacting kinase (NIK).” *Development* 128(9): 1559.

Yamada, J., J. L. Phillips, S. Petel, G. Goldfien, A. Calestagne-Morelli, H. Huang, R. Reza, et al. 2010. “A bimodal distribution of two distinct categories of intrinsically-disordered structures with separate functions in FG nucleoporins.” *Mol. Cell. Proteomics* 9(10): 2205-2224.

Yang, Q., M. P. Rout, and C. W. Akey. 1998. “Three-dimensional architectur of the isolated yeast nuclear pore complex: Functional and evolutionary implications.” *Molecular Cell* 1: 223-234.

Yao, X., X. Chen, C. Cottonham, and L. Xu. 2008. “Preferential Utilization of Imp7/8 in Nuclear Import of Smads.” *Journal of Biological Chemistry* 283 (33) (June): 22867-22874.

Yi, H., J. L. Friedman, and P. A. Ferreira. 2007. “The Cyclophilin-like Domain of Ran-binding Protein-2 Modulates Selectively the Activity of the

Ubiquitin-Proteasome System and Protein Biogenesis." *Journal of Biological Chemistry* 282(48) (September): 34770-34778. doi:10.1074/jbc.M706903200.

Zawel, L., J. Le Dai, P. Buckhaults, S. Zhou, K. W. Kinzler, B. Vogelstein, and S. E. Kern. 1998. "Human Smad3 and Smad4 are sequence-specific transcription activators." *Molecular Cell* 1(4): 611–617.

Zeng, Y. A., M. Rahnama, S. Wang, W. Sosu-Sedzorme, and E. M. Verheyen. 2007. "Drosophila Nemo antagonizes BMP signaling by phosphorylation of Mad and inhibition of its nuclear accumulation." *Development* 134(11) (June): 2061-2071.

Zhang, X., S. Chen, S. Yoo, S. Chakrabarti, T. Zhang, T. Ke, C. Oberti, et al. 2008. "Mutation in Nuclear Pore Component NUP155 Leads to Atrial Fibrillation and Early Sudden Cardiac Death." *Cell* 135(6) (December): 1017-1027.

Zhu, C. C., J. Q. Boone, P. A. Jensen, S. Hanna, L. Podemski, J. Locke, C. Q. Doe, and M. B. O'Connor. 2008. "Drosophila Activin-β and the Activin-like product Dawdle function redundantly to regulate proliferation in the larval brain." *Development* 135(3) (January): 513-521.

Appendix: Primary hits of the RNAi screen.

Candidates are listed ascendingly according to the score given by visual inspection. Hits that are characterized in this thesis are highlighted in grey.

Gene	CGs	Human Homologene	Nuc Cyto Ratio	Visual Score	DRSC Amplicon	Amp. Length	19 bp Matches
msk	CG7935	IPO7	1.844	1	DRSC23929	429	0
msk	CG7935	IPO7	2.063735	1	DRSC11340	501	1
CG5733	CG5733	NUP85	2.110022	1.5	DRSC06947	507	1
CG3898	CG3898		1.963377	2	DRSC18330	363	19
Pop2	CG5684	CNOT7	2.177269	3	DRSC10537	502	1
Pp4-19C	CG1459, CG18339, CG32505, CG1596	PPP4C	2.405957	4	DRSC20559	311	1
Pp4-19C	CG1459, CG18339, CG32505, CG1596	PPP4C	2.358362	4	DRSC20559	311	1
CG34104	CG34104, CG12102, CG12094		2.58209	4	DRSC25197	426	0
Cdc37	CG12019	CDC37	2.482043	4	DRSC27723	328	0
sec13	CG6773	SEC13	2.33088	4	DRSC14144	485	0
CG11092	CG11092	NUP93	2.347931	4	DRSC19344	509	0
CG11943	CG11943	NUP205	2.424338	4	DRSC19432	505	0
Cdc37	CG12019	CDC37	2.365422	4	DRSC08648	518	1
Pp4-19C	CG1459, CG18339, CG32505, CG1596	PPP4C	2.577226	4.5	DRSC21251	515	1
Pp4-19C	CG1459, CG18339, CG32505, CG1596	PPP4C	2.585115	4.5	DRSC21251	515	1
CG9339	CG9339, CG14399, CG9340	TBC1D24	2.217	4.5	DRSC03214	263	0

CG2158	CG2158	NUP50	2.291576	4.5	DRSC06827	510	1
Uba1	CG1782	UBE1	2.313767	4.5	DRSC07567	516	1
put	CG7904	ACVR2A	2.419291	4.5	DRSC17039	510	0
Ntf-2	CG1740		2.363126	4.5	DRSC20552	200	1
CG6583	CG6583		2.402576	4.5	DRSC02972	207	1
			1.88281	4.5	DRSC36529	299	0
CG17665	CG17665		2.387269	5	DRSC21215	176	0
CG12460	CG12460, CG40051		2.418299	5	DRSC20970	134	2
CG17665	CG17665		2.290855	5	DRSC21215	176	0
CG12460	CG12460, CG40051		2.400496	5	DRSC20970	134	2
trus	CG5333	PDCD2L	2.12066	5	DRSC25521	307	0
upd2	CG5988		2.66533	5	DRSC24190	408	0
ras	CG11485, CG1799	IMPDH2	2.450879	5	DRSC27137	365	0
TER94	CG2331	VCP	2.584463	5	DRSC27600	320	0
CG3173	CG3173	INTS1	2.31775	5	DRSC27942	427	0
geminin	CG3183		2.317669	5	DRSC29794	386	0
poe	CG14472	ZUBR1	2.411179	5	DRSC03593	483	0
me31B	CG4916	DDX6	2.543134	5	DRSC03569	501	0
CG3173	CG3173	INTS1	2.152977	5	DRSC04343	495	1
defl	CG18176	INTS7	2.169792	5	DRSC10300	509	0
omd	CG9591		2.031163	5	DRSC16507	500	1
CG8211	CG8211	INTS2	2.201703	5	DRSC20094	503	0
dia	CG1768	DIAPH2	2.373998	5	DRSC03519	505	9
geminin	CG3183		2.38619	5	DRSC04984	508	2
BRWD3	CG6400, CG31132, CG18670	BRWD1	2.272912	5	DRSC16032	515	0
omd	CG9591		2.245437	5.4	DRSC29369	303	0
BRWD3	CG6400, CG31132, CG18670	BRWD1	2.206151	5.4	DRSC15369	508	9
l(1)G0060	CG3125	INTS6	2.249478	5.4	DRSC18281	504	3

snoRNA:U31:54Ec, snoRNA:snR38:54Eb, snoRNA:U27:54Eb, snoRNA:snR38:54Ec, snoRNA:U27:54Ec, snoRNA:snR38:54Ea, snoRNA:U31:54Ed, Uhg1, snoRNA:U31:54Eb, snoRNA:U29:54Ed, snoRNA:U27:54Ea	Uhg1: CG14486		2.287774	5.4	DRSC06458	2394	4
CG40282	CG40282, CG17706		2.427413	5.4	DRSC07814	464	3
CG5491	CG5491	INTS12	2.083407	5.4	DRSC15818	495	0
CG6619	CG6619		2.465679	5.5	DRSC08791	519	3
Mes2	CG11100		2.520626	5.5	DRSC11593	278	0
CG6619	CG6619		2.397858	5.5	DRSC08791	519	3
CG13779	CG13779		2.50665	5.5	DRSC30061	229	2
CG30151	CG30151		2.80161	5.5	DRSC24759	286	0
CG15269	CG15269		2.769486	5.5	DRSC24737	303	0
CG9235	CG9235		2.98227	5.5	DRSC26087	350	0
CG15263	CG15263		2.44419	5.5	DRSC27309	330	0
CG15374	CG15374		2.438166	5.5	DRSC27325	216	0
CG8008	CG8008		2.290436	5.5	DRSC27395	370	0
DppIII	CG7415	DPP3	2.55619	5.5	DRSC27801	451	0
CG17292	CG17292		2.614519	5.5	DRSC27746	301	0
CG32353	CG32353, CG6239		2.542148	5.5	DRSC27481	329	0
CG34123	CG34123, CG30079, CG30078, CG16805		2.588073	5.5	DRSC27597	512	0
mbl	CG14477, CG10941, CG33197	MBNL1	2.737744	5.5	DRSC28319	321	0
Rpn5	CG1100	PSMD12	2.699169	5.5	DRSC28279	544	0
Uba1	CG1782	UBE1	2.563883	5.5	DRSC28350	419	0
Itp-r83A	CG1063	ITPR1	2.529816	5.5	DRSC28770	300	0

CG12932	CG12932		2.354414	5.5	DRSC29170	303	0
shi	CG18102	DNM1	2.422113	5.5	DRSC29498	305	0
tkv	CG14026	BMPR1A	2.510634	5.5	DRSC03623	509	2
CG9314	CG9314		2.553812	5.5	DRSC03194	517	1
CG3975	CG3975		2.519396	5.5	DRSC01961	515	1
CG10531	CG10531		2.193149	5.5	DRSC04079	562	1
CG30281	CG30281, CG6676	FCN1	2.193796	5.5	DRSC04528	501	0
CG14471	CG14471		2.281233	5.5	DRSC04865	506	1
TER94	CG2331	VCP	2.327177	5.5	DRSC07560	513	1
CG4282	CG4282		2.289546	5.5	DRSC06865	508	0
CG5859	CG5859	INTS8	2.253403	5.5	DRSC07417	484	0
CG16807	CG16807	RC3H1	2.121173	5.5	DRSC10227	490	0
zfh1	CG1322	ZEB1	2.449715	5.5	DRSC17098	516	6
CG2116	CG2116		2.257611	5.5	DRSC18206	509	4
CG6506	CG6506		2.254038	5.5	DRSC19997	488	3
l(1)G0095	CG12113	INTS4	2.323491	5.5	DRSC17810	485	0
cmet	CG6392	CENPE	2.449095	5.5	DRSC03511	513	0
Nipped-A	CG33554, CG2905, CG10549	TRRAP	2.400973	5.5	DRSC04883	236	0
CG30169	CG30169, CG13584, CG13583		2.420928	5.5	DRSC04219	518	0
CG17048	CG17048		2.263541	5.5	DRSC06649	273	0
Arf51F	CG8156	ARF6	2.240902	5.5	DRSC05921	285	0
CG13335	CG13335, CG6183		2.287998	5.5	DRSC06966	575	0
CG13340	CG13340		2.221772	5.5	DRSC06374	514	2
CG13443	CG13443		2.415307	5.5	DRSC06403	520	0
Lcp65APsi	CG18775		2.18599	5.5	DRSC10342	226	1
mus301	CG7972	HEL308	2.162939	5.5	DRSC10939	491	0
rols	CG5679, CG17155, CG32096, CG12277	TANC2	2.196289	5.5	DRSC10536	505	0
CG18265	CG18265		2.070831	5.5	DRSC10310	509	0

MICAL	CG18667, CG18484, CG18668, CG33208, CG11687, CG33190, CG11685, CG33186	LOC729269	2.101503	5.5	DRSC14351	242	0
CG13658	CG13658		2.2555	5.5	DRSC14659	499	2
CG31156	CG31156, CG5253, CG5257	SRBD1	2.193412	5.5	DRSC15755	221	0
CG15786	CG15786		2.220728	5.5	DRSC18092	477	0
HDC20619 ('+' in Hild et al)			2.149558	5.5	DRSC21237	300	0
ari-1	CG5659	ARIH1	2.203919	5.5	DRSC21603	500	1
CG30049	CG30049		1.973251	5.5	DRSC21345	311	0
Ptp99A	CG2005, CG11517, CG11516, CG11515	PTPRG	2.200032	5.5	DRSC22125	148	0
twin	CG31137, CG17741, CG5534	CNOT6	2.199761	5.5	DRSC21363	500	1